PAUL SCHERRER INSTITUT

PSI

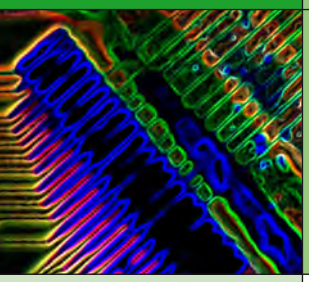

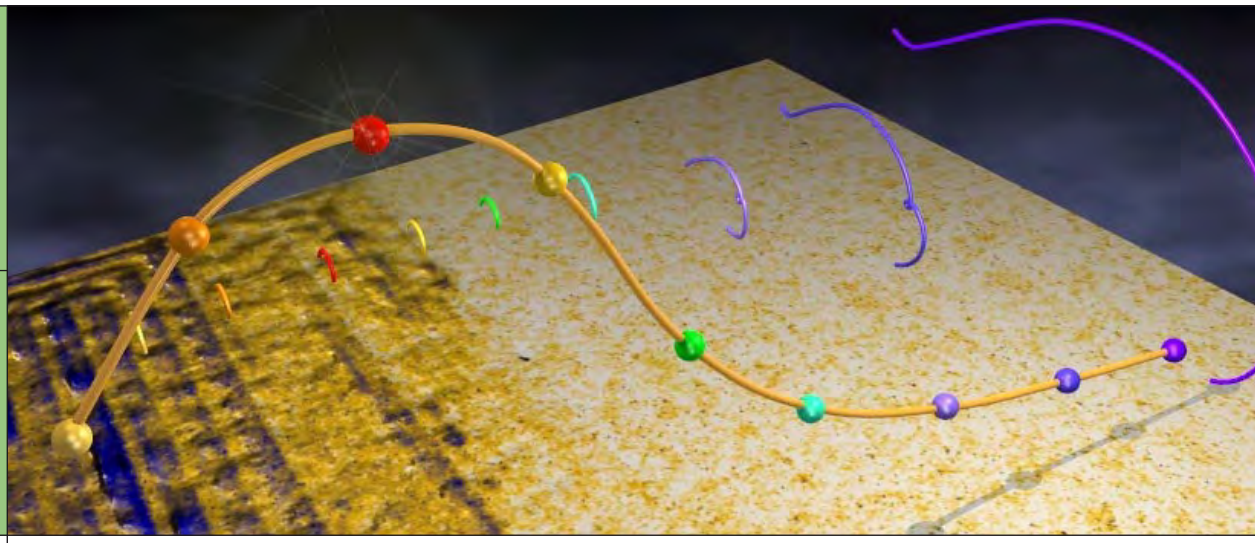

Annual Report 2005

Electrochemistry Laboratory

http://ecl.web.psi.ch

COVER PHOTO:

Center: Diagnostics are essential for fuel cell development. The picture shows a collage of different spatially resolving in situ methods simultaneously applied to a fuel cell. The base is formed by a neutron image showing the water distribution within a small scale PEFC. The larger curve shows the local current generation, and the winding curves are representations of the local impedance response of the device. From the combined measurements, detailed information about local processes and limitations can be obtained.

Left: View inside a special polymer electrolyte fuel cell for measuring current distribution on the micro meter scale (false colours).

© Paul Scherrer Institut

PAUL SCHERRER INSTITUT

Electrochemistry Laboratory

Annual Report 2005

Hardcopies of this report are available from:
Isabella Kalt (isabella.kalt@psi.ch)
Paul Scherrer Institut
5232 Villigen PSI
Switzerland

A full version of this report is also available on the web:
http://ecl.web.psi.ch

Paul Scherrer Institut
Electrochemistry Laboratory
5232 Villigen PSI
Switzerland

Secretary
Phone +41 (0)56 310 29 19
Fax +41 (0)56 310 44 15

IMPRESSUM

Publisher
Electrochemistry Laboratory
Paul Scherrer Institut
5232 Villigen PSI

Editorial Team
Isabella Kalt
Rüdiger Kötz
Günther G. Scherer

Printing
Paul Scherrer Institut

ISSN 1661-5379
PSI Electrochemistry Laboratory – Annual Report 2005

© Paul Scherrer Institut

CONTENT

EDITORIAL

The past year 2005 exhibited several highlights for the Electrochemistry Laboratory, three of them will be mentioned here: The 2005 Technology Award of the Battery Division of the Electrochemical Society was dedicated to PD Dr. Petr Novak, Head of our Battery Group, to honour his longstanding contributions to battery research. On the occasion of the 3rd European Polymer Electrolyte Fuel Cell Forum, Lucerne, members of our Fuel Cell Group became recipients of the Christian Friedrich Schönbein "Contribution to Science" Medal for their contributions to the "Understanding of the fundamentals of the spatially resolved characterization of polymer electrolyte fuel cells". A joint one-day-symposium of Seoul National University and Paul Scherrer Institut took place at SNU, Seoul, illustrating the high level efforts of R & D in electrochemical energy conversion and storage at both institutions. This and further joint seminars will strengthen the collaboration with our colleagues of SNU.

Currently, the laboratory is organized into the following four research groups: Fuel Cells, Fuel Cell Systems, Batteries, and Capacitors, as well as the Nanocat and Interface Analysis Projects. The head of the former project is also responsible for the construction of the IR beam line at PSI's synchrotron SLS. Within this Annual Report each of the research groups is represented by several contributions, highlighting their research efforts and their results of the past year 2005. Among others, this years report features the continuing development of *in situ* diagnostic methods and combinations thereof. These methods will become more and more important to understand inhomogeneous and transient performance patterns in devices of technical relevance.

According to the laboratory's philosophy we carry out research and development of electrochemical energy conversion and storage systems at the materials, cell, and systems level. This is the reason why many of our projects are materials development oriented. Surface, interface, and inter-phase aspects of materials play an important role, for the processes occurring in electrochemical conversion and storage systems. Materials aspects will influence cell and systems design, hence the development of more sophisticated and over all cheaper materials will allow working on more efficient but simpler cells and systems.

Continuous education of our students and co-workers is another primary goal of our laboratory. Our Electrochemistry Seminar (a Monday afternoon affair), was organized in several cycles to various topics by either our PhD-students, post-doctoral fellows, or the group leaders and took place 38 times, with 20 external speakers. Participation of our co-workers at national or international conferences, including numerous lectures or poster presentations, served as a means to expose the Laboratory to the international scientific community. Further, several diploma and summer students spent time with us to carry out their thesis in one of our research groups.

Communication to our partners in research projects, within the Paul Scherrer Institut, and to the scientific community outside of PSI is of utmost importance to us. For this reason, the laboratory again organized successfully a One-Day-Symposium with international participation. The 21st One-Day-Symposium took place on the 11th of May, addressing the subject of "Electrochemistry in Automotive Industry". Presentations were given by P. Schmutz, EMPA, Dübendorf; G. Nauer, Univ. Wien; G. Broussely, SAFT SA, Poitiers; W. Tillmetz, ZSW, Ulm; and M. Ullrich, Volkswagen AG Wolfsburg.

We look forward to the 22nd Symposium, which will take place on May 11th, 2006, addressing topics of "Electrochemistry in Biology and Medicine".

In summary, we look back again to a successful year 2005. This gives us great confidence to further contribute to the field of Electrochemistry and transfer our know-how to industrial partners as well as to support education of students. We see our work in the wider context of a sustainable energy development, which also has been identified as a general future goal of the Domain of the Swiss Federal Institutes of Technology in the context of its recently founded Competence Center for Energy and Mobility.

Günther G. Scherer

SCIENTIFIC CONTRIBUTIONS 2005

IN SITU DIAGNOSTICS

ADVANCED CHARACTERIZATION OF PEFCS USING NEUTRON RADIOGRAPHY AND LOCALLY RESOLVED IMPEDANCE SPECTROSCOPY

I.A. Schneider, D. Kramer, A. Wokaun
G.G. Scherer
+41(0)56 310 2795
ingo.schneider@psi.ch

The performance as well as the longevity of polymer electrolyte fuel cells (PEFCs) have to be increased to be further competitive to conventional power conversion technologies. Proper water management in PEFCs is one of the most critical factors to ensure high cell performance.
Therefore, for further optimization the impact of water on ohmic, electrochemical as well as mass transport losses has to be better understood in operating PEFCs [1]. A novel method for performing neutron radiography [2] and locally resolved impedance spectroscopy [3] simultaneously *in situ* in an operating Polymer Electrolyte Fuel Cell (PEFC) is presented. The new spatially resolved method [4] provides information about the local cell performance, the locally limiting processes, and the liquid water distribution at a glance. Information about the impact of water on cell performance and limiting processes can be gained *in situ* on a local scale in an operating PEFC.

Experimental

For the experiments described here, we used a PEFC (area 29.2cm^2) similar to our segmented cell for locally resolved EIS described earlier [2]. Several technical changes were taken into consideration [4] to ensure high neutron transparency. Locally resolved impedance measurements were performed *in situ* at the neutron radiography facility NEUTRA [3].
The nine-fold segmented cell is placed into the collimated neutron beam as shown in Fig.1. The neutron beam becomes attenuated while passing through the fuel cell perpendicular to the flow field area. The relative transmission of the neutron beam is a measure for the local amount of water in the cell, provided that the neutron image of the dry cell is used as reference [3]. The locally resolved impedance measurements were performed simultaneously in galvanostatic mode under the conditions described in Fig. 2, once the segment voltages and currents stabilized.

Results and Discussion

The gases are fed to the cell in co-flow mode as shown in Fig. 2a. The amount of water formed due to reduction of oxygen gradually increases as the gases flow along the gas channels from the gas inlets (segment 1) towards the gas outlets (segment 9).

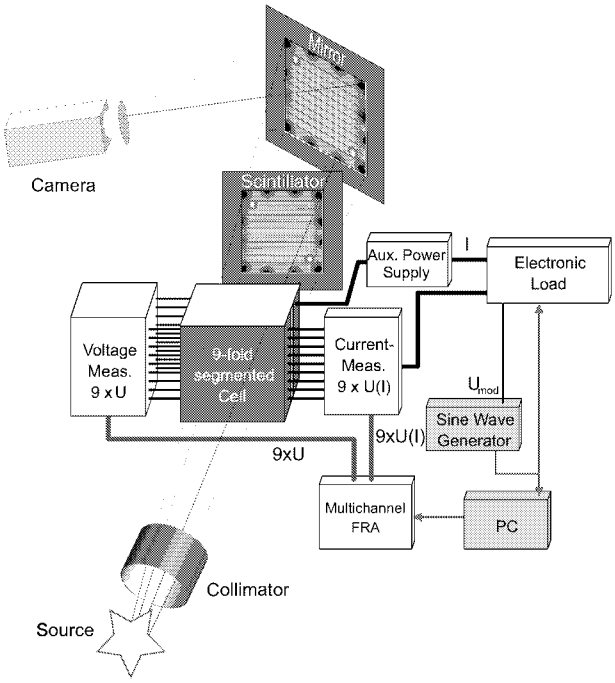

Fig. 1: *Experimental setup used in this study.*

Neutron radiogram and liquid water profile: According to the referenced neutron radiogram (Fig. 2a) and the liquid water profile (Fig. 2b) no liquid water is present in segments 1-5 (undersaturated region). Large parts of the cell are dry. The gases flow a long way through the cell until liquid water is formed in segment 6 (transition region), which is partly flooded (Fig. 2a). The liquid water content then strongly increases towards the gas outlets from segment 7 to segment 9 (flooding region).

Current density distribution: The current density (Fig. 2c) shows highest values in the fully humidified flooding region (segment 7-9), but decreases strongly towards the gas inlets as the cell becomes dry (segments 1-5). The results indicate that liquid water formation is necessary for ensuring high cell performance. However, strong flooding seems to have some detrimental effect on cell performance, even in a PEFC operated on pure H_2/O_2. With the strongly increasing liquid water content in the flooding region (Fig. 2b) the local current density slightly decreases from segment 7 to segment 9 (Fig. 2c).

The local impedance spectra shown in Figures 2d, 2e provide more insight to understand the impact of water on local cell performance. For the discussion of the local "two electrode" impedance spectra we use again a simplistic approach [1, 4]. We define an overall kinetic resistance R_{kin} as the distance from the high frequency intercept with the real axis (ohmic resistance) to the next lower frequency intercept.

Local impedance spectra of the transition and undersaturated region: The strong performance loss in the undersaturated region (Fig. 2c) can be attributed to drying effects. Liquid water is present only in part of segment 6 (transition region) and segments 1-5 are dry (Fig. 2a, 2b). In this region the

relative humidity of the feed gases decreases along the gas channels towards the gas inlets.

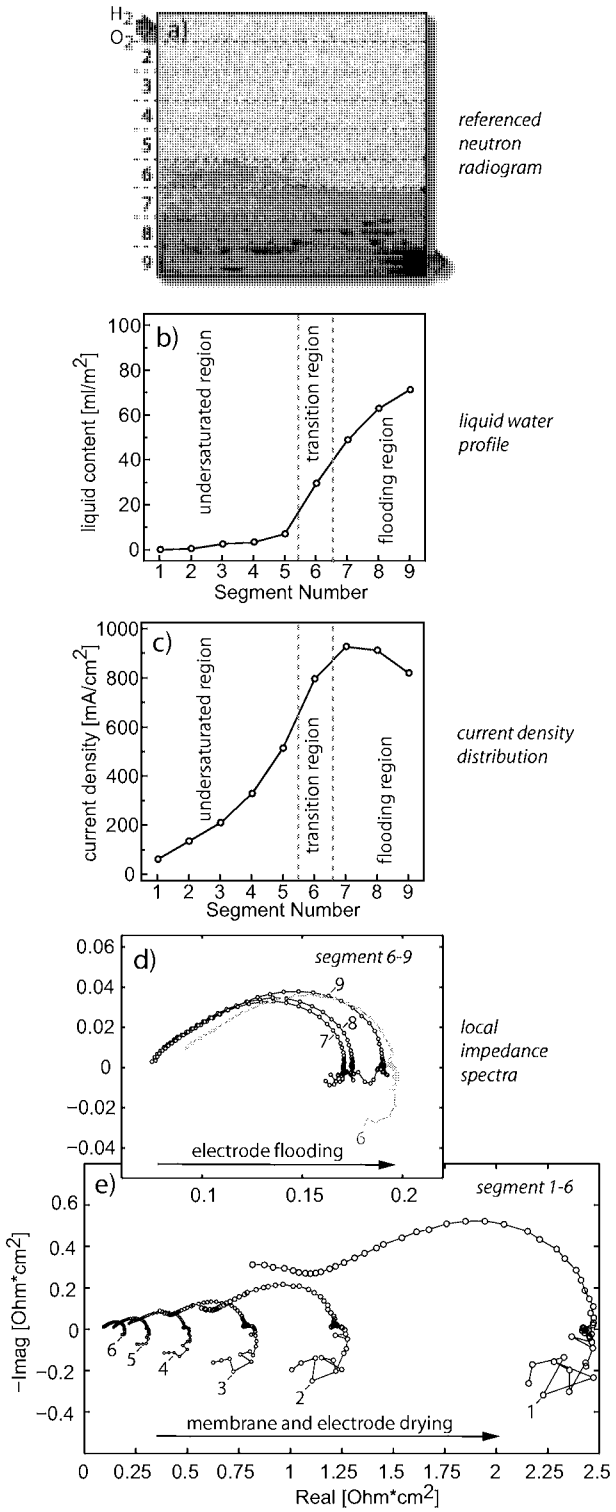

Fig. 2: *Results in co-flow mode: T_{cell}=70°C, I_{cell}=14.6A, A_{cell}=29.2cm², λ_{H2}= λ_{O2}=1.5, r.h.(H_2)=40%, dry O_2, f_{mod}=10mHz-10kHz, Nafion 112 membrane, ETEK ELAT V3.1 electrodes, 250µm PTFE gaskets, (numbers denote segment).*

The decreasing membrane water content with decreasing feed gas humidity towards the gas inlets is clearly reflected in an increasing value for the ohmic resistance in the local impedance spectra (Fig. 2d, 2e).

The ohmic resistance is constant in the flooding region (segment 7-9 in Fig. 3d), but increases instantly when parts of the cell become dry in segment 6 (Fig. 2d). The strong increase continues from segment 6 to segment 4 (Fig. 2e) with decreasing gas humidity towards the gas inlets. For segments 1-3 in the gas inlet region no value for the ohmic resistance (HF real axis intercept) could be identified. However, the most important feature of the local impedance spectra in the undersaturated region is the strongly increasing kinetic resistance [4] from segment 6 to segment 1 towards the gas inlets (Fig. 2e). We attribute this effect to drying of the ionomer incorporated into the catalyst layer with decreasing gas humidity, which results in poor interfacial kinetics. It is highly probable that both, anode and cathode become dry in this region and contribute to this effect, since no liquid water is present in the undersaturated region (segments 1-5).

The results show that under dry conditions in the gas inlet region the detrimental effect of poor interfacial kinetics might actually exceed the impact of the increasing membrane resistance on cell performance.

Local impedance spectra of the flooding region: The high performance in this region can be attributed to liquid water formation. The local impedance spectra for segments 7-9 show a minimum value for the ohmic resistance (Fig. 2d). This correlates well with the results obtained from neutron radiography.

In contrast, the overall kinetic resistance slightly increases (Fig. 2d) with the increasing liquid water content (Fig. 2b) from segment 7 to segment 9. Segment 7 with the lowest liquid water content in the flooding region (Fig. 2b) and the lowest overall kinetic resistance at all (Fig. 2d) shows the highest local performance within the cell (Fig. 2c).

The results show that under low humidity operating conditions severe drying and strong flooding can occur at the same time in different sections of a PEFC, when the cell is operated in co-flow mode. Liquid water formation is crucial for ensuring high proton conductivity/activity in the ionomer incorporated into the active layer of a PEFC electrode. Strong flooding seems to have only little effect on cell performance (Fig. 2c, 2d) in a PEFC operated on pure H_2/O_2.

References

[1] I.A. Schneider, H. Kuhn, A. Wokaun, G.G. Scherer, J. Electrochem. Soc. **12**, A2383 (2005).

[2] I.A. Schneider, H. Kuhn, A. Wokaun, G.G. Scherer, J. Electrochem. Soc. **10**, A2092 (2005).

[3] D. Kramer, J. Zhang, E. Lehmann, A. Wokaun, G.G. Scherer, Electrochim. Acta **50**, 2603 (2005).

[4] I.A. Schneider, D. Kramer, A. Wokaun, G.G. Scherer, Electrochem. Comm. **7**, 1393 (2005).

THE ADVANTAGE OF COLD NEUTRON IMAGING FOR LIQUID WATER DETECTION IN POLYMER ELECTROLYTE FUEL CELLS

D. Kramer, G. Kühne, G. Frei, P. Boillat, E. Lehmann, A. Wokaun, G.G. Scherer
+41(0)56 310 4140
denis.kramer@psi.ch

As has been shown recently, neutron imaging is a potent *in situ* diagnostic method for the investigation of liquid water accumulation in polymer electrolyte fuel cells [1,2,3]. In the past, mainly beam lines at facilities that provide neutrons in the thermal energy range (12-100 meV) were available.

With the realization of the new ICON beam line at PSI, a facility that provides neutrons in the cold energy range (0.12-12 meV) for imaging purposes has become available. This bears several improvements in terms of image quality compared to thermal beam lines.

Neutron cross-section of liquid water

The interaction probability of neutrons with matter is a function of the neutron energy. Generally, lower neutron energies result in higher interaction probabilities. The relative neutron transmission of liquid water as function of the water layer thickness for thermal (NEUTRA) and cold (ICON) neutrons is compared in Fig. 1. The stronger decline in the case of cold neutrons is evidence for a higher interaction probability, whereby the cross-section is nearly doubled in comparison to the thermal beam. This is beneficial for the sensitivity of the method.

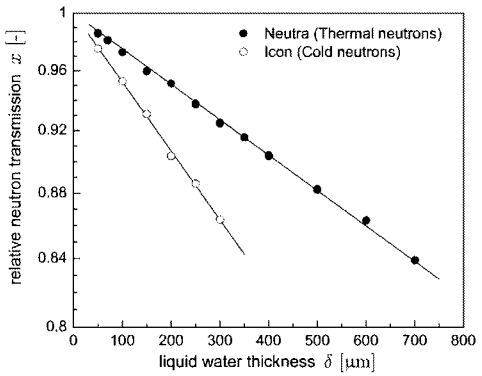

Fig. 1: *Relative neutron transmission as function of liquid water layer thickness for cold (ICON) and thermal (NEUTRA) neutrons.*

Signal to noise ratio (SNR)

Beside the cross-section, the SNR determines the lower detection limit. The noise is a function of the neutron flux and exposure-time due to the shot-noise dominance. The standard deviation (reciprocal of the SNR) of referenced openbeam images (no sample) as function of exposure-time for ICON and NEUTRA is compared in Fig. 2. For both experiments the same CCD-based detector setup was used. Although, the neutron fluxes are comparable for both beam lines, the use of ICON bears a considerable reduction of the image noise. This arises to a large extend from the higher capturing probability of cold neutrons within the scintillator.

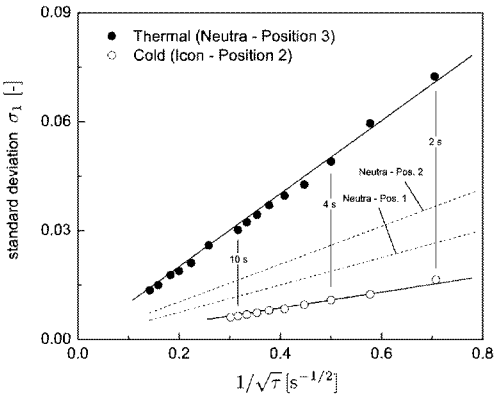

Fig. 2: *Standard deviation of referenced openbeam images as obtained from ICON (cold neutrons) and NEUTRA (thermal neutrons); the dashed lines show estimates for other measurement positions at NEUTRA.*

This enables either a higher accuracy in quantifying thin water layers, which is of extremely high importance for the investigation of liquid accumulation within the porous structures of a membrane-electrode-assembly, or a significant reduction of the exposure-time, which allows investigating fast phenomena like the removal of droplets from the flow field.

Conclusions

The availability of the cold neutron beam line ICON for imaging purposes entails a significant improvement in terms of image quality due to two effects: (1) a higher cross-section for water improves the sensitivity, and (2) the higher detection probability lowers the image noise. Hence, measuring the liquid distribution in polymer electrolyte fuel cells becomes possible with unprecedented accuracy. In addition, the low noise level brings fast neutron imaging into reach, which will enable the dynamic investigation of two-phase flow within the flow fields. Finally, the high flexibility of the facility allows tailoring the beam properties according to the needs of the experiment, e. g. the possible high beam collimation will improve high resolution measurements [4] in the future.

References

[1] D. Kramer, J. Zhang, R. Shimoi, E. Lehmann, A. Wokaun, K. Shinohara, G.G. Scherer, Electrochimica Acta **50**, 2603 (2005).

[2] J. Zhang, D. Kramer, R. Shimoi, Y. Ono, E. Lehmann, A. Wokaun, G.G. Scherer, Electrochimica Acta **51**, 2715 (2006).

[3] I.A. Schneider, D. Kramer, A. Wokaun, G.G. Scherer, Electrochem. Comm. **7**, 1393 (2005).

[4] D. Kramer, J. Zhang, Y. Ono, E. Lehmann, A. Wokaun, K. Shinohara, G.G. Scherer, PSI Scientific Report 2004, **V**, 101, ISSN 1423-7342 (2005).

EFFECT OF GAS FLOW RATE ON LOCAL VOLTAMMOGRAMS IN PEFCS

I.A. Schneider, H. Fuchs, L. Gubler, A. Wokaun, G.G. Scherer
+41(0)56 310 2795
ingo.schneider@psi.ch

Measurement of H_{upd}-adsorption is widely used for determining the electrochemically active Pt area (ECA) in Polymer Electrolyte Fuel Cell (PEFC) electrodes. Cyclic Voltammetry (CV) in PEFCs is carried out on the electrode of interest (working electrode) over a range of 0-1V. Humidified hydrogen flows through the flow field channels of the counter electrode, which also serves as hydrogen reference electrode. Humidified nitrogen flows through the flow field channels of the working electrode. Hydrogen adsorption/desorption occurs in a potential range of approximately 0.05-0.3V. The area (charge) under the H_{upd}-adsorption or desorption peak is used as a quantitative measure of the electrochemically active Pt area.

However, the adsorption peak always includes a contribution from the hydrogen evolution current (HEC). Hydrogen generated in the hydrogen evolution reaction (HER) will accumulate in the nitrogen stream at the working electrode from the gas inlet towards the gas outlet. Since the HER is mass transport controlled [1], the flow velocity of the nitrogen gas should strongly influence the contribution of the HEC to the local CVs.

Experimental

Local CVs were recorded in a potential range from 0.05V to 1V using the setup and the nine-fold segmented PEFC described in [2]. The electronic load was replaced by a four quadrant potentiostat. The segment currents and the overall cell current were recorded during the sweep to obtain local and integral voltammograms. The cell was operated on fully humidified H_2 and N_2. The local and the integral voltammograms were taken using nitrogen flow rates of n_{N2}=20ml/min and n_{N2}=200ml/min, respectively.

In addition, ECA measurements were performed using CO stripping voltammetry. Therefore, the working electrode was purged with a fully humidified CO/N_2 (1%CO) gas mixture and subsequently with fully humidified nitrogen gas, for 30 minutes (@ 0.125V) respectively. The local and the integral stripping voltammograms were recorded using nitrogen gas flow rates of n_{N2}=20ml/min and n_{N2}=200ml/min.

Results and Discussion

Local and integral CVs for nitrogen flow rates of n_{N2}=200ml/min and n_{N2}=20ml/min are shown in Fig. 1a, b and Fig. 1c, d. In addition, integral CVs were calculated from the local CVs for n_{N2}=200ml/min and n_{N2}=20ml/min, respectively. The calculated and the respective measured integral CVs shown in Fig. 1b, d are equal.

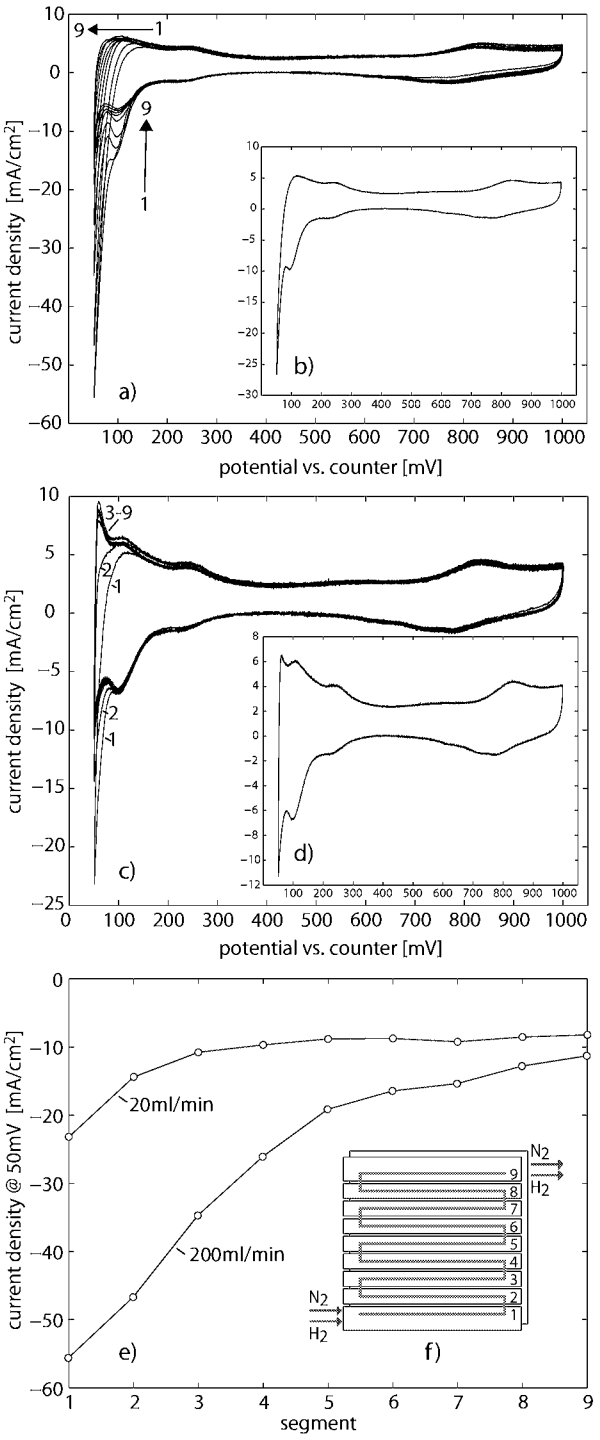

Fig. 1: *Local and integral CVs (2nd sweep) for nitrogen flow rates of (a, b) n_{N2}=200ml/min and (c, d) n_{N2}=20ml/min, e) local current density at minimum potential f) gas flow direction (n_{H2}=200ml/min, v=20mV/s, E_{start}=125mV, E_{low}=50mV, E_{high}=1000mV, T_{cell}=70°C, T_{gas}=70°C (fully humidified), ETEK W140 electrodes, N1135 membrane, 250µm PTFE gaskets, A_{cell}=29.2 cm²), numbers denote segment.*

The local contribution of the HEC to the local H-adsorption peak currents decreases towards the nitrogen outlet (Fig. 1a, c). The local contribution of the HEC strongly increases with increasing N_2 flow rate (Fig. 1e). In a first approach, this effect could be explained by a mass transport controlled HER, i.e,

diffusion of molecular hydrogen away from the electrode limits the HEC. Hydrogen generated in the HER accumulates along the channels towards the gas outlet of the working electrode. This results in an increasing hydrogen concentration in the nitrogen stream towards the gas outlet and by this to an increasing gas phase mass transport limitation for the HER. By this, the contribution of the local HEC to the local H adsorption peak currents decreases towards the nitrogen outlet (Fig. 1e).

At high gas flow rate the local hydrogen concentration in the channels is kept at an overall lower level, the diffusion of molecular hydrogen away from the electrode is promoted. The local and integral HEC and its contribution to the H adsorption peak increase (Fig. 1a, b vs. Fig. 1c, d). The promotion of hydrogen diffusion away from the electrode with decreasing segment number and increasing gas flow rate can also explain the decreasing values observed for the anodic charge required to oxidize molecular and adsorbed hydrogen in the same direction (Fig. 1a, c).

The large differences in the local contribution of the HER in the H_{upd} region, which become strongly pronounced at higher gas flow rate, hamper the evaluation of reliable and comparable values for local ECA values from H_{upd} adsorption/desorption currents.

However, besides H_{upd} adsorption/desorption measurements CO-stripping voltammetry can be used to determine the ECA of Pt catalysts in PEFC electrodes, using the CO electro-oxidation peak, which occurs at potentials higher than 600mV..

Local stripping voltammograms for nitrogen flow rates of $\dot{n}_{N2}$=20ml/min and $\dot{n}_{N2}$=200ml/min are shown in Fig. 2a, b (500mV to 700mV). The respective calculated and measured integral voltammograms are shown in Fig. 1b, d for the entire sweep range. Again, no difference could be observed between measured and calculated integral data.

The local peak potential slightly decreases from the gas inlet to the gas outlet and also depends on the gas flow rate (Fig. 2e). However, no trend similar to the H_{upd} currents could be observed in the local ECA values (Fig. 2e), which were determined from the respective peak areas.

Further work is required to gain more insight into the effects of experimental conditions on local voltammograms in PEFCs and into the impact of coupling via the gas phase along the channels.

However, according to the preliminary results shown here, local CO stripping voltammetry and local cyclic voltammetry at very low gas flow rates can be used to determine local ECA values. These novel methods will be valuable to study the impact of local inhomogeneities in operating conditions (e.g. humidity, reactant or temperature gradients) on local catalyst degradation.

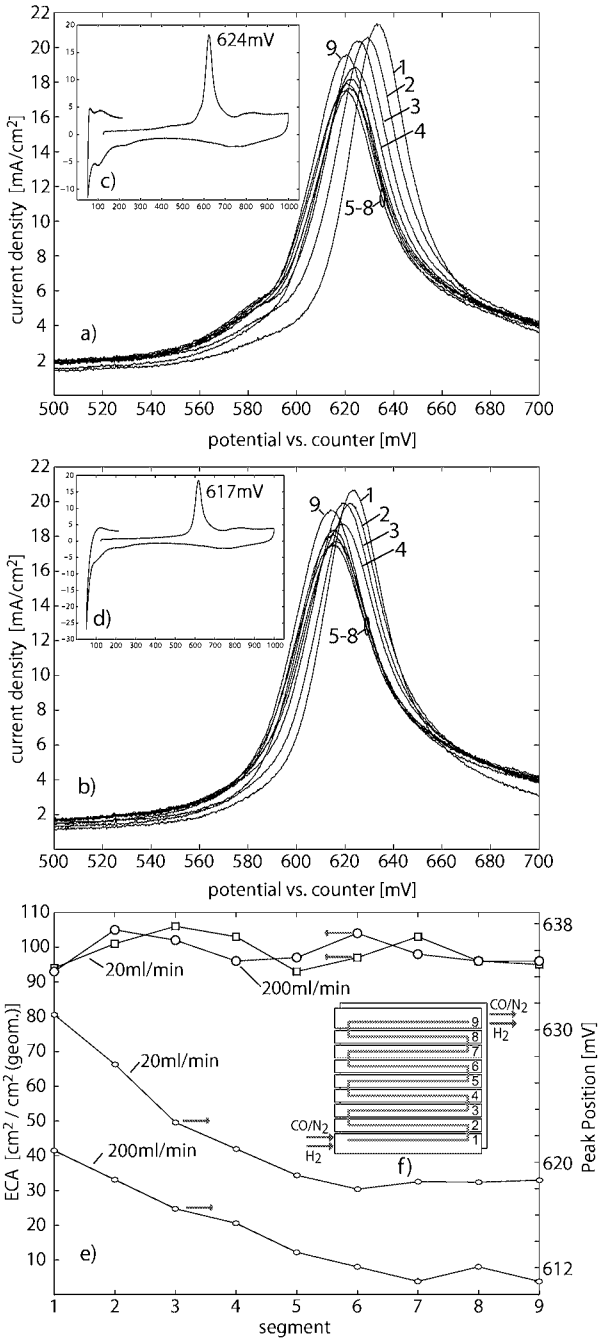

Fig. 2: *Local CO stripping voltammograms a) $\dot{n}_{N2}$=200 ml/min, b) $\dot{n}_{N2}$=20ml/min, c, d) respective integral voltammograms for whole sweep potential range, e) local ECA and peak position f) gas flow direction (1st sweep, $\dot{n}_{H2}$=200ml/min, ν=20mV/s, E_{start}=125mV, E_{low}=50mV, E_{high}=1000mV, T_{cell}=70°C, T_{gas}=70°C (fully humidified), ETEK W140 electrodes, Nafion N1135 membrane, 250µm PTFE gaskets, A_{cell}=29.2 cm²) , numbers denote segment*

References

[1] T. Biegler, D.A. Rand, R. Woods, J. Electroanal. Chem. **29**, 269 (1971).

[2] I.A. Schneider, H. Kuhn, A. Wokaun, G.G. Scherer, J. Electrochem. Soc. **10**, A2092 (2005).

TRANSPORT PHENOMENA IN POLYMER ELECTROLYTE FUEL CELLS

H. Kuhn, A. Wokaun, G.G. Scherer
+41(0)56 310 2350
holger.kuhn@psi.ch

Recent experiments have demonstrated the influence of a pressure gradient across a polymer electrolyte fuel cell (PEFC) onto the cell's impedance response [1]. These experiments were now repeated, introducing a pseudo reference electrode arrangement. This allows for an investigation of the pressure dependence on the single electrode reactions and, furthermore give an insight into the proton transport within the solid polymer electrolyte. Additionally, this method allows for an allocation of single processes to a specific electrode, which is not possible in impedance measurements over the entire cell.

Experimental

Basically, the same experimental setup and operating conditions were used as described in [1], except that a pseudo reference electrode was placed between the two electrolyte membranes [2]. ETEK electrodes with a platinum loading of 0.5 mg/cm^2 and a standard ionomer impregnation and two Nafion 1135 membranes were applied as membrane electrode assembly.

Results and Discussion

The fuel cell was operated at a constant current density of 500 mA/cm^2. An excess pressure ranging from 0 to 100 mbar was applied to the oxygen side, supporting the transport of water from the cathode back to the anode side, in order to compensate for the lack of water due to the electro-osmotic drag at high current densities.

As the pressure difference is increased, the impedance strongly decreases. We are able to address two major effects by the help of the half-cell measurements. First, we observe a decreasing semi-circle at low frequencies (Fig. 1). This characteristic is directly accounted for the proton transport within the liquid phase of the solid electrolyte. A priori it is impossible to assign this characteristic to whether it is the water transport from the cathode to the anode or the proton transport off the anode to the cathode. The half-cell impedance measurements clearly show that this effect has its origin at the anode side. This supports the fact that at high current densities the proton transport, in particular the electrolyte conductivity, is improved by the excess pressure avoiding a decreasing water content of the electrolyte at the anode side [3].

Second, at medium frequencies we observe an impedance decrease, which is governed by an effect at the cathode side. As we increase the oxygen pressure, we enhance the oxygen kinetics by providing more oxygen to the catalyst sites. This reduces the charge transfer resistance, the diameter of the semi-circle at medium and high frequencies respectively. We did not observe any diffusion limitations at the cathode side, hence assuming a sufficient supply of all reactants.

Surprisingly, an excess pressure of 15 mbar is enough to enhance the performance. The impedance is reduced by a factor of 20%, resulting in a higher cell voltage increasing from 396 mV at 10 mbar to 441 mV at 15 mbar. Between 15 mbar and 100 mbar, only a negligible improvement can be achieved, which is also reflected in the cell voltage changing from 441 mV to 451 mV at 100 mbar. Only the kinetics of the ORR is improved further, however not processes according to proton transport within the solid electrolyte, as can be seen in Figure 1, where the semi-circle at low frequencies stays almost unchanged.

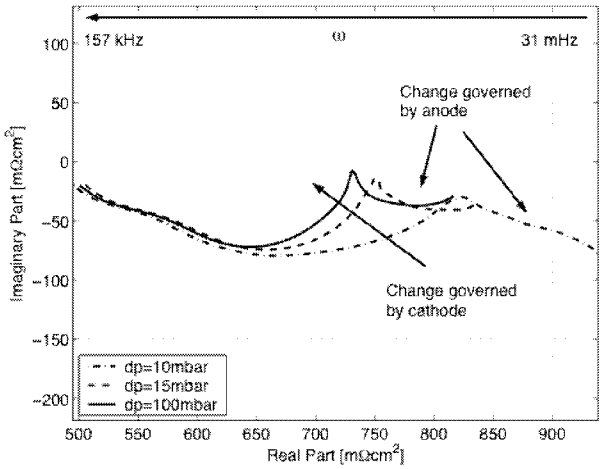

Fig. 1: *Impedance spectra between anode and cathode. Two major effects can be addressed to processes at the anode and cathode side.*

The pressure difference has a minor effect on the electrolyte resistance, as this value is almost constant. This is contrary to experiments with thicker membranes [1]. This may indicate that diffusion limitations within the solid electrolyte are due to the water diffusion within the liquid phase, which influences the local water content of the membrane and hence the proton mobility.

Conclusions

Electrochemical impedance spectroscopy (EIS) offers to investigate processes linked to the electrochemical reactions of species in a fuel cell, without directly participating in the charge transfer processes. With the pseudo reference electrode setup we can distinguish between processes at single electrodes of the fuel cell and address some of their limitations.

References

[1] H. Kuhn, B. Andreaus, G.G. Scherer, A. Wokaun, PSI Scientific Report 2004, **V**, 105 (2005).

[2] H. Kuhn, B. Andreaus, A. Wokaun, G.G. Scherer, Electrochim. Acta **51,** 1622 (2006).

[3] F.N. Büchi, G.G. Scherer, J. Electroanal. Chem. **404**, 37 (1996).

MEASURING THE CURRENT DENSITY DISTRIBUTION IN PEFC WITH SUB-MILLIMETER RESOLUTION

M. Reum, S.A. Freunberger, J. Evertz[1], F.N. Büchi
+41(0)56 310 2127
mathias.reum@psi.ch

In today's PEFCs the current density distribution on all scales is of high interest for the optimization of cell structures with respect to power density, which is associated to performance and costs. On the sub-millimeter scale where the current density is inhomogeneous over *flow field ribs* and *gas channels*, solely simulations i.e. [1-3] are available for describing the local current generation. Experimental data is restricted to the correlation of integral cell performance to channel and rib spacing [4].
A novel method for measuring the current density distribution on a scale smaller than the channel and rib spacing is presented [5]. This new tool is able to bring light in the limiting processes on the sub-mm scale.

Methodology

The method is based on the idea to use the electron conductors in a plane perpendicular to the membrane and the channel direction as a two-dimensional shunt resistor. The local potential is probed at the GDL – catalyst layer interface by fine gold wires (see Fig.1). Hence, the current density is obtained from the solution of Laplace's equation for Ohm's law with the potentials at catalyst layer and current collector as boundary conditions.

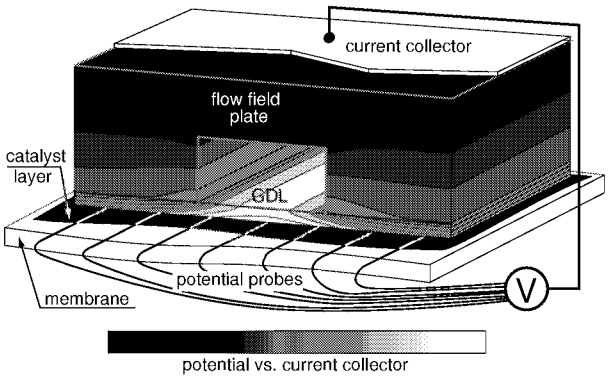

Fig. 1: *Scheme of the measurement setup, gold wires probe the potential at the GDL - catalyst layer interface.*

Using the ohmic drop for calculating the local current, the precise knowledge of all resistances involved is of prime importance. In particular, the strongly pressure dependent contact resistance between GDL and flow field rib causes a substantial fraction of the total ohmic drop in addition to the anisotropic bulk resistance and requires therefore careful consideration by ex situ measurements.
FEM simulations of the GDL's structural mechanics were made to obtain the distribution of stress in the bulk of the GDL and of the contact pressure under the flow field rib. Therewith, the local contact resistance and the spatial distribution of the conductivity in the GDL's cross section are obtained from ex-situ data. Using four point measurement technique, GDL and flow field plate electric conductivities and the appropriate contact resistance can accurately be determined as a function of pressure.

Experimental

A specialized test cell with a square active area of 1.0 cm^2 was developed. The flow field structure consisted of 2 channels and 3 ribs, all of the width of 2.0 mm and a length of 10 mm. Fig. 2 shows the setup with fine gold wires with a diameter of 25 µm to probe the electronic potential at the interface of gas diffusion medium and active layer. The wires were placed with 0.5 mm spacing parallel along the channel. Experiments were conducted with air and oxygen as oxidant.

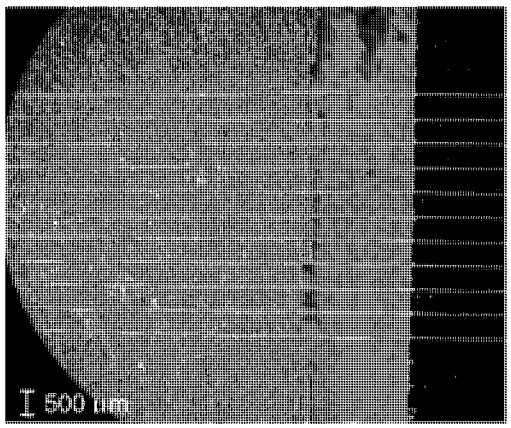

Fig. 2: *View on the GDL and the edge of the flow field of the test cell, probe wires (25 µm gold) are arranged along the flow field structure at the GDL – reaction layer interface.*

Results

Accurate potential measurements at the reaction layer interface are obtained. Results show that the local current production is highly inhomogeneous, in particular at high loads. Exemplary a set of data is presented in Fig.3 for H_2/air operation. On the left side, the diagram shows the potential distribution across channel and rib. On the right side the corresponding current density distribution is shown, calculated using the highly anisotropic and pressure dependent 2D-resistances of the conducting components.
The right side of Fig.3 illustrates that the general pattern of the sub-mm current distribution is strongly current dependent. Up to integral loads of 0.4 A/cm^2 the current maximum lies under or at the edge of the rib. This is due to the differences in electron pathway

[1] *Tribcraft AG, Binzstrasse 7, 8045 Zürich*

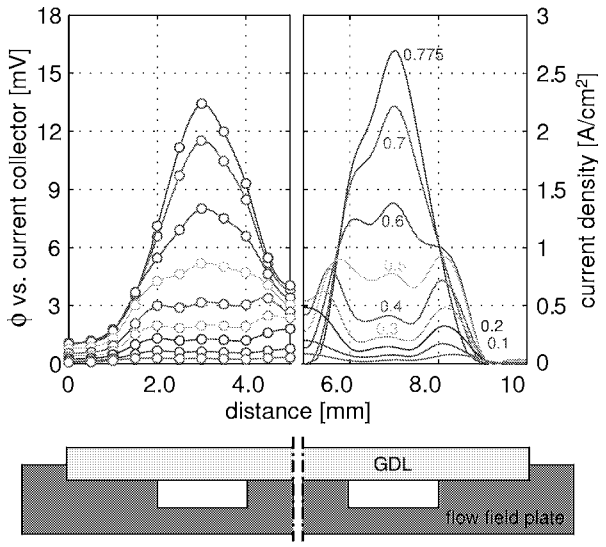

Fig. 3: *Measured potential and calculated current density distribution across channel and rib for a cell operated with air as oxidant up to a maximum load of 0.75 A/cm².*

length of current produced under channel and rib and the distribution is governed by ohmic drop mainly.

At higher loads, the regime determining the position of the current maximum is changing. With increasing integral current, reactant starvation begins to take place under the rib, promoting the current production under the channel. The large inhomogeneities now developing are due to reaction rate limitation by oxygen transport. As displayed in Fig.4, current production under the middle of the rib is approaching zero when operating on air near the limiting current density. This leads to high local current peaks of more than three times (!) the integral current density under the channel.

Using oxygen, the same effects can be observed in an alleviated way: the regime change from resistance to diffusion control occurs at a higher integral current density of 0.8 to 1.0 A/cm^2. Also, for oxygen operation the current under the center of the rib is only diminished but seems not to be completely suppressed, as it is the case with air.

The transition from resistance- to diffusion controlled current distribution can be observed for both oxidants (shown exemplary for air operation in Fig.3 at a load of 0.3 to 0.4 A/cm^2) with maxima occurring at the rib edges. This phenomena, proposed by *Meng et.al.* [3] in modeling calculations, is experimentally confirmed for the first time.

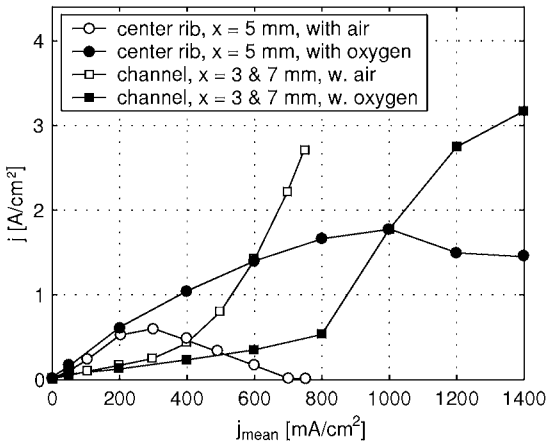

Fig. 4: *Calculated current in the middle of the channels and the center rib as a function of the integral current density for both, oxygen and air operation.*

Conclusions

A novel method for measuring the local current density distribution on a sub-millimeter scale has successfully been developed. First results show that prominent differences are observed as function of the oxygen partial pressure at the cathode. Systematic measurements and combination with models will allow for optimization of the structures for higher performance and lifetime.

Acknowledgements

Financial support by the Swiss Federal Office of Energy (BfE) is gratefully acknowledged. Great appreciations to R. Schraner (LOG) and F. Glaus (LMN) for the valuable support in manufacturing of the test cell.

References

[1] W.M. Yan, C.Y. Soong, F. Chen, H.S. Chu, J. Power Sources **125**, 27 (2004).

[2] W. Sun, B.A. Peppley, K. Karan, J. Power Sources **144**, 42 (2005).

[3] H. Meng, C.Y. Wang, J. Electrochem. Soc. **151**, A358 (2004).

[4] J. Scholta, G. Escher, W. Zhang, L. Kuppers, L. Jorissen, W. Lehnert, J. Power Sources, in press, (2006).

[5] S.A. Freunberger, M. Reum, J. Evertz, F.N. Büchi, J. Electrochem. *Soc*, submitted (2006).

INFLUENCE OF THE COOLING STRATEGY ON THE LOCAL PERFORMANCE OF PEFC

S.A. Freunberger, U. Frischknecht, F.N. Büchi
+41(0)56 310 2410
stefan.freunberger@psi.ch

System efficiency concerns limit the coolant flow rate, restrict the energetically costly gas humidification to an extent well below cell operation temperature, and allow only for stoichiometric ratios that are not capable of completely removing product water as vapor. On the one hand prehumidification of the feed gases is necessary to prevent drying at their inlets. On the other hand product water is formed inside the cell that humidifies both the reactants and the membrane. Liquid water in turn is prone to impede the transport of the educts through the porous gas diffusion layers (GDL) to the reaction layers and therefore to limit the performance. Limited coolant flow leads to temperature inhomogeneities in the cell-plane which might be employed to beneficially counteract local drying at gas inlets and flooding in downstream regions. Influences of the cooling strategy on the cell performance have been investigated theoretically [1, 2] and are subject to the present experimental study.

Experimental

Experimental data were obtained with a current mapping technique based on a segmented cathode end-plate and unsegmented MEA in cell with an active area of 200 cm^2 and parallel linear channels. The electrochemical components used were Elat-A7-Type E-Tek gas diffusion electrodes with a Pt loading of 0.6 mg/cm^2 and Nafion 115 as the membrane. Hydrogen and air are fed at a stoichiometry of $\lambda_{H_2/air} = 1.5/2$ and atmospheric pressure. The cell temperature was controlled by water-fed cooling jackets placed adjacent to both the anode and cathode endplates

Results

Figure 1 shows the resulting current distributions for counterflow operation with 10 °C temperature rise and drop along the air path and a constant mean value. The current at the dry H_2 inlet rises, even at increased temperature, steeply while heat up at the air inlet shows a particular strong response in local performance. This is because air flowing from the opposite direction becomes saturated towards the H_2 inlet which is humidified by water exchange through the MEA. For the case of falling temperature along the air path already slight undersaturation of air leads to lower current (see top left graph) which occurs more, the lower the humidification. Counterflow of hydrogen and low current are less able to humidify the air. This leads to an increasingly confined region of current production. The inverse effect is achieved when the dry air inlet is cooled. The current remains roughly homogeneous down to 50 % relative humidity.

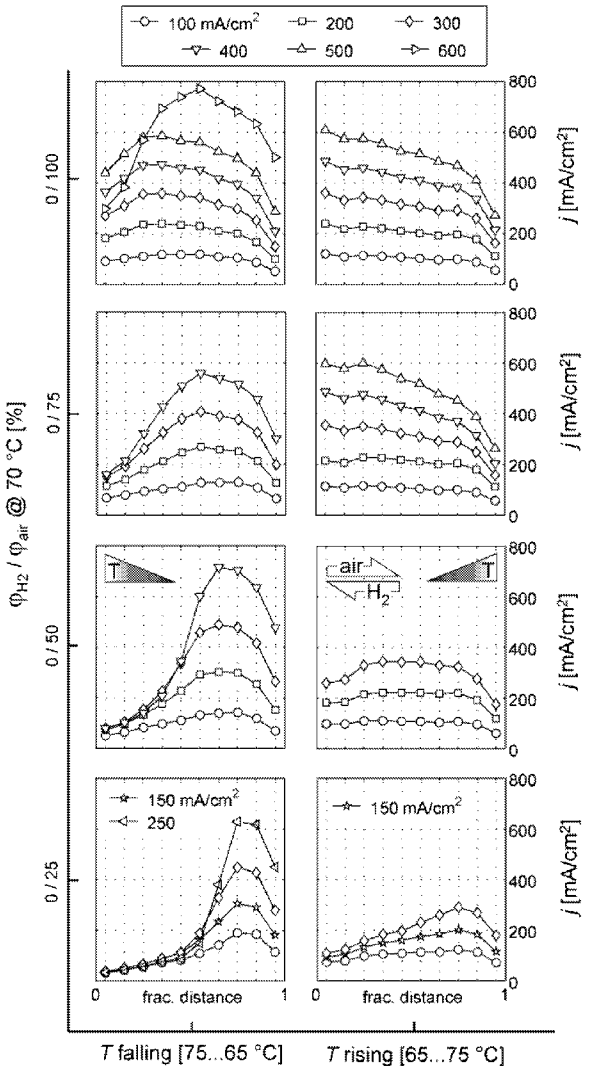

Fig. 2: *Current density distribution for counterflow operation with dry hydrogen and variously humidified air at different total current. Air enters at the left side. Left column: temperature rises along the air path from 65 to 75 °C. Right column: Inverse profile with decline from 75 to 65 °C. Air humidification decreases along the columns.*

Conclusions

Due to the serious impact of temperature on all processes in the PEFC both the relative direction of the coolant stream to the gas streams and its mass flow turns out to significantly affect the cell performance. Besides influencing the electrochemical reaction and all kinds of mass transfer temperature variations predominantly alter the local membrane hydration and consequently its conductivity.

References

[1] S.A. Freunberger, M. Santis, I.A. Schneider, A. Wokaun, F.N. Büchi, J. Electrochem. Soc. **153**, A396 (2006).

[2] S.A. Freunberger, A. Wokaun, F.N. Büchi, J. Electrochem. Soc. **153**, A909 (2006).

EXPERIMENTAL INVESTIGATION OF COUPLING PHENOMENA IN POLYMER ELECTROLYTE FUEL CELL STACKS

M. Santis, S. A. Freunberger, M. Papra, F. N. Büchi
+41(0)56 310 2125
marco.santis@psi.ch

In an *ideal* fuel cell stack geometry, compenents and mechanics of every single cell, as well as the operating conditions for all individual cells are identical throughout the complete stack. In a *real* stack however, individual cells may operate at different working conditions because of differences in manufacturing tolerances and/or location in the stack. Differences in local working conditions lead to performance changes at individual cell level. These performance variations are often not confined to individual cells only, but are sometimes accompanied by coupled performance variations of adjacent cells.

Classically, performance variations are detected monitoring cell voltage. Nevertheless, this provides only limited information on effects giving rise to performance changes and endows almost no particulars about coupling phenomena between individual cells.

In the present work, measurement of local current density in adjacent cells in a stack has been implemented to study two types of non-uniformities: i) air starvation anomaly at single cell level, and ii) thermal anomaly as encountered in peripheral cells in a stack.

Experimental

2- and 3-cell technical fuel cell stacks (active area per cell of 205 cm^2) have been modified implementing local current measurement by a semi-segmented plate principle [1] in both peripheral cells of the stack. Furthermore, a second independent media supply was implemented separating the stack in two cell-groups (1+1 and 1+2), allowing them to be operated at different operating conditions (see Figure 1).

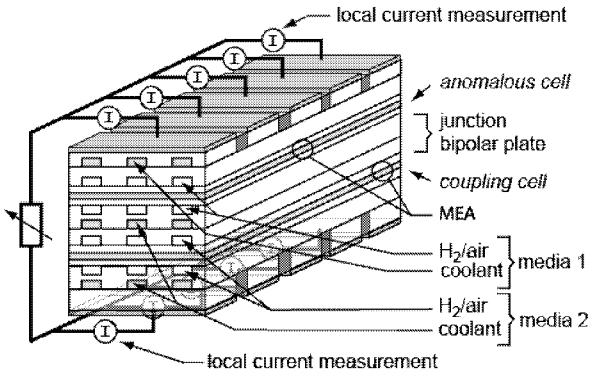

Fig. 1: *Schema of a two part 2-cell stack with independent media supplies and location of the local current density measurement in the stack.*

The two cell-groups are connected electrically and thermally via the junction bipolar plate separating the two media streams. Emulation of anomalies in the stack was realized by varying the operating conditions in one cell (anomalous cell), while keeping them constant in the second cell-group (coupling cells). Table 1 gives an overview of the presented cases. Measurements were carried out in constant current mode at an average current density of 390 mA cm^{-2} (80 A total stack current) with fully humidified gases. Local current density is mapped at six positions located at 3%, 11%, 34%, 66%, 89% and 97% from the beginning of the air path, respectively. Membrane electrode assemblies were prepared using Nafion® 112 membranes and E-Tek Elat A7 gas diffusion electrodes. In- and trough-plane conductivities of the bipolarplate material (SGL BMA5-type graphite) are 100 S cm^{-1} and 20 S cm^{-1}, respectively.

Table 1: *Overview of the studied cases with the status and working conditions of the cells in the indicated stacks.*

Case	Stack	Anomalous cell	Emulated anomaly	Operating condition varied		
				Cell 1	Cell 2	Cell 3
1	1+1	1	air starvation	λ_{air}	all constant	-
2	1+2	1	air starvation	λ_{air}	all constant	all constant
3	1+1	1	thermal losses	coolant temperature	all constant	-

Results and discussion

Cases 1 and 2– emulation of air starvation – coupling to an immediate and non-immediate adjacent cell

Starvation of air at single cell level was emulated in 1+1 and 1+2 stacks by gradually reducing air stoichiometry in the anomalous cell only, while keeping the working conditions of adjacent cells unaltered (coupling cells). Local current density in the immediate adjacent cell was recorded in a 1+1 stack.

Figure 3a shows changes in individual cell voltages as function of the air stoichiometry of the anomalous cell. The anomalous cell shows the expected decrease in cell voltage when its air stoichiometry is reduced. But also the coupling cells show qualitatively the same behavior, even though the operating conditions are kept constant. An examination of Figure 3b clarifies this behavior: air starvation induces a non-uniform current density profile in the anomalous cell [2, 3]. The non-uniform current pattern is passed to the adjacent cells via the common bipolar without complete homogenization due to its finite thickness and in-plane conductivity. Hence, the current takes a path in the coupling cells which is non-optimal from the resistances point of view, increasing the sum of overpotentials and diminishing cell voltage.

For the studied type of cell geometry and material, changes in local current density propagate to an adjacent cell with a coupling factor of 0.64 +/- 0.02 and to a subsequent cell by a factor of 0.40 +/- 0.04. Induced changes in cell voltage propagate with a factor of 0.59 +/- 0.04 and 0.32 +/- 0.05, respectively.

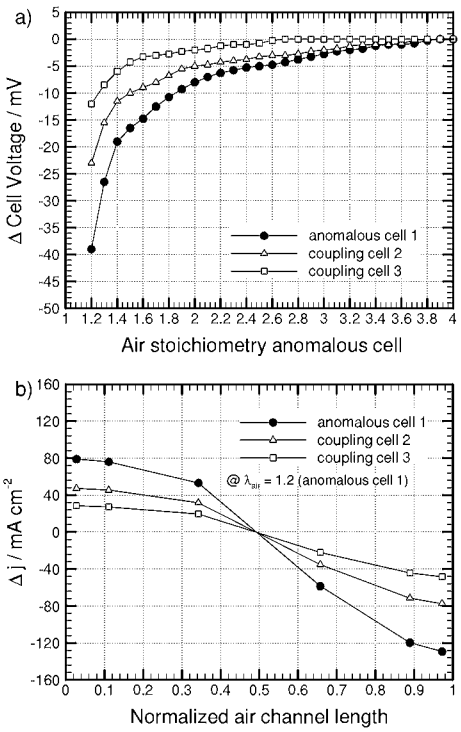

Fig. 3: *a) Cell voltage changes of the anomalous cell 1 and coupling cells 2 and 3 as function of the air stoichiometry in the anomalous cell 1; b) changes in local current density j in the anomalous cell 1 and coupling cells 2 and 3 as function of the normalized air channel length for the given air stoichiometry in the anomalous cell 1. Changes are given with reference to values obtained at an air stoichiometry of 4.0 for the whole stack.*

Case 3 – emulation of thermal losses –

Increased thermal losses in a peripheral cell were emulated in a 1+1 stack by decreasing coolant inlet temperature in the anomalous cell. An external heating device was used to simulate the presence of a continuous stack behind the coupling cell. Changes in individual cell voltage are shown in Figure 4a. The anomalous cell experiences evident performance changes depending on its working temperature. Conversely, and very surprisingly indeed, the performance of the adjacent cell seems not affected at all.

An inspection of Figure 4b clarifies these results. For the lowest experimentally realized working temperature in the anomalous cell (inlet coolant temperature of 30 °C) changes in local current density (under the given working conditions of fully humidified reactant streams) are small (< 25 mA cm^{-2}). Consequently, the induced changes in the adjacent cell are minor.

The drastic voltage changes in the anomalous cell are due to changes in the activation overpotential and membrane conductivity. Since the temperature of the coupling cell is kept constant (coolant inlet/outlet temperature difference of 1 °C) and the electronic coupling is minimal, as a result, its individual performance remains practically unchanged.

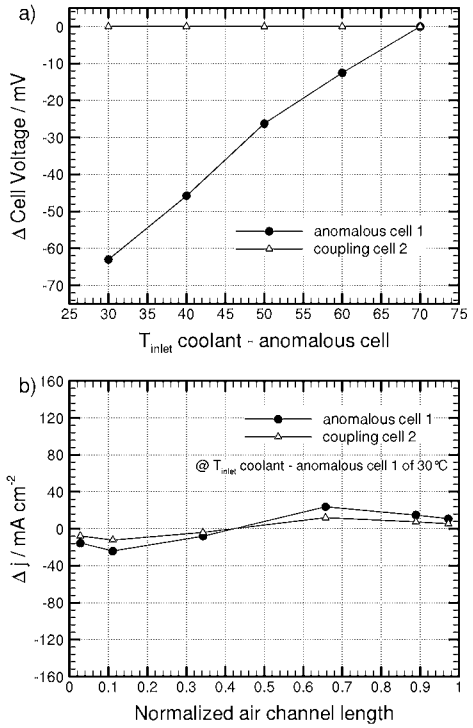

Fig. 4: *a) Cell voltage changes in the anomalous cell 1 and coupling cell 2 as a function of the coolant inlet temperature T_{inlet} of the anomalous cell 1; b) changes in local current density j in the anomalous cell 1 and coupling cell 2 as function of the normalized air channel length for the given T_{inlet} of the anomalous cell 1. Changes are given with reference to values obtained at a temperature of 70 °C for the whole stack.*

Conclusions

The experimental results show that performance changes inducing considerable variations in local current density, such as air starvation, can propagate even to non-immediate adjacent cells. The coupling has an electronic origin taking place via the common bipolar plate. Local current changes originated in an anomalous cell are not completely smoothed in the common bipolar plate due to its finite thickness and in-plane conductivity. Consequently, a current density profile is impressed onto the coupling cells which would not arise from their distribution of overpotentials under their individual working conditions. Therefore, the current takes a path through the electrochemical part of the cell, which is non-optimal, leading to a decrease in cell voltage. Conversely, anomalies which do not induce considerable changes in local current density, such as a thermal anomaly (under the studied working conditions), do not propagate to adjacent cells.

References

[1] F. N. Büchi, A. B. Geiger, R. P. Neto, J. Power Sources **145**, 62 (2005).

[2] M. Santis, S. A. Freunberger, A. Reiner, F. N. Büchi, Electrochim. Acta, in press (2006).

[3] D. J. L. Brett, S. Atkins, N. P. Brandon, V. Vesovic, N. Vasileiadis, A. R. Kucernak, Electrochem. Commun. **3**, 628 (2001).

PRESSURE EVOLUTION IN CARBON / PROPYLENE CARBONATE BASED SUPERCAPACITORS

M. Hahn, O. Barbieri, A. Foelske, R. Kötz
+41(0)56 310 2128
matthias.hahn@psi.ch

Increasing the cell voltage of supercapacitors (SC) is one route to increase energy density and power density simultaneously. Increased voltage may, however, introduce faradaic reactions such as ion insertion and electrolyte decomposition, which limit the lifetime of the device. Using a purpose designed pressure cell, we have for the first time determined the pressure increase in capacitor cells based on real SC electrode coils in 1 M $(C_2H_5)_4NBF_4$ (TEABF$_4$) / propylene carbonate (PC) electrolyte. The measurements were carried out during cycling between 0 and 2.5 V and at constant cell voltages up to 3 V. During cycling a reversible pressure decrease was observed upon charging, while an irreversible pressure increase was monitored during load tests at constant cell voltages above 2.5 V. The absolute amount of gases evolved during the load tests could be determined by means of simultaneous compressibility monitoring.

Experimental

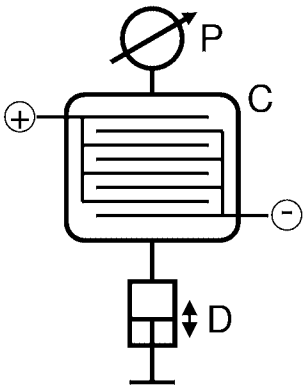

Fig. 1: *Sketch of the set-up used to determine the pressure and volume changes during charging. P: pressure transducer; C: cell case containing the electrode coil; D: motor driven dispenser for periodic injection/removal of a small liquid volume. The set-up is placed into a temperature chamber held at 25°C ± 0.1 °C.*

The set-up used to measure the volume changes upon charging is sketched in Figure 1. A D-size electrode coil (350 F rated capacitance, containing about 25 cm^3 activated carbon) is mounted inside a thick-walled plastic (PEEK) case (C). The electrode coil comprises two aluminum foil supported activated carbon electrodes with a paper separator in between. The cell is connected to a pressure transducer P and a motor driven dispenser D, then filled with about 40 cm^3 of the argon saturated electrolyte solution, 1 M TEABF$_4$ in PC. Before starting the actual experiment, the cell pressure is increased to around 2 bars by adding some electrolyte solution by means of the dispenser. Then, after a settling period of several hours, the run is started by applying a voltage between the two electrodes.

During the experiment the compressibility of the set-up (depending on the gas buffer above the liquid, the stiffness of the cell container and the sensor) is determined by periodic injection/removal of a small electrolyte volume ΔV (about 0.015 ml). The corresponding pressure change ΔP is recorded as an extra hump on the otherwise smooth pressure curve. From the ratio $(\Delta V/\Delta p)_p$ the volume change is calculated according to equation 1.

$$V_p = \int_{p_0}^{p} (\Delta V / \Delta p)_p dp \qquad (1)$$

In the case of gas evolution, the amount of gas is further computed as n = (pV)/(RT).

Volume change above 2.5 V

The total volume changes at constant voltages of 2.5, 2.75 V, 3.0 V and finally once again at 2.5 V are shown in Figure 2. Based on our previous DEMS measurement on the same electrode material in the same electrolyte [1], we conclude that gas evolution is the origin of the pressure rise. The two curves obtained for the very first and the final plateau at 2.5 V are markedly different during the first few hours, while their slopes become almost identical after some 10 hours. The much more pronounced gas evolution during first charging is in agreement with previous DEMS measurements [1] and might indicate some initial passivation of the electrodes.

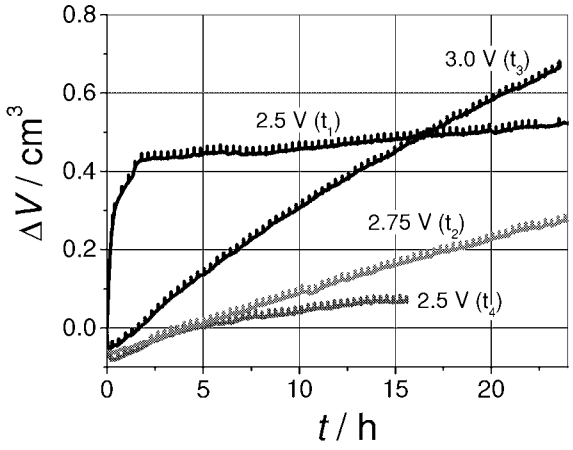

Fig. 2: *Total volume change during the voltage hold periods. The experiments were carried out in the sequence t1, t2, t3, t4. Spikes are caused by the procedure used to determine the compressibility.*

Assuming ideal gas behaviour, gas evolution rates dn/dt of 0.5, 1.4, and 3.3 µmol/hour can be derived for 2.5 V, 2.75 V and 3.0 V, respectively (calculated for t = 15 h). Further on, relating the gas evolution to the recorded residue current i by means of Faraday's law yields z, the number of electrons needed to produce one gas molecule: z = i / (F dn/dt), where F is the Faraday constant. The results shown in Figure 3 clearly reveal that at all cell voltages only a minor part of the leakage current results in gas formation. During the initial hold period at 2.5 V z drops to about 450 electrons per gas molecule. The corresponding

values at 2.75 and 3.0 V are 140 and 65, respectively. The markedly lower z value for the final hold period at 2.5 V, about 150 electrons per gas molecule (compared to the initial value z = 450), suggests that the cell is still far from stationary operation at the end of the initial hold period at 2.5 V. In general, the calculated number of electrons per gas molecule is very large, indicating that in fact only a small portion of the leakage current is responsible for gas formation.

In contrast to the earlier DEMS investigation [1], the present pressure measurement does not allow for on-line determination of the evolved gases. However, it is possible to take samples with a syringe and analyse the gas composition off-line. First results of such an analysis using GCMS indicate propene and CO_2 as main products, confirming the DEMS results [1].

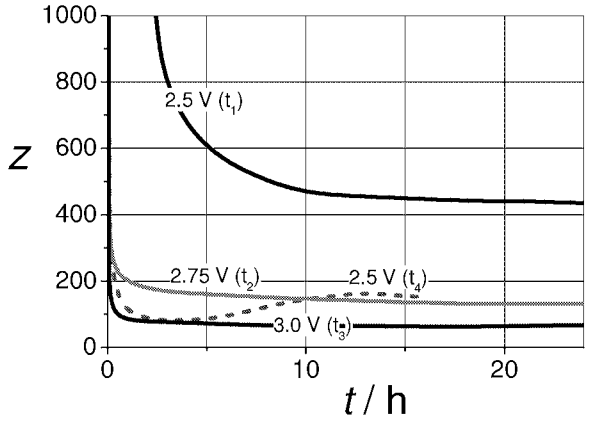

Fig. 3: *Number of electrons needed to produce one gas molecule. Calculation is based on the assumptions that i) the pressure change is solely caused by gas evolution, ii) the residue current is purely faradaic (without any capacitive contribution). Time labels refer to Figure 2.*

Volume change below 2.5 V

Besides gas evolution another volume (pressure) related effect can be observed during a voltage sweep (CV) experiment (Figure 4). As a striking fact, a signifant volume contraction occurs while increasing the cell voltage, and the opposite effect when again discharging the capacitor. Clearly, this charge induced volume change is not related to gas evolution. Instead, the effect can be attributed to the fact that the space requirement of a given molecule/ion depends on its chemical and sterical environment (for mixtures commonly expressed as the component's partial molar volume). In fact, according to the Debye-Hückel theory, the partial molar volume of strong electrolytes decreases upon dilution. Therefore, the depletion of the bulk electrolyte during charging (upon which ions leave the bulk and enter the pores) might explain the observed volume contraction. On the other hand, the same argument predicts an opposed volume expansion for the pore electrolyte. Obviously, on the basis of the present results, it is not possible to distinguish quantitatively between the above contributions. Further experiments to elucidate the findings are under way.

It is worth noting that the measured total volume change (electrode plus electrolyte) is of the same magnitude but of opposite sign as the volume change of the solid electrode alone (dashed line in Figure 4, adopted from previous dilatometric investigations carried out on the same electrode material [2]).

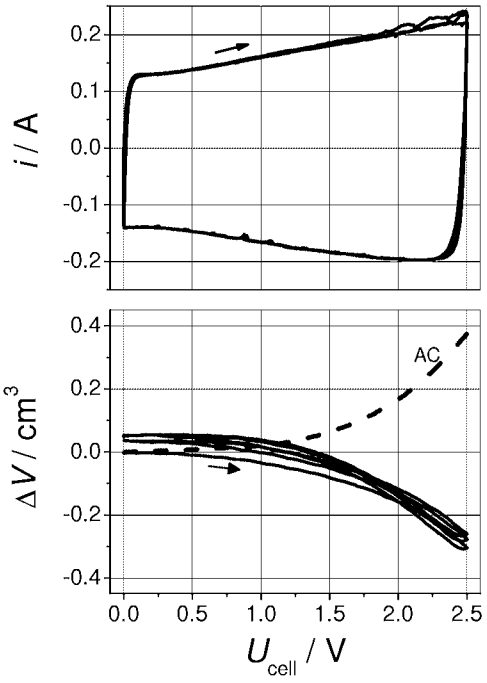

Fig. 4: *Cyclic voltammogram (top) and simultaneous total volume change (solid line). The dashed line shows the volume change of the AC electrodes alone (adopted from Ref. [2] assuming isotropic expansion). Electrolyte: 1M $TEABF_4$ in PC. Scan rate: 0.5 mV/s.*

At a second glance the latter finding is not surprising, since in a rough approximation, the total volume change (electrodes plus electrolyte) is zero: The ions entering the electrodes leave the bulk solution at the same time. According to this simplistic picture, the electrode expansion is just compensated by the contraction of the bulk electrolyte solution. The actually observed volume contraction thus simply indicates a denser packing of the involved species/phases in the charged state.

References

[1] M. Hahn, A. Würsig, R. Gallay, P. Novák, R. Kötz, Electrochem. Comm. **7**, 925 (2005).

[2] M. Hahn, O. Barbieri, F.P. Campana, R. Kötz, R. Gallay, Applied Phys. **A82**, 633 (2006).

IN SITU ATOMIC FORCE MICROSCOPY STUDY OF EXFOLIATION PHENOMENA ON GRAPHITE BASAL PLANES

F. Campana, H. Buqa, A. Foelske, M. Hahn, R. Kötz, P. Novák
+41(0)56 310 2057
ruediger.koetz@psi.ch

Various types of carbon play an important role in electrochemical energy storage devices such as electrochemical double layer capacitors and lithium-ion batteries. While for double layer capacitors, utilizing organic electrolytes, activated carbons are the prefered material, special graphites are used for the negative electrode of Li-ion batteries. In order to investigate and understand the stability of such electrodes HOPG (highly oriented pyrolytic graphite) was investigated as a model electrode using *in situ* atomic force microscopy (AFM) during the insertion of Li^+ ions from organic electrolyte. In particular the phenomenon of SEI formation and exfoliation processes was studied.

Experimental

In situ AFM measurements were carried out with a PicoLE Scanning Probe Microscope (Molecular Imaging MI, Arizona, USA). The film morphology was probed by contact mode AFM with low constant force. All measurements were performed with a 100 µm scanner, a scan rate of 1 Hz, and a contact Si CSC38/no-Al cantilever (Micromash, SchaeferTec, Switzerland) with a typical force constant of 0.03 N/m. Further experimental details were described before by Campana et al. [1]. A solution of 1 M $LiClO_4$ in ethylene carbonate (EC) : propylene carbonate (PC) (1:2 by weight, Merck, 99.9%, < 20 ppm H_2O), served as the electrolyte.

Results

Fig. 1 depicts a typical polarisation curve (CV) of HOPG in 1 M $LiClO_4$ / EC:PC (1:2) recorded with a scan rate of 5 mV/s from 3 V to 0.005 V vs. Li/Li^+ in the *in situ* AFM cell. The negative current wave at 0.75 V clearly indicates the SEI formation.

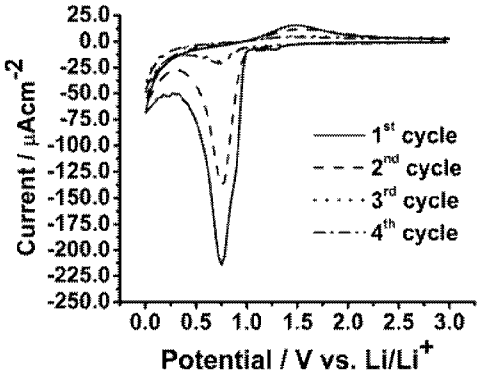

Fig. 1: *CV of HOPG in EC:PC (1:2) / 1 M $LiClO_4$. Potential range from 3 V to 0.005 V vs. Li/Li^+, with a scan rate of 5 mV/s.*

Figure 2 shows the evolution of surface topography starting from the pristine HOPG at 3.0 V vs. Li/Li^+ (2a) and after holding the electrode at a potential of 5 mV for increasing time (2b-2d). After about 6 min, the SEI becomes visible, changing the surface topography drastically (see Fig. 2b).

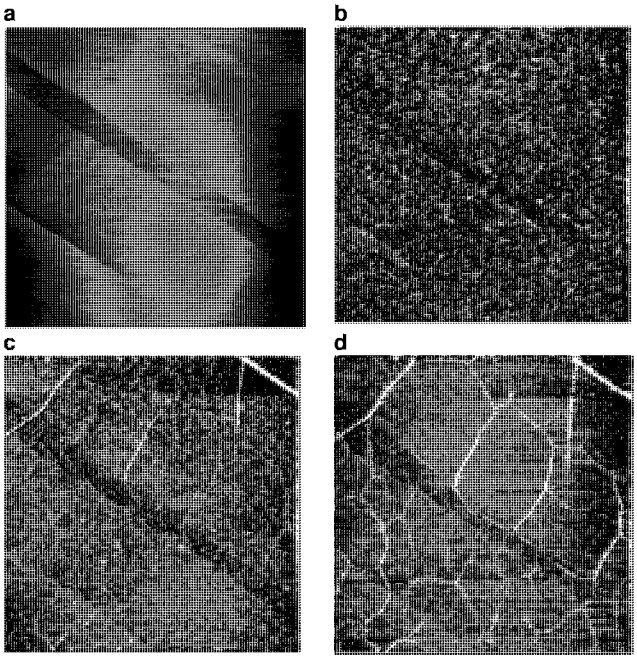

Fig. 2: *Contact mode AFM images of HOPG in EC:PC (1:2) / 1 M $LiClO_4$. Scan size is 10 x 10 µm and image scan rate was 1 Hz. a) At 3 V vs. Li/Li^+; Δz = 10 nm b) after 6 min at 5 mV vs. Li/Li^+; Δz = 25 nm c) after 41 min at 5 mV vs. Li/Li^+; Δz = 15 nm d) after 71 min at 5 mV vs. Li/Li^+; Δz = 15 nm.*

After 41 min (2c) at 5 mV vs. Li/Li^+ crack-like features developed on the basal planes. These features had a height between 5 and 55 nm and a cross section of about 500 nm for "small" branch-like features, and about 4 µm for the larger features. The "cracks" extended beyond the scanned area, which excludes any possibility of a tip-induced effect. The features could not be removed by scratching of the surface with the AFM tip at an increased force set point. These crack-like structures can be explained as elevations, induced by the gaseous decomposition products of intercalated PC.

The present study demonstrated that exfoliation phenomena do not only occur on the edge planes but also on the basal planes of graphite.

References

[1] F.P. Campana, R. Kötz, J. Vetter, P. Novák, H. Siegenthaler, Electrochem. Commun. **7**, 107 (2005).

AN *IN SITU* RAMAN MICROSCOPIC INVESTIGATION OF LITHIUM INTERCALATION INTO ANATASE TITANIUM DIOXIDE

L. J. Hardwick, M. Holzapfel, P. Novák
+41(0)56 310 2174
laurence.hardwick@psi.ch

Lithium-ion batteries continue to be the primary choice of power source for the ever increasing number of portable electronic products which are available; such as phones, cameras, music-playing devices, to name but a few. This has created a demand for this battery system to provide higher power and energy densities. The search for electrode materials with a greater specific charge continues. One such material is titanium dioxide (TiO_2). In the anatase form TiO_2 has a maximum theoretical specific charge of 168 Ah/kg when lithium is intercalated into half the vacant octahedral holes, giving a composition of $Li_{0.5}TiO_2$. This material is of interest as either a possible intercalation cathode or anode in the lithium-ion battery. Though the potential difference is ca. 1.5 V lower compared to other oxide materials ($LiCoO_2$, $LiMn_2O_4$) vs. Li/Li^+, possible advantages maybe its rapid discharge and charge properties. Raman microscopy is a very suitable tool to investigate the surface of the electrode as it can offer information about the local disorder and changes in bond lengths and coordination environments. Furthermore because of the sensitive volume resolution of Raman microscopy, the heterogeneity of the electrode reaction can be investigated. Earlier Raman studies on anatase TiO_2 were only performed *ex situ* [1]. Here for the first time a real time *in situ* Raman study of the intercalation of lithium into nano anatase TiO_2 is presented.

Experimental

The *in situ* Raman cell set-up is described in detail elsewhere [2]. Here the working electrode comprised of anatase TiO_2 (AK1, BASF) and metallic lithium acted as both the counter and reference. *In situ* Raman spectra were collected at 23°C with a confocal Raman microscope (Labram series, Jobin Yvon SA, ex DILOR SA), using a HeNe laser with a wavelength of 632.8 nm as the excitation source. An 80x objective (Olympus) was used to focus the laser light onto the electrode surface and filter lowered the laser power to ca. 1 mW to avoid electrode degradation during the long term measurements. The cell had an open circuit potential (OCP) of ca. 3 V (all quoted potentials are vs. Li/Li^+) and was galvanostatically cycled using a Computer Controlled Cell Capture device from OCP down to 1.0 V and then between 1.0 V and 3.0 V. The charge/ discharge current employed was 15 µA/mg of TiO_2.

Results and Discussion

The Raman spectra observed for anatase TiO_2 during the first lithium insertion are shown in Figure 1. The potential vs. lithium content first lithiation curves are as an insert with numbered points corresponding to the spectrum number in the spectral series. The maximum lithium intercalation is ca. $Li_{0.85}TiO_2$. The potential and the amount of lithium intercalated into anatase TiO_2 for each spectrum are displayed in Table 1. Table 2 lists the *in situ* Raman wavenumbers (cm^{-1}) measured for Li_xTiO_2 when x = 0, 0.09, 0.1-0.5 and >0.5.

TiO_2 anatase has the point group D_{4h} and according to the factor group analysis, the 15 optical modes have the irreducible representation: $\Gamma_{opt} = 1A_{1g} + 1A_{2u} + 2B_{1g} + 1B_{2u} + 3E_g + 2E_u$. The A_{1g}, B_{1g} and E_g modes are Raman active, therefore six fundamental transitions are expected in the Raman spectrum of TiO_2 anatase. At OCP (ca. 3 V vs. Li/Li^+) five bands measured are present (with vibration mode in brackets) at 143 (E_g), 190 (E_g), 393 (B_{1g}), 516 (A_{1g}, B_{1g}) and 637 (E_g) cm^{-1}. The band at 516 cm^{-1} only resolves into two components at 507 (A_{1g}) and 519 cm^{-1} (B_{1g}) only at 73 K [3]. At 1.81 V x ~ 0.09 (spectrum no. 4) the first change in the spectrum is observed. The E_g band at 143 cm^{-1} has shifted to 149 cm^{-1} and has weakened in intensity and two shoulder peaks at 165 and 178 cm^{-1} are now present. The peak at 190 cm^{-1} shifts to 232 cm^{-1}. New peaks are observed at 315, 339, 527 and 554 cm^{-1} and the E_g 637 cm^{-1} band has shifted down to 629 cm^{-1}.

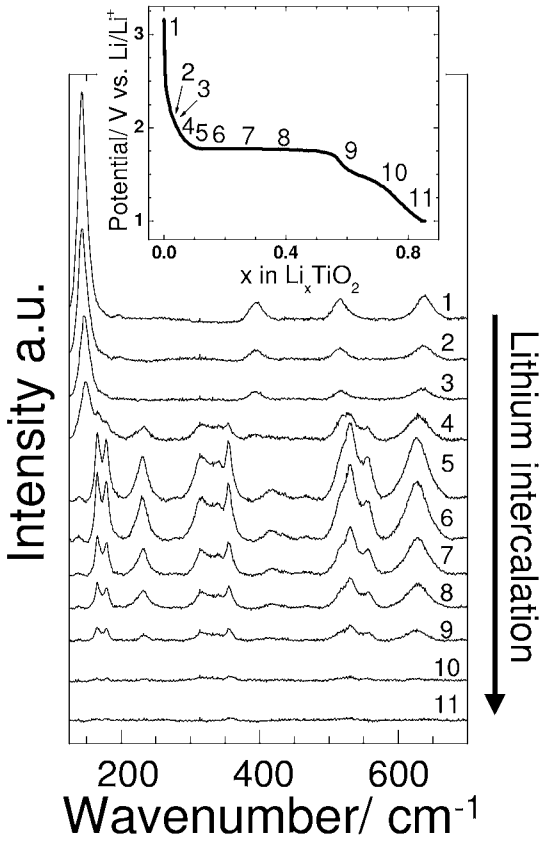

Fig. 1: *In situ Raman spectra series of the first lithium intercalation into anatase TiO_2. The charge curve showing the numbered regions where the spectra were measured is displayed above as an insert.*

This observation differs from Baddour-Hadjean et al. [1], where they first saw changes in the spectrum at x = 0.3. The spectrum at x = 0.15 was observed by them to have the identical form of the x = 0 for Li_xTiO_2. Upon further lithium intercalation x = 0.1 (spectrum no. 5); the spectrum radically changes. The band at 149 cm^{-1} disappears completely replaced by intensified doublet peaks at 165 and 178 cm^{-1}. The 393 cm^{-1} peak also vanishes. Additionally the bands seen at higher wavenumbers at 848 and 931 cm^{-1} were not observed by us. These bands were perhaps hindered by electrolyte bands appearing in this region. These bands are thought to originate from Li-O bonds.

Tab. 1: *The potential and the amount of lithium intercalated into anatase TiO_2.*

Spectrum Number	E/ V vs. Li/Li^+	x in Li_xTiO_2
1	3.16	0
2	2.05	0.04
3	1.84	0.07
4	1.81	0.09
5	1.79	0.10
6	1.78	0.11
7	1.77	0.24
8	1.77	0.38
9	1.60	0.58
10	1.38	0.71
11	1.03	0.83

The 637 cm^{-1} E_g band continues to shift down from 629 cm^{-1} to 626 cm^{-1}. This band is described as an asymmetric breathing motion of the TiO_2 octahedral i.e. Ti-O stretch. The small shift observed indicates that lithium insertion does not greatly disrupt this vibration. Whilst 141 cm^{-1} peak is a O-Ti-O bending motion and the presence of lithium is obstructive.

Tab. 2: *In situ Raman wavenumbers (cm^{-1}) for Li_xTiO_2[a].*

Spectrum 1	Spectrum 4	Spectra 5-8	Spectra 9-11
x = 0	x ~ 0.09	x = 0.1-0.5	x > 0.5
143s	149m		
	165w	165	165w
	178w	177	177w
190	232	232	232w
	315	315	315w
	339	339	339w
	355	355	355w
393	393		
		416	416vw
		467	467vw
516	516	516	516w
	527	527	527w
	554	554	554w
637	629	626	626w

[a] *s, strong; m, medium; w, weak; v, very*

At x = 0.5 the tetragonal TiO_2 anatase (D_{4h}) arrangement (a = b = 3.8 Å, c = 9.61 Å) slightly changes to an orthorhombic (D_{2h}) structure (a = 3.81 Å, b = 4.07 Å, c = 9.04 Å). Here $3A_g$, $3B_{2g}$ and $3B_{3g}$ modes are Raman active. Therefore essentially the $Li_{0.5}TiO_2$ composition is a TiO_2 lattice perturbed with lithium interactions. As described earlier our *in situ* Raman results show this rearrangement occurs at x ~ 0.1. Accordingly the partial assignment of spectra 5-8 is shown in Table 3. The table shows that using the simulated Raman spectrum of $Li_{0.5}TiO_2$ by Baddour-Hadjean et al. [1] possible Li-O modes have been detected in the case of the bands at 467 and 554 cm^{-1}.

Tab. 3: *Band assignment and Raman wavenumbers (cm^{-1}) for $Li_{0.5}TiO_2$.*

Band/ cm^{-1}	Assignment	Comment
165, 177	O-Ti-O bend	Possible doublet band of the E_g 141 cm^{-1} in TiO_2 anatase. May arise from the splitting of E_g into B_{2g} and B_{3g} modes of $Li_{0.5}TiO_2$
232	O-Ti-O bend	Shifted band of 190 cm^{-1} E_g in TiO_2 anatase
315	Unassigned	New lattice mode
339	O-Ti-O bend	Arises from the splitting of the E_g mode at 190 cm^{-1} into B_{2g} and B_{3g} modes of $Li_{0.5}TiO_2$
355, 416	Unassigned	New lattice mode
467	Possible Li-O mode	B_{3g}, see [1]
516, 527	Ti-O stretch	Shifting and possible separation of the TiO_2 anatase A_{1g}, B_{1g} modes
554	Li-O mode	B_{3g}, see [1]
626	Ti-O stretch	Shifted band of E_g 637 cm^{-1} in TiO_2 anatase

At high lithium content x > 0.5 (spectra 9-11) all bands become less intense. This could be due to the possible development of a metallic behaviour of the sample. The remaining signal from the material surface probably results from traces of material with intermediate stoichiometry.

Conclusions

For the first time, to the best of our knowledge, *in situ* Raman spectra have been generated from the lithiation and delithiation of anatase TiO_2. Our results differ significantly from *ex situ* measurements previously performed by Hadjean et al. [1]. Primarily the spectra show that Li_xTiO_2 changes symmetry from D_{4h} to D_{2h} when x ~ 0.1. They did not detect the disappearance of either the 143 cm^{-1} or the 393 cm^{-1} band during lithium intercalation. However our measurements did support *ex situ* measurements with the detection of low wavenumber Li-O modes at 467 and 554 cm^{-1}. No high wavenumber peaks assigned as lithium-oxygen stretches were detected by us. This is because the electrolyte bands are visible in the same region. Consequently because of these measured differences, our results show the possible advantages in carrying out Raman measurements *in situ*.

References

[1] R. Baddour-Hadjean, S. Bach, M. Smirnov, J.-P. Pereira-Ramos, J. Raman Spectrosc. **35**, 577 (2004).

[2] P. Novák, D. Goers, L. Hardwick, M. Holzapfel, W. Scheifele, J. Ufheil, A. Würsig, J. Power Sources **146**, 15 (2005).

[3] T. Ohsaka, F. Izumi, Y. Fujiki, J. Raman Spectrosc. **7**, 321 (1978).

IMPROVED *IN SITU* METHOD FOR GASSING ASSESSMENT, APPLIED TO CO_2 EVOLUTION AT LITHIUM-ION BATTERY CATHODES

J. Vetter, M. Holzapfel, W. Scheifele, A. Würsig, P. Novák
+41(0)56 310 2165
jens.vetter@psi.ch

Gas evolution during storage and use, leading to internal pressure build-up and cell bulging, is a major failure mechanism of lithium-ion batteries. With the differential electrochemical mass spectrometry (DEMS) technique it is possible to detect the different gaseous reaction products that are evolved during electrochemical cycling. Hence, intensity changes in mass signals can be detected as a function of time and/or potential and, thus, can be correlated with current peaks in the cyclic voltammogram or plateaus on galvanostatic charging / discharging curves.

Cell design

For detection of small amounts of gases the existing equipment [1] had to be improved considerably, and a new test cell was designed (figure 1). The new measurement system is based on headspace analysis. The gaseous reaction products are pumped off continuously from the top of an electrochemical cell [2,3] via a capillary into a quadrupole mass spectrometer where they are analyzed on-line. The headspace is purged with argon gas in order to flush the reaction products to the mass spectrometer. For measurements at elevated temperature, the cell is also equipped with a heating unit.

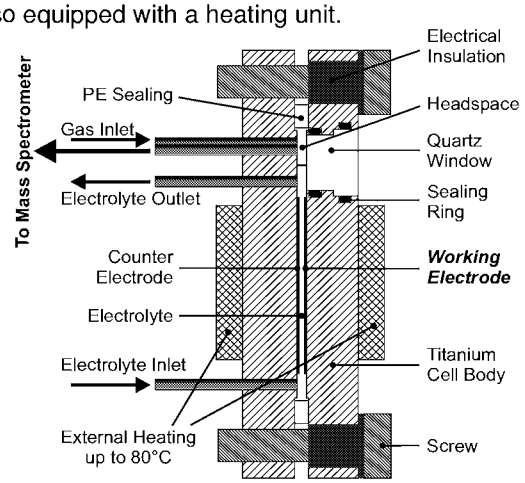

Fig. 1: *Schematic drawing of the improved DEMS measurement cell for headspace gas analysis.*

Measurement set-up

In order to avoid loss of volatile electrolyte compounds during long-term experiments, especially at elevated temperature, the purge argon is bubbled through a reservoir of the volatile compounds which is kept at the same temperature as the cell. After passing the cell, the volatile compounds are removed from the gases in a condensation trap before feeding the remaining gases to the mass spectrometer via a capillary (figure 2). This reduces the background signals and prevents liquid formation in the capillary. A mass flow controller ensures a constant gas flow to the mass spectrometer.

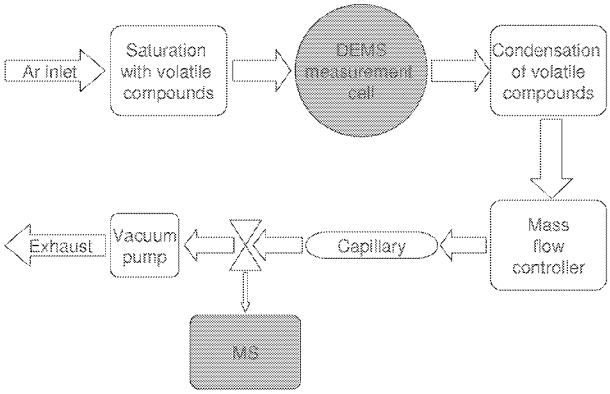

Fig. 2: *Schematic drawing of the improved DEMS measurement setup.*

With this electrochemical cell and set-up the identification and quantification of very small amounts of gas is possible. Compared to the previously existing equipment, the sensitivity is enhanced by ca. two orders of magnitude.

CO_2 formation at cathode materials

The improved cell and set-up was utilized to study the processes of electrolyte decomposition and to follow the formation of gaseous reaction products, especially CO_2, at lithium-ion battery cathodes during the first electrochemical cycles. During prolonged storage, especially at elevated temperature and high cell voltage, i.e., in the charged state, CO_2 is the main gaseous compound formed [4,5]. According to previous investigations, CO_2 is mainly formed at the positive electrode due to oxidation of the electrolyte [5,6].

Experimental

Since CO_2 readily reacts with lithium, further decreasing the already small amount of CO_2 formed during electrochemical cycling, a graphite counter electrode was used for the measurements. The electrodes were prepared by blade-coating the oxide and graphite electrode directly on the titanium body of the DEMS cell. For the oxide electrodes a mixture of 86.2 wt.% active material, 8.8 wt% conductive carbon, and 5 wt.% poly(vinylidene difluoride) binder was used. For the graphite counter electrode 95 wt% active material were mixed with 5 wt% poly(vinylidene difluoride) binder. In both cases the slurries were prepared in N-methyl pyrrolidone. After the coating of the electrode materials the cell parts were vacuum-dried at 120°C over night. The measurements cell was assembled in an argon filled glove-box with a moisture and oxygen level of less than 5 ppm. EC/PC/DMC 1/1/3 (v/v), 1 *M* $LiPF_6$ was used as the electrolyte.

DEMS measurements were carried out potentiodynamically at 60(±0.5)°C at a scan rate of 400 μVs^{-1}. The cycling voltammetry (CV) measurements were started at open circuit potential

and then varied between 4.5 V and 3.0 V with a potentiostatic hold period at the upper and lower voltage limit.

Lithium nickel cobalt aluminum oxide

In figure 3, the CO_2 traces from two slightly different DEMS experiments with a commercial standard cathode material, $Li[Ni,Co,Al]O_2$ are shown. Despite of a slightly different background, the two curves are quite similar, showing the reproducibility of the method.

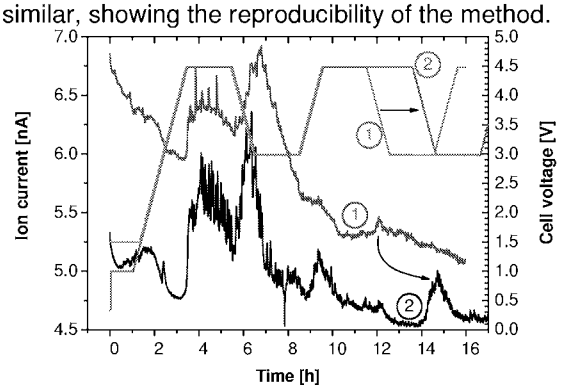

Fig. 3: *CO_2 evolution in cells with $Li[Ni,Co,Al]O_2$ cathodes and EC/PC/DMC 1/1/3, 1 M $LiPF_6$ electrolyte at 60 °C. MS traces and corresponding voltage profiles for two experiments are shown.*

During the first charge, a sharp increase of the CO_2 signal is observed at a cell voltage of ca. 4.2–4.3 V. The CO_2 evolution reaches a maximum shortly after the upper voltage limit is reached and then decays slowly during the two hour hold period. In the following discharge, the CO_2 signal again increases at a voltage of ca. 4.3–4.2 V, indicating the beginning of a second process releasing the gas. In the second cycle, similar signals are observed, but with much lower intensity, and the CO_2 signal at increasing cell voltage is shifted to lower voltages. In measurement (2), the hold period at 4.5 V in the second cycle was extended to 4 hours, resulting in a shift of the gas signal in time, indicated by arrows in figure 3. This shows that the CO_2 evolution is really associated with an electrochemical process during the lowering of the cell voltage. The most probable explanation for this kind of behavior seems to be the formation of a film or precipitate on the surface of the electrode or active material at high voltage above 4.3 V, and the dissolution or structural rearrangement of this compound at lower voltages, accompanied by the formation or release of CO_2.

Lithium nickel manganese cobalt oxide

As a second positive active material, $Li(Ni,Mn,Co)O_2$ was tested on its CO_2 evolution in dependence on the cell voltage. This material was developed within the European project CAMELiA with the goal of reducing CO_2 evolution.

Indeed, our experiments showed only a very small amount of CO_2 evolved from these electrodes at 60 °C. In fact, the signals detected could hardly be distinguished from the background noise and did not allow a reliable correlation with the cell voltage (figure 4).

Influence of Li_2CO_3 on CO_2 evolution

The $Li[Ni,Mn,Co]O_2$ contains only very small amounts of Li_2CO_3 impurity, which is a possible source of CO_2. In order to find out if carbonate content is a crucial parameter we added 2 % of Li_2CO_3 to the electrode. These DEMS experiments (figure 4) show a strong CO_2 signal at very low cell voltages, but gas evolution stops at ca. 3.5–3.8 V in the first charge. Neither during the hold period at 4.5 V, nor in the subsequent cycles, any influence of the added lithium carbonate on CO_2 formation is observed. This is a strong hint that inorganic carbonate present in the $Li[Ni,Mn,Co]O_2$ has only a minor impact on the evolution of CO_2 at high voltages and elevated temperatures.

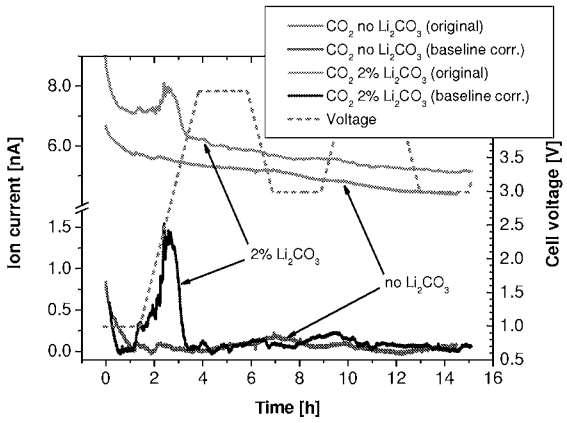

Fig. 4: *CO_2 evolution in cells with $Li[Ni,Mn,Co]O_2$ cathodes and EC/PC/DMC 1/1/3, 1 M $LiPF_6$ electrolyte at 60 °C. Original and baseline corrected MS traces and corresponding voltage profiles for experiments with and without Li_2CO_3 added to the electrodes are shown.*

Acknowledgment

Financial support by the European Community and the Swiss State Secretariat for Education and Research (contract no. 02.0004-1) under the framework of the European research project CAMELiA (ENK6-CT-2002-00636) is gratefully acknowledged.

References

[1] P. Novák, J.C. Panitz, F. Joho, M. Lanz, R. Imhof, M. Coluccia, J. Power Sources **90**, 52 (2000).

[2] A. Würsig, J. Ufheil, P. Novák, Proc. 205th ECS Meeting, San Antonio, TX, USA, May 9-13, 78, (2004).

[3] P. Novák, D. Goers, L. Hardwick, M. Holzapfel, W. Scheifele, J. Ufheil, A. Würsig, J. Power Sources **146**, 15 (2005).

[4] K.H. Lee, E.H. Song, J.Y. Lee, B.H. Jung, H.S. Lim, J. Power Sources **132**, 201 (2004).

[5] N. Takami, T. Ohsaki, H. Hasebe, M. Yamamoto, J. Electrochem. Soc. **149**, A9 (2002).

[6] R. Imhof, P. Novák, J. Electrochem. Soc. **146**, 1702 (1999).

COMPONENTS

NEDC-CONSUMPTION OF THE HY-LIGHT FUEL CELL/SUPERCAP CAR

F.N. Büchi, G. Paganelli[1], P. Dietrich, D. Laurent[1], A. Tsukada, D. Walser[1], P. Varenne[1], R. Kötz, S.A. Freunberger, A. Delfino[1]
+41(0)56 310 2411
felix.buechi@psi.ch

The main factors influencing fuel consumption of a vehicle are curb weight and drive train efficiency. In a joint project, Conception et Développement Michelin and Paul Scherrer Institut have dedicated a strong effort to achieve an exceptional tank to wheel efficiency with a new hydrogen/oxygen fuel cell powered concept car named HY-LIGHT, with low weight and a highly efficient drivetrain.

Vehicle and drive train development

HY-LIGHT is a compact two door vehicle designed for four passengers. It is equipped with the Michelin active wheel, which embeds an electric actuator for programmable active suspension and chassis control functions in all wheels. The two front wheels are equipped with electric motors for traction of 30 kW / 60 kW nominal/peak power. The traction motors have a mass of only 7 kg, keeping the unsprung mass small.

Big efforts have been made to reduce curb weight of the car to only 850 kg. This could be achieved with a chassis based on an aluminum structure, into which the hydrogen tank is integrated. The fuel cell system is positioned under the hood and the power electronics are located in the tunnel between driver and front passenger. The hybrid electric powertrain consists of a hydrogen/pure oxygen polymer electrolyte fuel cell system with 30 kW_{net} continuous power [1] and a 45 kW_{peak} (for 15 sec) super capacitor module with a usable energy content of 180 Wh. The hybrid powertrain lay-out was chosen to cover the peak power demand for acceleration and to profit from the characteristics of the electric drive train enabling recuperation of braking energy.

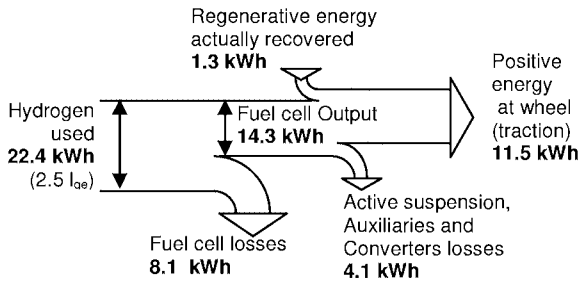

Fig. 1: *Energy Flow for 100 km in NEDC.*

New European Driving Cycle

In order to compare consumption between different vehicles standardized drive cycles are used. The new European driving cycle (NEDC) comprises an urban section with four accelerations to 60 km/h and an interurban section with maximum speed of 120 km/h. The total length is 11.2 km, the overall average speed 34 km/h.

Results

The hydrogen consumption of the HY-LIGHT vehicle for the NEDC, measured on the dynamometer, is 0.67 kg H_2/100 km. The energy flows are given in Figure 1. For comparison with vehicles based on H_2/air fuel cell systems, the energy for production and compression of the oxygen in case of the HY-LIGHT car has to be included into the consumption. When including this energy with an efficiency ratio of 63%, the NDEC consumption increases to 0.69 – 0.78 kg per 100 km depending on the route of oxygen production. The lower value is for oxygen and hydrogen produced by water electrolysis and the higher value for oxygen produced by distillation of liquid air [1]. In Table 1 the consumption values are compared to those of the pre-series vehicles of DaimlerChrysler (NeCar 4 [2]) and General Motors / Opel (Hydrogen 3 [3]).

Vehicle	NEDC consumption [kg H_2/100 km]	[l_{gas}/100 km]
HY-LIGHT (H_2 only)	0.67	2.5
HY-LIGHT (incl. O_2)	0.69 – 0.78	2.6 – 2.9
NeCar 4 [2]	1.1	4.0
HydroGen 3*	1.15	4.2

* official communication of GM-Opel

Table 1: *Vehicle NEDC consumption in hydrogen and gasoline equivalent values.*

The DC and GM vehicles are considerably heavier (1400 – 1600 kg) and therefore the results in Table 1 reflect the fact, that curb weight is a premier factor for the consumption in the NDEC. HY-LIGHT being the lightest vehicle, has an exceptional low consumption, even under consideration of the energy required for the oxygen production/compression.

References

[1] F.N. Büchi et al., Fuel Cells, submitted (2005).

[2] G. Friedlmeier, J. Friedrich, F. Panik, Fuel Cells **1**, 92 (2001).

[3] U. Winter, M. Herrmann, Fuel Cells **3**, 141 (2003).

[1] *Conception et Développment Michelin, 1762 Givisiez*

MEASURING THE EFFECTIVE RELATIVE DIFFUSIVITY OF GAS DIFFUSION MEDIA FOR PEFC

S.A. Freunberger, D. Kramer, F.N. Büchi, G.G. Scherer
+41(0)56 310 2410
stefan.freunberger@psi.ch

Despite considerable improvements, the major voltage losses in polymer electrolyte fuel cells (PEFC) arise from poor oxygen reduction kinetics, mass transport limitations and a high resistance of dehydrated ionomer. Mass transport limitations arise in the porous gas diffusion layer (GDL), in a possibly used micro porous layer and in the catalyst layer. In particular the link between electrochemical performance, the behaviour of liquid water in porous media, and the material properties is still poorly understood. Even more, there is no clear link between electrochemical performance and liquid water hold up in the GDL. Neutron radiography by Zhang et al. [1] has shown that different behaviour of GDL materials in terms of liquid water accumulation and its partitioning between areas under the channels and the ribs does not necessarily impede the integral cell performance. Much more detailed discrimination between mass transfer resistances in GDL and catalyst layer can be obtained by local current measurements with a resolution better than the channel and rib size as first shown by Reum et al. [2]. However, in order to gain the most possible information from such experiments model calculations are inevitable. For that, one key parameter is the effective diffusivity of porous transport media, whose compression and direction dependence is subject to this experimental study.

Experimental

Diffusion in a porous medium is represented by its effective diffusivity $D^{eff} = \varepsilon/\tau \cdot D$, where D is its value in free space, ε the porosity and τ the tortuosity. Instead of laborious diffusion experiments for gaining ε/τ, a physically analogous process like current conduction is suited likewise. Therefore, the conductivity change of an electrolyte volume due to insertion of a GDL sample with the free pore space soaked with this electrolyte is used. The appropriate test cell which allows for controlled compression of the sample is sketched in Figure 1.

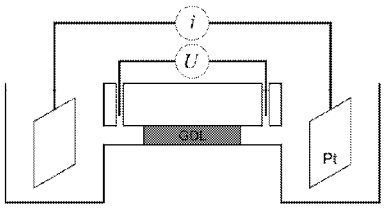

Fig. 1: *Schematic diagram of the measuring cell with 0.5 M H_2SO_4 as electrolyte.*

Electrolyte conductivity is best measured by high frequency impedance. However, when applying this to electrolytes in conductive porous materials current is capacitively coupled into the conductor. This phenomenon is known from porous electrodes and may be described by a transition line equivalent circuit [3] (see Figure 2). The value of ε/τ is equal to the ratio of ΣR_i and the resistance of the respective free space without GDL.

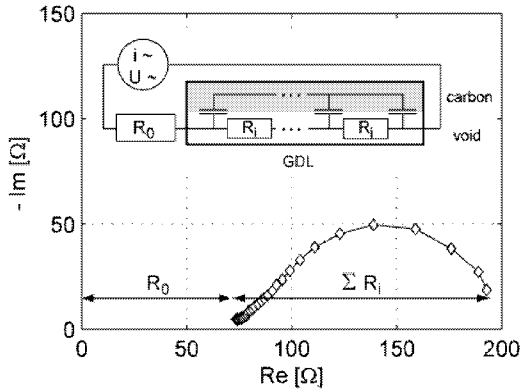

Fig. 2: *Typical impedance spectrum of an electrolyte soaked GDL and its interpretation by means of a transition line equivalent circuit [3].*

Results

Figure 3 shows exemplarily porosity, effective relative diffusivity, and consequential tortuosity for Toray TGP-H-060 carbon paper in the in-plane direction as a function of compressed thickness. Tortuosity values range from 1.3 at raw thickness to 3.4 at nearly 60 % compression. This is well below usually used values around 7 in most modelling works.

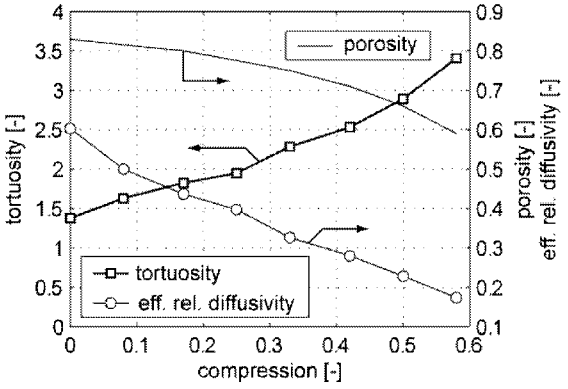

Fig. 3: *Porosity, effective relative diffusivity, and consequential tortuosity of Toray TGP-H-060 carbon paper in in-plane direction.*

References

[1] J. Zhang, D. Kramer, R. Shimoi, Y. Ono, E. Lehmann, A. Wokaun, K. Shinohara, G. G. Scherer, Electrochim. Acta, in press (2005).

[1] M. Reum, S.A. Freunberger, J. Evertz, F.N. Büchi, this report.

[3] R. de Levie, Electrochimica Acta **8**, 751 (1963).

MICROSTRUCTURING POLYELECTROLYTE MEMBRANES FOR IMPROVED MECHANICAL STABILTITY

P. Farquet, C. Padeste, S. Alkan-Gürsel, G.G. Scherer, H.H.Solak, A. Wokaun
+41(0)56 310 2580
patrick.farquet@psi.ch

The proton conducting membrane is a key element in polymer electrolyte fuel cell technology. When mounted in a fuel cell the membranes are subjected to high mechanical stress, which may cause failure of the cell. Membranes, which are prepared by radiation grafting a second component into a fluoropolymer film and subsequent sulfonation, are mechanically less stable than the originally base film. By covering part of the base film area with a metal mask during the exposure process, one can avoid grafting of shadowed areas leading to better mechanical stability [1, 2]. However, the non-grafted areas should be minimized in order to preserve high proton conductivity.

Experimental

ETFE films of 100 µm of thickness were exposed using a molybdenum X-ray source (40 kV, 30 mA). ETFE samples were placed in the incident beam just behind an 800 µm iron mesh with 51% of open area. Grafting and sulfonation of the irradiated samples were carried out as described elsewhere [3].

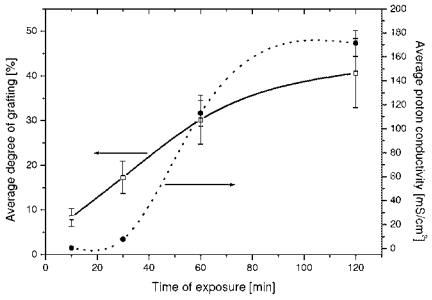

Fig. 1: *Degree of grafting and proton conductivity of microstructured membranes as a function of exposure time.*

Graft level and proton conductivity are increasing with exposure time (Fig. 1). However, below about 20% graft level only very low proton conductivity was measured, probably due to inhomogeneous grafting in the exposed areas. The saturation of graft level and conductivity at high exposure time is assigned to radical recombination during the exposure and grafting process.

The positive effect of microstructuring on the mechanical properties of grafted membranes is shown in Figure 2. The base polymer is highly flexible and breaks after an elongation as high as about 500%. Grafting and sulfonation procedures drastically diminish the film toughness, as seen from the lower force needed for expansion and the much lower elongation at break. Structured membranes showed an intermediate behavior, both in toughness and elongation at break.

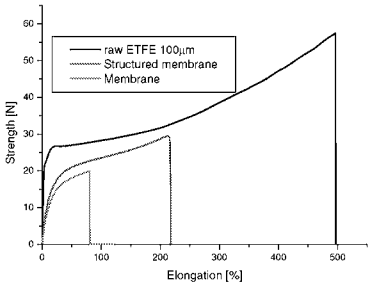

Fig. 2: *Tensile strength as measured by elongating 1 cm broad sample stripes. Membrane samples were tested in completely wet state.*

In order to loose less active area in the structuring process, exposures were performed using microfabricated 200 µm period nickel grids of 25 µm wide lines, which gives an open area of 87 %. These grids were electroplated with nickel in SU8 moulds prepared by UV lithography. A structure thickness of 80 µm ensured an attenuation of the x-rays by more than 95 %. Figure 3 shows micrographs of an ETFE film, which was exposed through such a nickel grid after grafting and sulfonation. A high discrimination between the grafted and non grafted areas was observed with a good resolution through the whole film thickness.

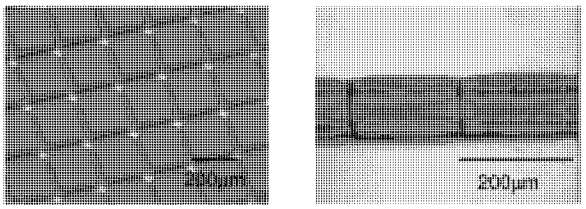

Fig. 3: *Top view and cross-section of a 200 µm period structured membrane, with 87 % of open area. The grafted areas appear dark in the micrographs.*

Conclusions

Lithographic structuring is a promising approach to increase the mechanical stability of radiation grafted proton conducting membranes. X-ray exposure through metal shadow masks results in a good discrimination between grafted and ungrafted regions. Using microfabricated metal grids as masks, non-grafted stabilization structures in the 10µm range appear feasible.

References

[1] H.P. Brack, C. Padeste, M. Slaski S. Alkan, H.H. Solak, JACS **126 (4)**, 1004 (2004).

[2] S.A. Gürsel, C. Padeste, H.H. Solak, G.G. Scherer, Nucl. Instr. Meth. Phys. Res. B. **236,** 449 (2005).

[3] L. Gubler, S. Alkan Gürsel, G.G. Scherer, Fuel Cells **5**, 317 (2005).

THERMAL PROPERTIES OF POLY-(ETHYLENE-*ALT*-TETRAFLUORO-ETHYLENE) BASED PROTON-CONDUCTING MEMBRANES

S. Alkan Gürsel, J. Schneider, G.G. Scherer
+41(0)56 310 2797
selmiye.alkan@psi.ch

Proton-conducting membranes for fuel cell applications require exhibiting both, chemical and thermal stability. The present investigation has been carried out to study the thermal behaviour of poly(ethylene-*alt*-tetrafluoroethylene) (ETFE) based proton-conducting membranes, both uncrosslinked and DVB-crosslinked, prepared by pre-irradiation grafting of styrene and subsequent sulfonation. We have studied the influence of various preparation steps on the thermal degradation and the crystallinity of grafted films and membranes with varying degree of grafting by thermogravimetric analysis (TGA) and differential scanning calorimetry (DSC).

Experimental

ETFE based radiation grafted membranes at varying graft levels (GL) were prepared as described previously [1]. TGA measurements were performed in inert atmosphere on a Perkin-Elmer TGA-7 system at a heating rate of 20ºC/min. The membrane samples were purged with a nitrogen flow for 10 minutes at 100 °C to remove excess water prior to TGA. DSC measurements were conducted on a Perkin-Elmer DSC-7 system at a constant heating rate of 20°C/min under nitrogen atmosphere. The membranes were converted to salt form and dried at 50 °C overnight prior to DSC in order to eliminate the interference of moisture on their melting process.

Results and Discussion

Similar to styrene-grafted FEP-films and membranes [2,3,4], the degradation of ETFE-based grafted films and membranes exhibited the typical two-phase behavior, demonstrating the non-compatibility of base polymer film and grafted component.

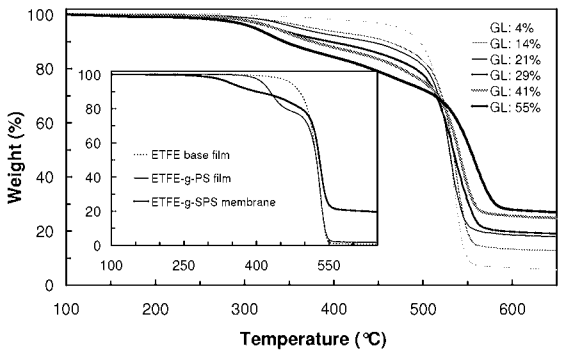

Fig. 1: *Degradation behavior of ETFE based crosslinked membranes with varying GL, as characterized by TGA. Inset shows the comparison of base film, grafted film, and membrane.*

Unlike the two-step degradation pattern of the grafted films, a three-step weight loss pattern was observed for radiation grafted membranes and has been ascribed to dehydration of the membrane, de-aromatization, and desulfonation, and finally degradation of the backbone [3]. In addition, the GL was found to affect the degradation pattern only to a minor extent. (Fig.1)

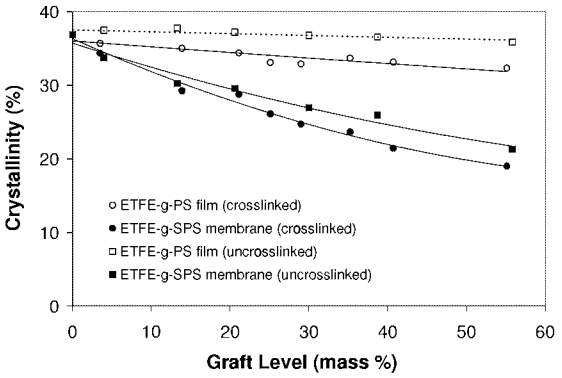

Fig. 2: *Comparison of crystallinity of ETFE based grafted films and membranes.*

The crystallinity of the films decreased slightly by grafting. However, the sulfonation of the grafted films caused a significant decrease in crystallinity (Fig. 2). Moreover, the decrease in crystallinity was more expressed for the crosslinked films and membranes. The loss in crystallinity in membranes may be attributed to the strong hydrophilic-hydrophobic stresses in the water swollen membrane, which lead to the distortion of the crystallites. An similar behavior was described previously for FEP based membranes [4]. The melting temperature of grafted films and membranes decreased only slightly, as compared to the base film.

Conclusions

Radiation-induced grafting and subsequent sulfonation caused significant changes on degradation behavior. However, GL and crosslinking have no considerable effect on thermal degradation. Although crystallinity changed only slightly by grafting, a considerable decrease in crystallinity was obtained after sulfonation. The melting temperature of the base polymer film was almost constant after grafting and sulfonation.

References

[1] L. Gubler, N. Prost, S. A. Gürsel, Solid State Ionics **176**, 2449 (2005).

[2] B. Gupta, G.G. Scherer, Die Angew. Makromol. Chem. **210**, 151 (1993).

[3] B. Gupta, J.G. Highfield, G. G. Scherer, J. Appl. Polym. Sci. **51**, 1659 (1994).

[4] B. Gupta, O. Haas, G. G. Scherer, J. Appl. Polym. Sci. **54**, 469 (1994).

MEMBRANE AND ELECTRODE DEGRADATION UNDER A DYNAMIC TESTING PROTOCOL

L. Gubler, M. Arcaro, G.G. Scherer
+41(0)56 310 2673
lorenz.gubler@psi.ch

Radiation grafted membranes developed at PSI have been successfully tested in the H_2/O_2 fuel cell without performance loss for over 4'000 h at a temperature of 80°C [1]. The cell operation was under constant current condition of 0.5 Acm^{-2}. In reality, however, load changes and start-stop cycles are likely to occur, which may lead to more rapid components degradation. In this study, the results of a durability test under dynamic conditions using a standard PSI membrane on the basis of 25 µm thick poly(tetrafluoroethylene-*co*-hexafluoropropylene) (FEP) film is reported [2].

Experimental

The radiation grafted FEP-25 membrane was hotpressed with carbon paper based electrodes, having a catalyst loading of 0.6 $mgPtcm^{-2}$, to form a membrane electrode assembly (MEA). The active area of the test cell was 30 cm^2. During testing, intermittent polarization experiments were carried out for performance evaluation, current-pulse measurements for membrane resistance, cyclic voltammetry for electrochemical catalyst surface area, leak test and H_2 permeation for assessing membrane integrity.

Results and Discussion

For the first 1'000 h, the cell was operated at constant current density of 0.5 Acm^{-2}. Subsequently, a dynamic cyclic protocol was used: 4 h at 0.5 Acm^{-2}, 10 min at open circuit voltage (OCV). The history plot of the experiment (Fig.1) shows a relatively stable performance with only 9 μVh^{-1} performance degradation and no apparent deterioration of OCV and membrane (ohmic) resistance. However, the MEA failed close to 3'000 h due to pinhole formation in the membrane, measured by crossover leak check.

The cell performance data shown in Fig.1 gives an inconclusive picture on the state of the MEA sub-components, i.e. membrane and electrodes. For the present MEA, both anode and cathode surface area show a steady decrease with only 50 % of the initial area left after 3'000 h (Fig.2). The impact on the performance, however, was minor. Catalyst aging may be caused by Pt particle ripening, dissolution, deactivation, corrosion of the carbon support, of loss of ionomer from the catalyst layer [3]. As for the membrane integrity, both H_2 permeation and leak rate increase gradually as a function of testing time, and, eventually, a large enough pinhole is formed to cause the collapse of the cell voltage and lead to MEA failure. The gradual degradation of the membrane does not appear to affect performance (Fig.1), probably because the pinhole area is small compared to the size of the active area.

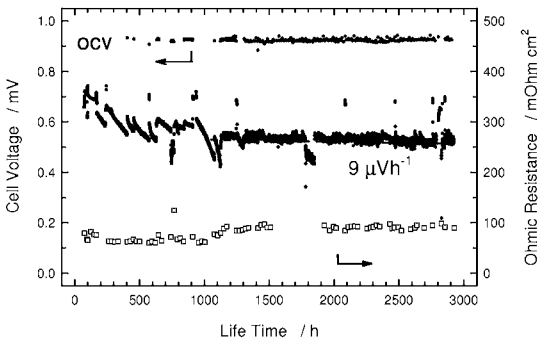

Fig. 1: *Durability experiment using MEA based on radiation grafted FEP-25 membrane. Cell temperature 80°C, stoichiometry H_2/air = 1.5/2.0, pressure 1 bar_a, gases fully humidified. Current density 0.5 Acm^{-2}, from 1'100 h onwards a dynamic dynamic test protocol was used, with excursions to OCV every 4 h for 10 min.*

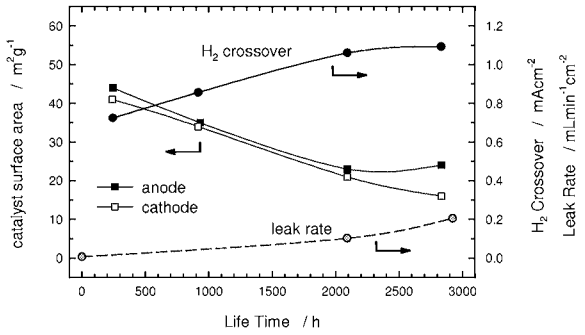

Fig. 2: *Breakdown of MEA performance shown in Fig. 1 into component characteristics. The electrochemical catalyst surface areas are a measure for the deterioration of the electrode structure, H_2 crossover and leak rate characterize the integrity of the membrane.*

Conclusions

The durability of a membrane electrode assembly (MEA) comprising a PSI membrane was assessed under a dynamic single cell testing protocol with sequences at 0.5 Acm^{-2} and open circuit voltage (OCV). Performance appeared to be stable, yet MEA failure occurred after 3'000 h due to a membrane pinhole. Advanced MEA components diagnostics revealed 50 % loss of electrochemical catalyst surface area and gradual deterioration of membrane integrity. These findings strengthen the insight that detailed MEA diagnostic tools are required to adequately assess the status and integrity of the MEA and its sub-components during evaluation in the fuel cell.

References

[1] L. Gubler, H. Kuhn, T.J. Schmidt, G.G. Scherer, H.P. Brack, K. Simbeck, Fuel Cells **4**, 196 (2004).

[2] J. Huslage, T. Rager, B. Schnyder, A. Tsukada, Electrochim. Acta **48**, 247 (2002).

[3] J. Xie, D.L. Wood III, D.M. Wayne, T.A. Zawodzinski, P. Atanassov, R.L. Borup, J. Electrochem. Soc. **152**, A104 (2005).

FUEL CELL PERFORMANCE OF α-METHYLSTYRENE GRAFTED MEMBRANES

L. Gubler, M. Slaski, G.G. Scherer
+41(0)56 310 2673
lorenz.gubler@psi.ch

Radiation grafted membranes using α-methylstyrene (AMS) as graft component offer the prospect of enhanced chemical stability in the fuel cell environment compared to styrene grafted membranes [1]. Due to the poor radical polymerization kinetics of pure AMS, methacrylonitrile (MAN) is used as co-monomer to obtain practical graft levels [2]. In this study, fuel cell performance and durability compared to styrene (S) grafted membranes and Nafion® 112 is reported.

Experimental

AMS/MAN based radiation grafted membranes were prepared as described in [1]. Styrene based membranes were made according to the standard procedure at PSI [3]. 25 µm thick poly(tetrafluoroethylene-*co*-hexafluoropropylene) (FEP) was used as base film. Optionally, the films were crosslinked using divinylbenzene (DVB) as additional monomer. Single cell testing was carried out in fuel cells of 30 cm^2 active area, using carbon cloth based Pt/C electrodes.

Results and Discussion

Ex situ membrane properties show encouraging conductivity for AMS based membranes (**Tab.1**). The graft level is about twice that of styrene grafted membranes for similar ion exchange capacity, because AMS is heavier than styrene and MAN is incorporated into the film along with AMS. The crosslinked AMS:MAN membrane has a higher water uptake compared to the crosslinked styrene based membrane, indicating that the degree of crosslinking can be potentially further increased.

Tab. 1: Ex situ *membrane properties, g- means radiation grafted and sulfonated membranes. Water content and conductivity at room temperature in water swollen state.*

membrane	graft level*	water content	conductivity
	[m-%]	[H_2O/SO_3H]	[mS/cm]
g-S	18.0	29.5 ± 0.7	72 ± 6
g-S:DVB	18.2	6.7 ± 0.7	41 ± 1
g-AMS:MAN	34.5	24.6 ± 0.8	98 ± 12
g-AMS:MAN:DVB	36.0	12.6 ± 0.9	89 ± 8
Nafion® 112	-	18.0 ± 0.9	82 ± 6
* weight increase through incorporation of graft component			

Single cell polarization data shows good performance (**Fig.1**), with the DVB crosslinked AMS:MAN membrane meeting the performance of Nafion® 112. The improved performance compared to the uncrosslinked AMS:MAN membrane is not understood to date, it may be an effect of improved membrane-electrode interface. The *in situ* membrane (ohmic) resistance is identical for all the membranes tested.

The single cells were operated until failure occurred (**Fig.2**). The failure mode was an excessive gas crossover through the membranes. The effect of crosslinking is shown dramatically for styrene based membranes. The AMS:MAN grafted membrane lasted for ~500 h, the AMS:MAN:DVB membrane for 1'000 h. As the crosslinking was rather moderate, the potential of the membrane is by far not fully exploited yet.

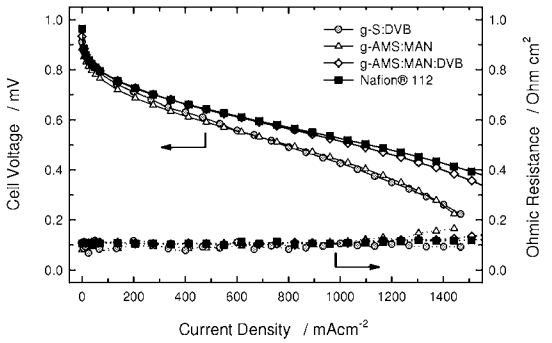

Fig. 1: *Single cell performance using radiation grafted and sulfonated membranes based on 25 µm FEP, compared to Nafion® 112. Electrodes: E-TEK 0.6 mgPtcm⁻², cell temperature 80 °C, reactants H_2/O_2 at a stoichiometry of 1.5/9.5, pressure 1 bar_a, gases fully humidified.*

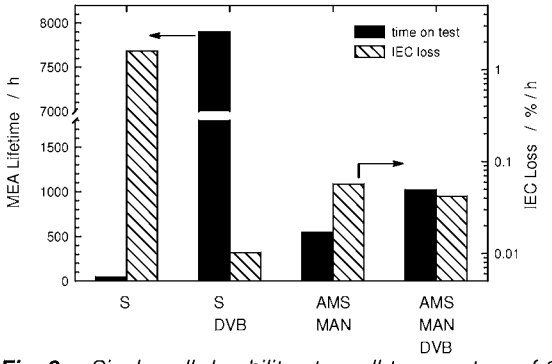

Fig. 2: *Single cell durability at a cell temperature of 80 °C and rate of ion exchange capacity (IEC) loss.*

Conclusions

Radiation grafted membranes based on α-methylstyrene (AMS) have been successfully tested in single cells. Results show higher stability compared to styrene based membranes. The performance and durability can be further improved by crosslinking using divinylbenzene (DVB). Crosslinking of AMS membranes has not been optimized yet, further improvements are required to exploit the full potential of the advanced monomer AMS.

References

[1] M. Slaski, L. Gubler, G.G. Scherer, A. Wokaun, this report.

[2] M. Slaski, L Gubler, G.G Scherer European Patent Application EP 05002875.

[3] L. Gubler, H. Kuhn, T.J. Schmidt, G.G. Scherer, H.P. Brack, K. Simbeck, Fuel Cells **4**, 196 (2004).

EFFECT OF SYNTHESIS PARAMETERS ON GRAFTING OF STYRENE ONTO POLY (ETHYLENE-*ALT*-TETRAFLUOROETHYLENE)

H. Ben youcef, S. Alkan Gürsel,
G. G. Scherer, A. Wokaun
+41(0)56 310 4188
hicham.ben-youcef@psi.ch

The influence of the synthesis parameters on the radiation induced grafting of styrene into poly (ethylene-*alt*-tetrafluoroethylene) (ETFE) without crosslinker has been studied. The grafting conditions are known to have significant effects on the degree of grafting. Pre-irradiation dose, reaction temperature, and their influence on the grafting kinetic were investigated.

Experimental

Reactions were carried out in a glass reactor (3 cm diameter, 18 cm height, 50 ml capacity) with 7cm x 7cm ETFE films (Tefzel® 100LZ, 25 µm, DuPont) using an isopropanol:water (7:1) (v/v) mixture under nitrogen atmosphere. The reference point for the studied parameters was: 1.5 kGy pre-irradiation dose, styrene (20%) (v/v), at 50 °C [1,2].

Results and Discussion

The grafting parameters were varied as follows: pre-irradiation dose from 1.5 to 30 kGy, monomer concentration from 5 to 100 % (v/v), temperature from 40 to 90 °C, and grafting time from 40 minutes to 24 hours. These parameters were optimized for poly (tetrafluoroethylene-co-hexafluoropropylene) for both, crosslinked and uncrosslinked grafted films [3,4].

The influence of pre-irradiation dose on grafting kinetics is shown in Figure 1. The degree of grafting shows an increasing trend with the increase in the pre-irradiation dose. This is a consequence of the increasing number of active sites in the polymer matrix.

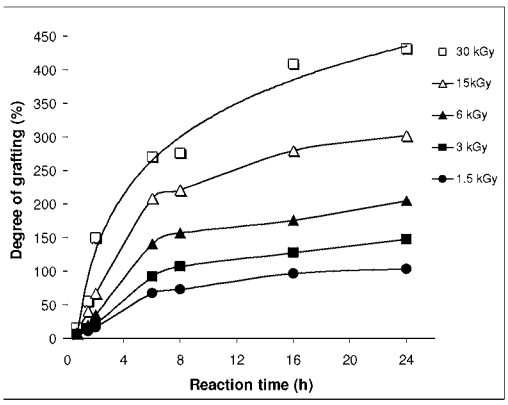

Fig. 1: *Grafting kinetics at different pre-irradiation dose.*

The effect of monomer concentration on the grafting kinetics is displayed in Figure 2. The degree of grafting increases with increasing monomer concentration up to 20% of styrene and then tends to decrease.

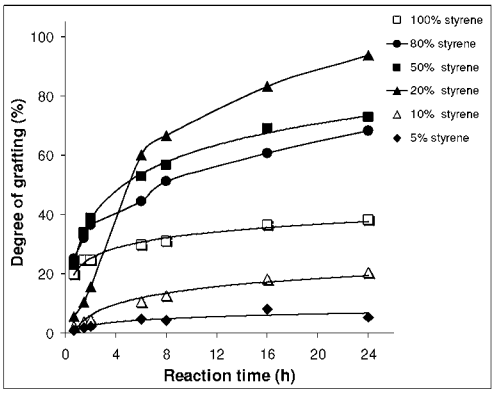

Fig. 2: *Grafting kinetics at different styrene concentrations.*

The grafting kinetics (time vs. degree of grafting) as function of temperature is shown in Fig. 3. The degree of grafting increases with increasing temperature up to 60 °C and decreases at temperatures above. At higher temperature the probabilities of homopolymer formation and recombination reactions increase and, as a consequence, the monomer diffusion may be hindered.

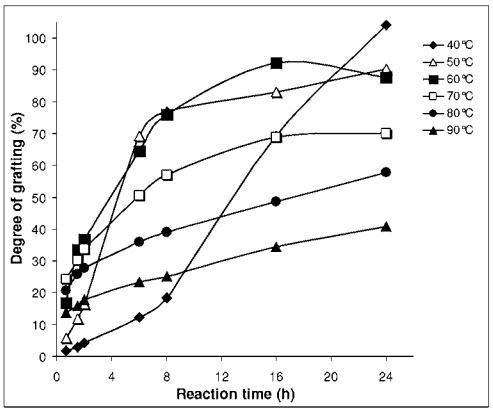

Fig. 3: *Grafting kinetic at different reaction temperature.*

Conclusions

From the results described above it can be concluded that "mild" conditions of grafting in terms of radiation dose, temperature, and concentration can be chosen, in order to achieve degrees of grafting interesting for fuel cell membranes. By taking these results into account, preparation conditions for crosslinked ETFE-membranes can therefore be set to evaluate the optimal crosslinker content.

References

[1] S. Alkan Gürsel, H. P. Brack, G. G. Scherer, PSI Scientific Report 2003, **V,** 101 (2004).

[2] S. Alkan Gürsel, L. Gubler, G. G. Scherer PSI Scientific Report 2004, **V,** 113 (2005).

[3] T. Rager, Helv. Chim. Acta **86**, 1966 (2003).

[4] T. Rager, Helv. Chim. Acta **87**, 400 (2004).

MATERIALS AND CATALYSIS

HYDROUS RUTHENIUM OXIDE FOR ELECTROCHEMICAL CAPACITORS: ELECTROCHEMICAL PROPERTIES

O. Barbieri, A. Foelske, M. Hahn, R. Kötz
+41(0)56 310 2132
olivier.barbieri@psi.ch

Due to promising high capacity per gram supercapacitors based on the pseudo capacitance of hydrous ruthenium oxide (RuO_2 xH_2O) have been the focus of numerous recent studies. In order to optimize the performance of this transition-metal-oxide compound a good understanding of the influence of the preparation parameters on its electrochemical behavior is required. Here we present some results on the influence of the annealing temperature on the capacitance and the ageing of RuO_2 upon electrochemical cycling.

The RuO_2 powders were prepared according to the sol-gel method presented by Zheng et. al. [1]. The black $RuO_2.xH_2O$ paste obtained was then dried on open air for one night and finally annealed at appropriate temperature for 17 hours in air. The capacitance values were determined from the cyclovoltammetric response in 3M H_2SO_4 at 2mV/s between 0V and +1.15V vs. SHE.

Capacitance

The evolution of the gravimetric capacitance with the annealing temperature T is shown in figure 1.

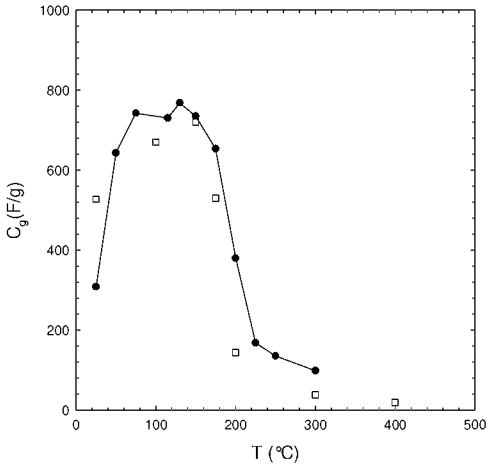

Fig. 1: *Gravimetric capacitance of hydrous ruthenium oxide powders as a function of the annealing temperature; black cycles: this study; white squares: from reference [1].*

The gravimetric capacitance increases with the annealing temperature until a temperature around 150°C is reached and then decreases for higher annealing temperatures. The results obtained are in good agreement with those of Zheng et al. also presented in figure 1. This behavior, with a maximum of $C_g(T)$= 750 F/g around T = 150°C (sample Z150), is due to the changes of morphology of the hydrous RuO_2 undergoing a phase transition from an amorphous hydrated morphology to a crystalline anhydrous structure [2]. The high capacitance of Z150 ($RuO_2.0.5H_2O$) is attributed to the optimum combination of electronic conductivity (increasing with crystallinity) on the one hand and proton accessibility on the other hand. The latter is increasing with the content of both physically and chemically bound water [3, 4].

Cycle stability

Three capacitors each comprising two identical RuO_2 electrodes (Z150) were cycled between zero cell voltage and upper voltage limits of 0.9, 1.0 and 1.1 V, respectively. The cell's capacitance evolution as a function of the cycle number is depicted in figure 2. For all voltages, the capacitance fading becomes negligible after several hundred cycles. The initial drop, however, is more pronounced at the higher voltages. After 600 cycles between 0 and 1.1 V the overall capacitance loss amounts to 9.5 %.

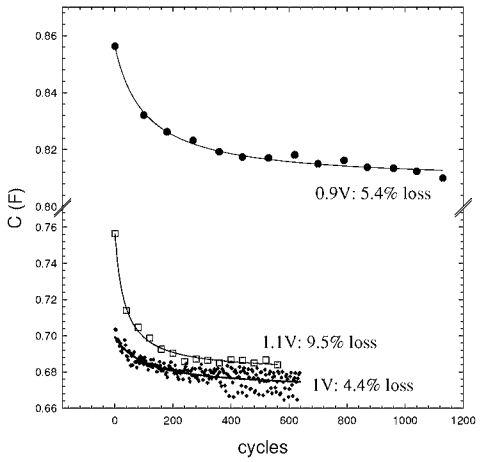

Fig.2: *Evolution of capacitance for three capacitors under cycling at three different maximum cell voltages. Electrolyte: 3 M H_2SO_4. Scan rate: 10 mV/s.*

These results show that hydrous RuO_2 is an attractive supercapacitor electrode material in terms of specific capacity and cycle stability. However, due to the high cost of ruthenium and the low decomposition voltage of the aqueous electrolyte, possible technical application will be restricted to small devices with low energy content.

References

[1] J. P. Zheng, P. J. Cygan and T. R. Jow, J. Electrochem. Soc.**142**, 8, 2699 (1995).

[2] A. Foelske; O. Barbieri; M. Hahn; R. Kötz, Electrochemical and Solid State Letters **9**, A268 (2006).

[3] W. Sugimoto, H. Iwata, K. Yokoshima, Y. Murakami, Y. Takasu, J. Phys. Chem. B **109**, 7330 (2005).

[4] C.-C. Hu, W.-C. Chen, and K.-H. Chang, J. Electrochem. Soc. **151**, A281 (2004).

HYDROUS RUTHENIUM OXIDE FOR ELECTROCHEMICAL CAPACITORS: AN XPS STUDY

A. Foelske, O. Barbieri, M. Hahn, R. Kötz
+41(0)56 310 4193
annette.foelske@psi.ch

Hydrous ruthenium oxide (RuO_2•xH_2O) is of great interest for electrochemical capacitors. In 3 M H_2SO_4 electrolyte the amorphous powder can provide specific capacitance values as high as 720 F/g under certain preparation conditions. One important parameter is the water content, and therefore the annealing temperature of the prepared powder. In order to investigate the influence of the annealing process on the chemical composition we performed XPS investigations of hydrous ruthenium oxide powders with a specific capacitance of 100-750 F/g. The determined water content is compared to the one obtained from weight loss measurements.

Experimental

Details of the preparation procedure and dependence of the electrochemical capacitance on the annealing temperature can be found in [1] and references therein. For the X-ray Photoelectron Spectroscopy (XPS) studies the hydrous ruthenium oxide powders were pressed between two cylindrical graphite pieces, glued to a sample holder, and subsequently transferred into the ultra high vacuum (UHV). Measurements were carried out with a monochromatic Al Ka X-ray source operated at a power of 200 W (10 kV, 20 mA).

Results

In order to quantify the different oxide species (H_2O, OH^- and O^{2-}) in dependence of the annealing temperature, the O 1s spectra were deconvoluted as shown in Fig. 1 for a sample heated at T = 250 °C.

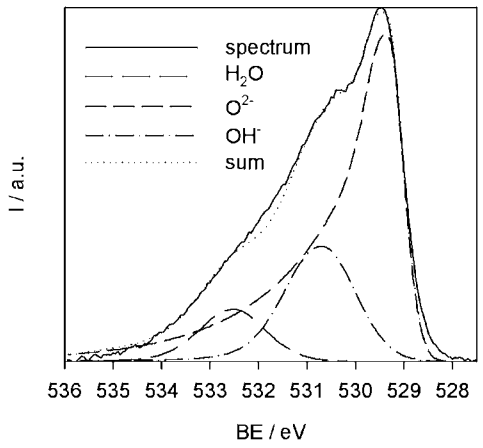

Fig. 1: *Deconvolution of the O1s signal from hydrous ruthenium oxide annealed at T = 250 °C for t = 17 h.*

Fig. 2 compares the water amount determined by XPS analysis with the one determined from the weight loss after heat treatment. The data reveal that for the materials annealed at lower temperatures less water is detected in the O 1s XP-signal than expected. At T > 160 °C the XPS results are in very good agreement with the calculation from weight loss measurements. Fig. 2 also depicts the changes of the ratio of ruthenium and oxygen in dependence of the annealing temperature. The ratio increases continuously from 0.27 (T = 25 °C) to 0.47 (T = 300 °C). In contrast, for the XPS analysis (black dots) only a slight increase of the ratio can be observed.

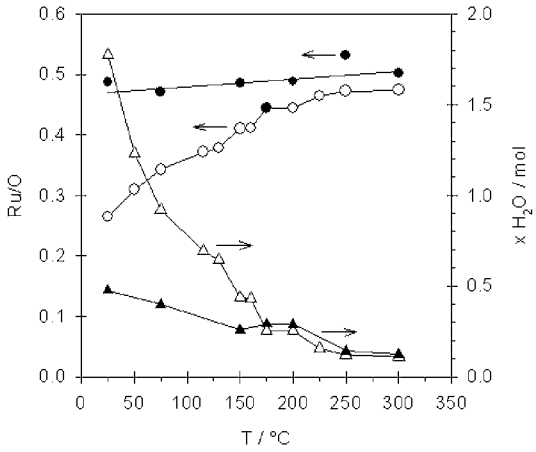

Fig. 2: *Comparison of the Ru/O ratio and water amount determined by gravimetric and XPS analysis; circles: ratio of ruthenium and oxygen (open symbols: gravimetric analysis; filled symbols: XPS analysis); triangles: x(H_2O) in RuO_2•xH_2O (open symbols: gravimetric analysis; filled symbols: XPS analysis).*

According to a model of Sugimoto et al. [2] the water is bound to material in two ways: chemically bound and physically adsorbed. Additionally, the size and the packing of the particles depend on the annealing temperature. Hydrous RuO_2•$0.5H_2O$ consists of small (2 nm) and loosely packed particles, whereas anhydrous RuO_2 consists of large (20 nm) and densely packed particles [2]. Our findings are in agreement with this model, as one can expect that the physically adsorbed water of hydrous RuO_2 evaporates under UHV conditions and therefore is not detected in the O 1s XP-signal. In contrast the chemically adsorbed water is detected. With the increase of particle size the number of adsorption sites at the surface decreases which leads to the observed decrease of water amount in the O1s signal with increasing annealing temperature.

References

[1] A. Foelske, O. Barbieri, M. Hahn, R. Kötz, Electrochem. Solid-State Lett. **9,** in print (2006).

[2] W. Sugimoto, H. Iwata, K. Yokoshima, Y. Murakami, Y. Takasu, J. Phys. Chem. B **109**, 7330 (2005).

TAILOR MADE NANO PARTICLES FOR BATTERIES BY FLAME SPRAY PYROLYSIS

J. Ufheil, F. O. Ernst[1], H. Buqa, S. E. Pratsinis[3], P. Novák
+41(0)56 310 2103
joachim.ufheil@psi.ch

Nanotechnology is becoming important for battery applications. It is well known that with decreasing size nano particles could change their abilities in respect to macro particles. For this, electroactive materials like, e.g., $LiMn_2O_4$ are of great interest for the improvement of lithium ion batteries because the small dimensions reduce diffusion lengths within the particles and the high specific surface area increases the number of active sites for surface active reactions. In addition, the local current density should be decreased as well, and for that reason the overpotential should be low and therefore higher charging/discharging rates are expected. However, not only the particle size is of general interest. Particles covered with other materials or hollow particles open a wide field of investigation. Production of these nano particles can be easy performed by a flame spray pyrolysis process.

Experimental

Figure 1 shows the experimental setup for the synthesis of nanoscale powders by flame spray pyrolysis (FSP) [1]. The organometallic precursors were dissolved in an organic solvent with a certain metal ion concentration. This precursor was fed into the reactor by a syringe pump and dispersed into fine droplets by a gas-assist nozzle. The spray was ignited and maintained by a flame ring of a methane/oxygen mixture surrounding the spray capillary. In addition, an oxygen flame surrounds the setup to assure the complete conversion of the reactants. The liquid feed rate and the dispersion oxygen flow rate were varied in order to adjust the product particle size which could be collected on a glass fiber filter.

A number of electroactive materials like Co_3O_4, Mn_3O_4, $LiMn_2O_4$, $Li_4Ti_5O_{12}$, and $LiFe_3O_4$ with spinel structure (normal, normal distorted, mixed, and mixed inverse) were produced by a flame spray pyrolysis process. The purity of the obtained powders of controlled size in the range from 8 to 30 nm was verified by X-ray diffraction. Sinter experiments showed high temperature stability of these powders produced at rates of 10 to 20 g/h.

The electrochemical properties as measured by slow scan cyclic voltammetry and charge/discharge cycling tests are reported here for one example, the nano $LiMn_2O_4$ particles as possible cathode materials in secondary lithium-ion batteries. For the characterization the nano particles were mixed with carbon black, polyvinylidenefluoride, and N-methylpyrrolidone. This slurry was doctor-bladed on a copper foil to form an electroactive and easy-treatable film. Circular working electrodes of 13 mm diameter were punched out from the coated sheets and then vacuum-dried overnight. In most cases, electrochemical experiments were performed in two-electrode arrangement in standard laboratory cells described elsewhere [2]. Lithium foils were used as the counter and also as the reference electrode, a glass fleece membrane as separator, and EC/PC 1:1 with 1 M $LiPF_6$ as electrolyte.

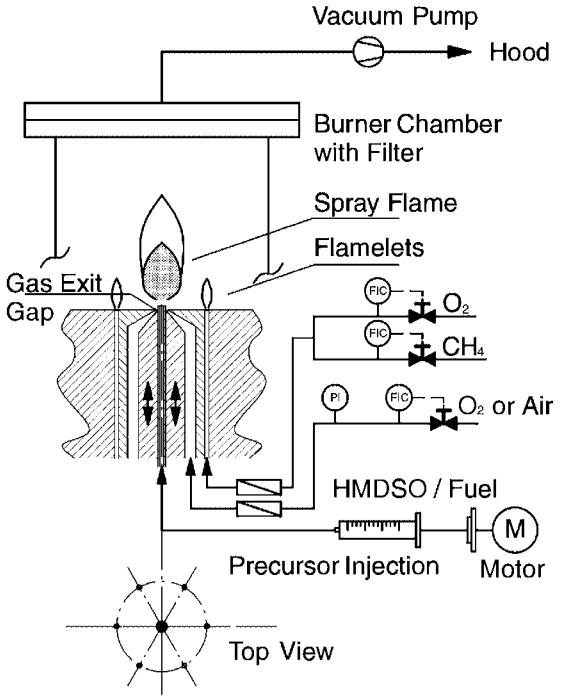

Fig. 1: *Experimental set-up of flame spray pyrolysis.*

Results

Figure 2 shows the XRD and the corresponding TEM image (inset) of as-prepared $LiMn_2O_4$.

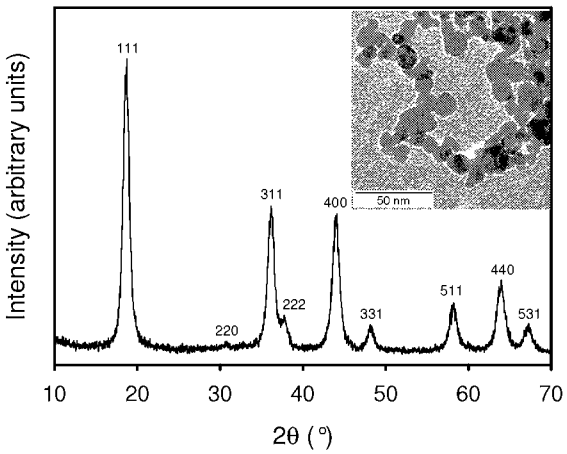

Fig. 2: *X-ray diffraction patterns of as-prepared normal spinel $LiMn_2O_4$. The main diffraction peaks are marked with their corresponding hkl indices. The inset shows a TEM image of the product powder with particle sizes in the nanometer range.*

[1] *ETH Zürich*

This powder contains no XRD-detectable impurities and the d_{XRD} is 11 nm, while the corresponding d_{BET} is 11 nm, indicating monocrystalline particles.

By varying the precursor feed rate from 3 to 8 mL/min and the dispersion gas from 6 to 3 L/min and increasing the precursor concentration up to 1.8 M, particle sizes from 7 nm (200 m^2/g) to 22 nm (65 m^2/g) were produced. The d_{BET} and d_{XRD} were always in close agreement and the phases produced were XRD-free of impurities (pattern not shown). This possibility in controlling the size of nanoparticles is representative for all powders produced here.

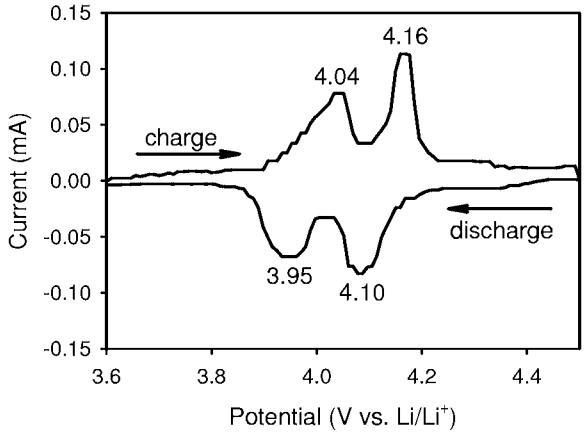

Fig. 3: *Cyclic voltammogram of $LiMn_2O_4$ recorded at 0.02 mV s^{-1} from 3.6 to 4.5 V vs. Li/Li^+ in EC/PC 1:1 with 1 M $LiPF_6$. The clearly separated pairs of oxidation and reduction peaks are characteristic for materials with a high degree of crystallinity.*

Figure 3 shows a slow scan cyclic voltammogram recorded at a scan rate of 0.02 mV/s for the $LiMn_2O_4$ sample shown in Figure 2. The charging and discharging pairs of peaks reflect the reversible oxidation and reduction reactions corresponding to lithium extraction and insertion, respectively, taking place as expected in two stages. The first peak at about 4.04 V is attributed to the removal of lithium ions from half of the tetrahedral sites in which Li-Li interactions occur. The second peak observed at about 4.16 V is caused by the removal of lithium ions from the other tetrahedral sites in which lithium ions do not have Li-Li interactions. The areas of the two oxidation and reduction peaks are essentially equal indicating that in each stage lithium ions occupy half of the total available crystallographic sites. The peaks are rather sharp and show well-defined splitting. These are the characteristics of materials with high degree of crystallinity.

Figure 4 shows charge/discharge cycling behavior as recorded with a rate of 5 µA/mg for the first cycle and 50 µA/mg for the following cycles. The specific charge seems to decrease to a limit value of approximately 77 Ah/kg. This relatively low value in contrast to commercial manganese spinels could be lead back that not all nano particles are well contacted with conductive additive carbon black.

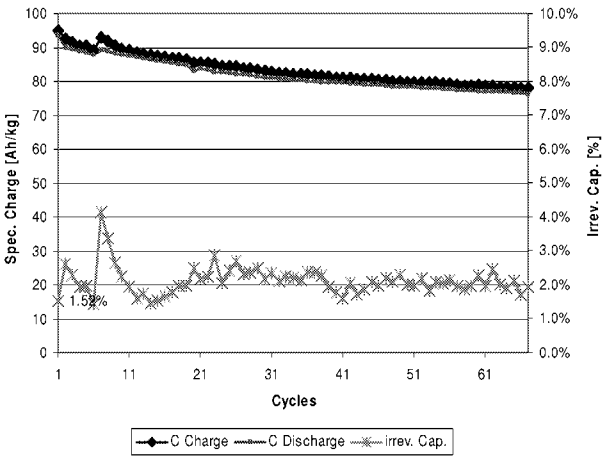

Fig. 4: *Typical charge/discharge cycling behaviour of nano particles of $LiMn_2O_4$ in EC/PC 1:1 with 1 M $LiPF_6$.*

Conclusions

Flame spray pyrolysis was used to make nano-sized, spinel-structured materials exemplified here with lithiated normal spinel ($LiMn_2O_4$). The fine control on the SSA (specific surface area), as typical for FSP, was used to representatively produce electrochemically active $LiMn_2O_4$ from 200 to 65 m^2/g by changing the precursor flow rate, initial metal ion concentration, and the dispersion gas flow rate. Its electrochemical activity was confirmed by cyclic voltammetry. Product particle stoichiometry and phase composition can be controlled by the Li/Me ratio as shown elsewhere [3]. Its electrochemical activity was demonstrated also for this potential battery anode material by cyclic voltammetry. Our work shows that, electrochemical active nano particles produced by flame spray pyrolysis could be used in lithium-ion batteries not only for their electrochemical properties but also because they could be fast and cost-effective produced.

References

[1] L. Madler, H.K. Kammler, R. Mueller, S.E. Pratsinis, Aerosol Science **33**, 369 (2002).

[2] P. Novák, W. Scheifele, F. Joho, O. Haas, J. Electrochem. Soc. **142**, 2544 (1995).

[3] F.O. Ernst, H.K. Kammler, A. Roessler, S.E. Pratsinis, W.J. Stark, J. Ufheil, P. Novák, Materials Chemistry and Physics, submitted.

A NEW TYPE OF NANO-SIZED SILICON/CARBON COMPOSITE ELECTRODE FOR REVERSIBLE LITHIUM STORAGE

M. Holzapfel, H. Buqa, W. Scheifele, P. Novák; F.-M. Petrat[1]
+41(0)56 310 2116
michael.holzapfel@psi.ch

Lithium-ion batteries are among the most useful devices for electrochemical energy storage, because of their high specific energy (more than 170 Wh/kg) and very high efficiency (up to 95% overall), which lets their use in electric vehicles (EVs) and hybrid-electric vehicles (HEVs) an option for the future.

The material mostly used for the negative electrode is graphitic carbon which suffers from a relatively low electrochemical specific charge (theoretical value: 372 mAh/g). Since many years, therefore, research has been conducted to find alternative negative electrode materials, above all in the field of lithium-metal alloys, as lithium-silicon [1-3]. They can show a very high theoretic specific charge of approx. 4200 mAh/g. Nevertheless, the insertion (alloying) of lithium is accompanied by a huge volume change which leads to strong mechanical stress on the crystallites and, thus, to breaking and amorphisation of the particles and loss of the electrical contact [4-6].

A reduction of both, the particle and the crystallite size into the nm-range should have a positive influence on the cycling behaviour. In this study, we present a nano-scale silicon material prepared by reductive decomposition of a silicon precursor and the results obtained on its electrochemical cycling in graphite/silicon composite electrodes. This composite shows impressive results with respect to its very high reversible charge capacity and low irreversible capacity upon prolonged cycling and both, long cycle life and low fading.

Experimental

Scanning electron microscopy (SEM) was conducted at 5 keV using in-lense detection. The electrodes were prepared as follows: the silicon material (20 wt%) is mixed with 70 wt% of a small particle size graphite (TIMREX® KS6, TIMCAL SA, Bodio, Switzerland) (8 wt%) and 10% of SOLEF® PVdF 1015 binder (Solvay SA, Belgium) in a N-methylpyrrolidone solution, mixed thoroughly and cast on a pre-treated (with a polymer based primer from Contitech, Nordhausen, Germany) copper foil which serves as current collector. Lithium metal is used as counter electrode. The electrolyte used is a battery grade mixture of ethylene carbonate (EC) and dimethyl carbonate (DMC) (1:1), with 1M $LiPF_6$ to which 2% of vinylene carbonate (VC) were added. The electrochemical measurements were conducted using a galvanostatic-potentiostatic protocol with a computer-controlled cell capture system CCCC (Astrol Electronics AG, Oberrohrdorf, Switzerland).

Results and discussion

The nano-silicon material is obtained as highly structured aggregates with primary particles in the order of 50 nm with a specific BET surface area of 12 m^2/g. The SEM image of the composite electrode, using 20 wt% of nano-silicon (Figure 1) shows a homogeneous mixture of the silicon particles and the graphite matrix.

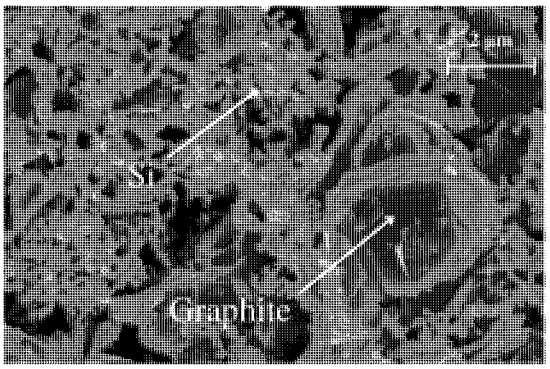

Fig. 1: *SEM-image of the nano-silicon/graphite composite electrodes.*

Figure 2 shows the cycling behaviour of the 20% Si composite electrode. Using a non-restricted cycling procedure an initial specific charge of 1350 mAh/g of active material (Si + graphite) is obtained whereas the specific charge for the following discharge is ~ 900 - 1000 mAh/g. This shows that, even when taking into account the specific charge of the graphite matrix itself (about 430 mAh/g for the first reduction), the nano silicon inserts about the theoretical amount of lithium.

Upon the delithiation the impressive amount of 3200 mAh/g is liberated from the silicon part of the electrode. This shows the beneficial effect of the presence of the large amount of graphite to accommodate the volume change of the silicon. The irreversible capacity (Q_{irrev}) loss upon the first cycle is about 26%. The fading of the reversible charge capacity for continued cycling is low.

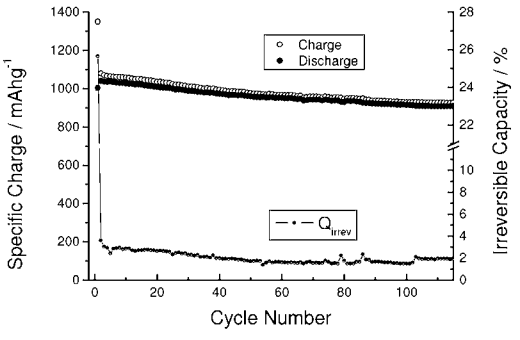

F

Fig. 2: *Cycling behaviour of a composite electrode with 20% nano-silicon in EC:DMC (1:1), 1M $LiPF_6$, 2% VC.*

[1] *Degussa AG, 45764 Marl, Germany*

The present results are new when compared to literature data where stable cycling with about 1000 mAh/g are seldom obtained for macroscopic electrodes. If so, it is for a smaller number of cycles [7,8]. Our material seems, hence, to show a much smaller mechanical degradation upon the intercalation/deintercalation process when compared to traditional silicon material. This is probably due to the very small particle size and the good interaction with the supporting graphite matrix.

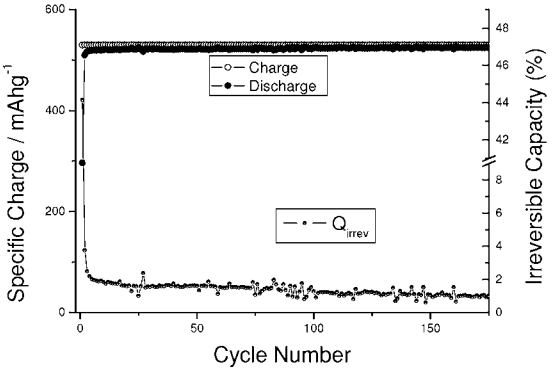

Fig. 3: Cycling behaviour of a composite electrode with 20% nano-silicon in the capacity-limited mode in EC:DMC (1:1), 1M $LiPF_6$.

We also tried a second cycling procedure, consisting in the deliberate fixation of the charge capacity. It is set to 530 mAh/g in this case (which corresponds to about 1.5 times the capacity of graphite), while keeping free the discharge capacity. The typical result of such an experiment is shown in Figure 3. The cycling can be maintained in a stable manner for more than 170 cycles. By this way the mechanical stress on the nano-silicon particle is somewhat reduced, as the reversible charge capacity, calculated for the silicon part of the electrode is of the order of 1000 – 1100 mAh/g. In effect, as the scanning electron micrograph in Figure 4 (obtained after 75 cycles at the capacity controlled regime) shows, the integrity of the electrode is unaltered and only the formation of a homogeneous passivation film can be acknowledged.

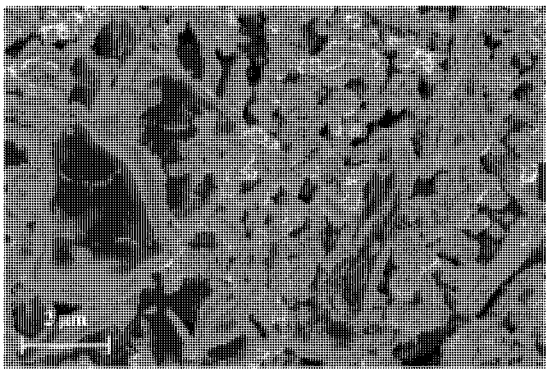

Fig. 4: *SEM-image of the nano-silicon/graphite composite electrode after 75 cycles in the capacity-limited mode.*

TIMCAL SA (Bodio, Switzerland) is acknowledged for supplying the graphite sample.

References

[1] W. J. Weydanz, M. Wohlfahrt-Mehrens, M. Winter, J. Power Sources **82**, 237 (1999).

[2] R. N. Seefurth, R. A. Sharma, J. Electrochem. Soc. **124**, 1207 (1977).

[3] T. D. Hatchard, J. R. Dahn, J. Electrochem. Soc. **151**, A838 (2004).

[4] M. Winter, J. O. Besenhard, M. E. Spahr, P. Novák, Adv. Mater. **10**, 725 (1998).

[5] J. Yang, M. Winter, J. O. Besenhard, Solid State Ion. **90**, 281 (1996).

[6] S. Bourderau, T. Brousse, D. M. Schleich, J. Power Sources **82**, 233 (1999).

[7] G. X. Wang, J. Yao, H. K. Liu, Electrochem. Solid State Lett. **7**, A250 (2004).

[8] Y. Liu, K. Hanai, J. Yang, N. Imanishi, A. Hirano, Y. Takeda, Solid State Ion. **168**, 61 (2004).

NOVEL MONOMERS FOR RADIATION GRAFTED FUEL CELL MEMBRANES

M. Slaski, L. Gubler, A. Wokaun, G.G. Scherer
+41(0)56 310 4003
michal.slaski@psi.ch

Radiation grafted fuel cell membranes based on pre-irradiation grafting of α-methylstyrene (AMS) and methacrylonitrile (MAN) have shown superior stability in fuel cells as compared to well known membranes based on styrene [1, 2]. The solvent influence on graft level and film composition is reported in this work.

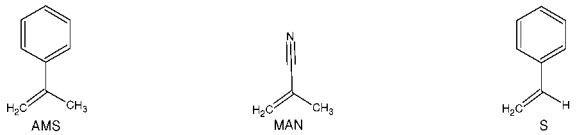

Fig. 1: *Structure formula of α-methylstyrene (AMS), methacrylonitrile (MAN), and styrene (S).*

Experimental

Poly(tetrafluoroethylene-*co*-hexafluoropropylene) (FEP) films (25 µm, DuPont) were e-beam irradiated in the presence of air with a dose of 25 kGy. The irradiated films were stored at -80ºC until used. In preparation of an experiment, films were taken from the freezer to room temperature and placed in the tube-type reactor (about 1g of film in 60 ml reactor). The reactors were filled with grafting solution containing monomers and a solvent. Monomers were used in a molar ratio of 1.5 (AMS/MAN). The reactors were purged with nitrogen for 1 h, then sealed and placed in a water bath for 22 h at 60º C. After the reaction, the reacting mixture was removed and films were washed with acetone. The dried films were weighed to determine the graft level given via the equation:

$$Graft\ Level = \frac{mass_{substrate} - mass_{product}}{mass_{substrate}} \cdot 100\%$$

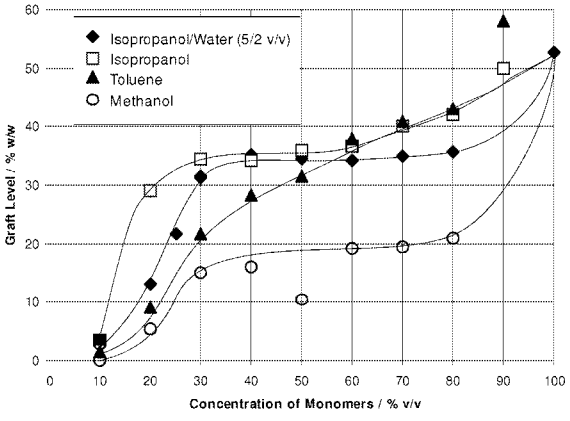

Fig. 2: *Graft level as a function of monomer concentration for four solvent systems (monomers = both AMS and MAN).*

The grafted films were investigated with FTIR spectroscopy for quantitative analysis of the graft components AMS and MAN.

Results & Discussions

The graft level was found to be dependent on monomer concentration (Fig. 2) and type of solvent. The highest graft level was obtained for the sample grafted without a solvent. Surprisingly, the lowest graft level was obtained with methanol as a solvent, not with toluene. The opposite effect was found by Rager [3] for styrene grafted onto FEP, where higher graft levels were obtained with methanol as solvent as compared to toluene.

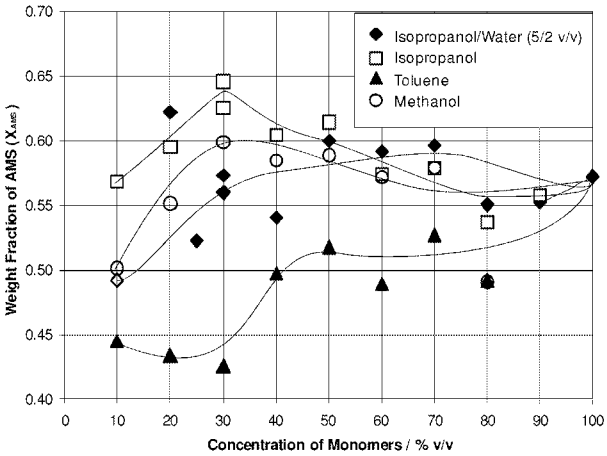

Fig. 3: *AMS weight fraction in the grafted AMS:MAN copolymer for four solvent systems as a function of monomer concentration in the grafting solution.*

The monomer concentration as well as the type of solvent was found to have an influence on film composition (Fig. 3). The highest AMS fraction was found in the sample grafted in isopropanol/water mixture at 30 % monomer concentration. For less polar solvents, such as isopropanol and methanol, the AMS fractions are moderate. The lowest AMS concentration was obtained with toluene as a solvent with the lowest polarity.

Conclusions

Solvent polarity has an influence on both film composition and graft level. A highly polar solvent, such as a mixture of isopropanol and water, increases the monomer concentration in the film by influencing the partitioning coefficient. A polar solvent tends to increase the concentration of a non-polar monomer such as AMS in the film. Consequently, the graft level increases, if a polar solvent is used, except for methanol.

References

[1] L. Gubler, M. Slaski, G.G. Scherer, A. Wokaun, this report.

[2] M. Slaski, L Gubler, G.G Scherer, European Patent Application EP 05002875.

[3] T. Rager, Helv. Chim. Acta **86**, 1966 (2003).

CHARACTERIZATION OF SURFACE PROCESSES AT CATALYSTS EXPOSED TO BIOMASS-DERIVED SYNTHESIS GAS

I. Czekaj, F. Raimondi, J. Wambach, A. Wokaun
+41(0)56 310 4464
izabela.czekaj@psi.ch

The surface modifications of a commercial Ni/Al_2O_3 catalyst during the production of methane from synthesis gas were investigated by *quasi in-situ* X-ray photoelectron spectroscopy (XPS). The effect of the synthesis gas on the surface properties of the catalyst and on its activity under methanation conditions was studied on atomic level. Additionally, composition of other commercial catalysts, e.g. for desulphurization of biomass-derived synthesis gas, were investigated.

Results and Discussion

Using our high pressure cell (HPC) [1], XPS studies on Ni/Al_2O_3 catalysts under fixed-bed conditions were made and a detailed investigation at molecular level of the surface Ni-particles modifications was done (see Figures 1, 2 and 3).

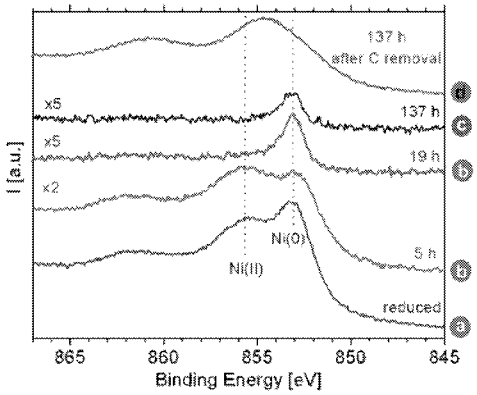

Fig. 1: *Comparison of XP spectra (Ni $2p_{3/2}$ region) showing the surface changes during a methanation run on a Ni/Al_2O_3 catalyst.*

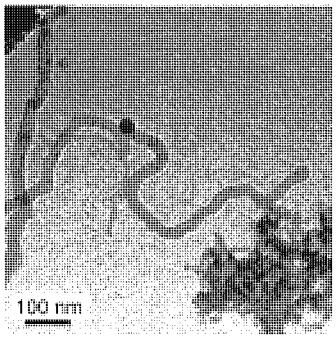

Fig. 2 *HR-TEM image showing carbon whiskers. Black dots: Ni clusters.*

The fresh catalyst surface consisted of different Ni particles both in oxidized + hydratized form. Activation under H_2 lead to a partial reduction of the surface Ni(II) species forming Ni^0. The reactive surface consisted of Ni^0 and NiO_x particles. During the methanation process (reaction of mainly CO + CO_2 with H_2), the surface became decorated with carbon species, which under fixed bed-conditions resulted even in a severe C-whiskers formation detaching Ni-particles from the support (see the HR-TEM image). Mechanically the formed carbon was removed easily. Figure 3 summarises the suggested surface processes.

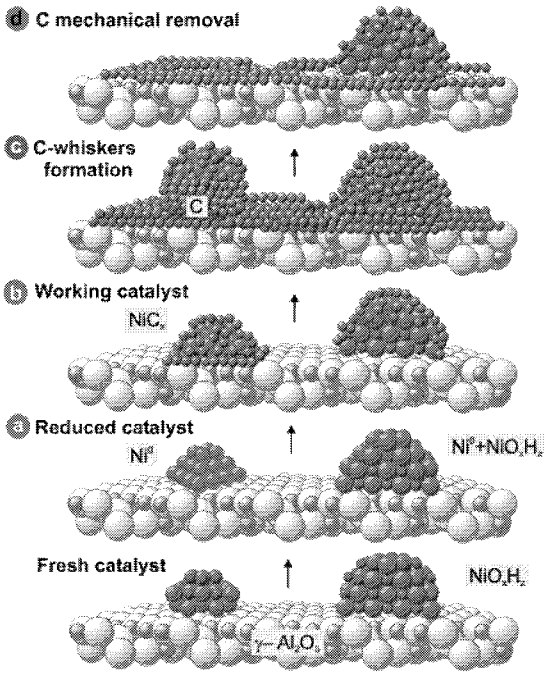

Fig. 3: *Suggested mechanism of processes during methanation at Ni/Al_2O_3 surface.*

Additionally, several series of XPS measurement were done, including: i) commercial Ni/Al_2O_3 catalyst samples in different phases of deactivation, ii) catalysts used in preliminary desulphurization processes: ZnO and $Mg/CaCO_3$, $CoMoO_x$, iii) nickel carbide samples. From detailed XPS analysis of catalysts in different phases of deactivation, it was possible to link the catalyst with a) a carbon deposition at the surface, and b) with a slight uptake of S species. Sulphur as one of the most active catalyst poison can effectively block active Ni^0 centres leading to a deactivation. The origin of the sulphur is not known yet.

Conclusions

Future investigations are planned for distinguishing different carbon components at the catalyst surface by e.g. vibrational spectroscopic methods (IR and Raman experiments), as well as theoretical modelling of the Ni-based catalysts surface and of the mechanisms of the molecule adsorption and reaction. The theoretical modelling is presently using Density Functional Theory with cluster models.

References

[1] F. Raimondi, M. Seemann, S. Biollaz, J. Wambach, A. Wokaun, PSI Scientific Reports 2003, **V**, 116 (2004).

FILM FORMATION ON ELECTRODE MATERIALS IN LITHIUM-ION BATTERIES

H. Buqa, M. Holzapfel, A. Würsig,
F. Krumeich[1], M. E. Spahr[2], P. Novák
+41(0)56 310 4406
hilmi.buqa@@psi.ch

The successful operation of Li-ion batteries is attributed mainly to the surface films on carbonaceous anode materials called Solid Electrolyte Interphase (SEI) [1]. A similar protective film has also been reported for cathode materials such as $LiMn_2O_4$, $LiCoO_2$, and $LiNiO_2$, but the discussion about the SEI on positive electrodes is still controversial and the parameters influencing the formation of this film are still a matter of intense investigation [2]. The identification of the material parameters that influence the SEI formation will be an important achievement to facilitate further improvements of the electrode materials for lithium-ion batteries. In recent years, there have been numerous investigations of SEI-related phenomena and this field is an ongoing topic of research [3].

In order to get a direct view on the surface of the negative and positive electrode in lithium-ion batteries, which allows to observe and to classify the SEI, post mortem scanning electron microscopy (SEM) analyses were performed in this work.

Experimental

The negative electrodes were prepared by blade-coating the TIMREX® SFG44 graphite (TIMCAL SA, Bodio) on a copper foil. 10 wt% polyvinylidene difluoride (SOLEF 1015, Solvay SA) was used as binder. The positive electrodes were prepared by blade-coating the oxide on an aluminum foil. They were composed of 85.7 wt% active mass ($LiCoO_2$, Ferro GmbH), 4.75 wt% Oppanol binder (B200, BASF AG), and 9.55 wt% mixture of carbon black (Ensaco® 250, 15 wt%) and graphite (TIMREX® MB15, 85 wt%). Before the cell assembly, the electrode as well as the glass fibre separator were dried at 120 °C under vacuum for 12 h and then stored in a dry argon atmosphere.

The graphite electrodes for the post mortem scanning electron microscopy (SEM) studies were first galvanostatically charged at 10 mA/g to 0.3 V vs. Li/Li^+, and were then equilibrated at this potential for 48 h as described elsewhere [4]. Unless otherwise stated, a galvanostatic charge of the oxide electrodes was performed with a specific current of 50 mA/g of oxide. After a potential of 4.3 V vs. Li/Li^+ was reached in the first galvanostatic Li^+ deintercalation, the charge was continued potentiostatically until the specific current dropped below 10 mA/g. The cells were then dismantled, the electrodes washed thoroughly twice with dry DMC (dimethyl carbonate), and dried over night in an argon filled glove box [4].

Post mortem scanning electron microscopy was performed on a LEO 1530 Gemini microscope, which was operated at low voltage (usually 1 kV) to achieve a suitable contrast of the surface details in the secondary electron images and to minimise charging of the uncoated samples. The electrodes were mounted on stubs. The acquisition of the SEM images was performed using the secondary electron detector in order to optimise the topographical information.

SEI Film Formation on Graphite Electrodes

An interesting approach to improve graphite electrodes for their use in lithium-ion batteries is the mixing of graphite with small amounts of conductive carbon materials and to use highly active film forming additives. Conductive carbon black or graphite can enhance the electrode conductivity. The film forming additives could enforce the protection against the continued reduction of the electrolyte itself at the surface of the low potential graphite. In most cases the additives form a stable film before the reduction of the electrolyte itself takes place. In Figure 1 we present a result demonstrating the stable cycling over 500 cycles, with only very small capacity fading, of an optimised SFG44 graphite electrode with carbon black in EC (ethylene carbonate) /DMC (1/1), 1 M $LiPF_6$ electrolyte containing 2 % VC (vinylene carbonate).

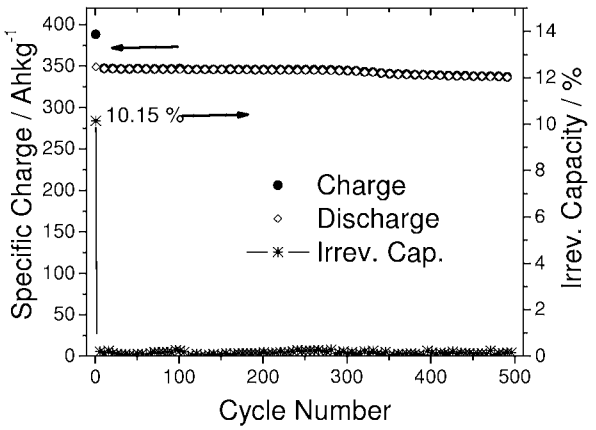

Fig. 1: *Cycling performance and irreversible capacity loss of an optimised TIMREX® SFG44 graphite electrode measured vs. Li. Electrolyte: EC/DMC (1/1) with 2% VC, 1 M $LiPF_6$.*

In order to address the question of the nature of the film formed on the surface, we performed a SEM study. Figure 2 shows a SEM image of optimised TIMREX® SFG44 graphite electrode (with carbon black as conductive additive) after cathodic polarisation to a limit of 0.3 V vs. Li/Li^+ in an EC/DMC (1/1) with 2% VC, 1M LiPF6. At 0.3 V the formation of the surface film can be considered to be complete. The specific current passing below this limit is mostly related to the intercalation of lithium into the graphite host.

[1] *ETH Zürich*
[2] *Timcal SA, 6743 Bodio*

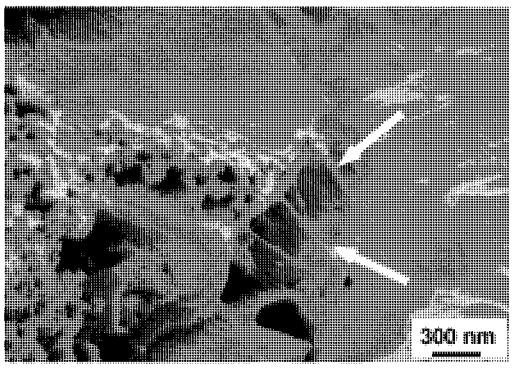

Fig. 2: *Post mortem SEM-image of an optimised TIMREX® SFG44 electrode stabilised at 0.3 V vs. Li/Li⁺ in EC/DMC (1/1) with 2% VC, 1 M $LiPF_6$.*

The image of the electrode shows a uniform and relatively dense film on the surface of the graphite particles, obviously the passivation film formed by the products originating from the electrolyte decomposition during the electrochemical reduction process. Furthermore, the polymer-like nature of the SEI formed under these conditions becomes obvious, since filament-like connections between the graphite layers (indicated by arrows) can be observed. Due to functional SEI-film formed on the graphite surface, it is possible to cycle the electrode for over 500 cycles as shown in Figure 1.

SEI Film Formation on Oxide Electrodes

Figure 3 shows the surface of an uncycled $LiCoO_2$ oxide electrode. One can distinguish between single oxide particles, small grains consisting of carbon black adhering at the oxide and several graphite flakes.

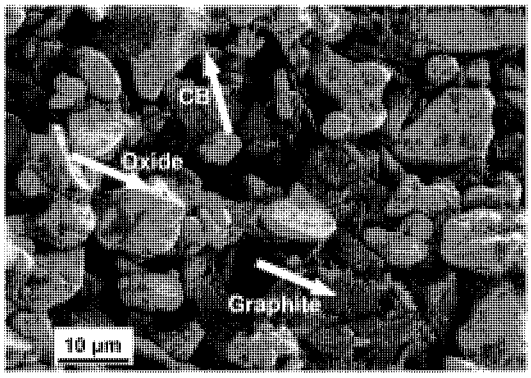

Fig. 3: *SEM-image of an $LiCoO_2$ electrode (uncycled). The arrows indicate the oxide particles, carbon black grains (CB) on the oxide surface, and graphite flakes in between.*

In order to probe the expected SEI formation on the positive electrode, $LiCoO_2$ electrodes were cycled vs. Li in a half cell with different electrolyte solutions. Figure 4 shows the post mortem SEM image of a $LiCoO_2$ electrode in EC/PC (1/1), 1M $LiPF_6$ electrolyte. The surface of the oxide particles is crumbled, and a film can be identified between the grains.

As is already known from studies of the SEI formation on anode materials, additives can be used to enhance the chemical characteristics of the surface. This leads to an improved performance of the material.

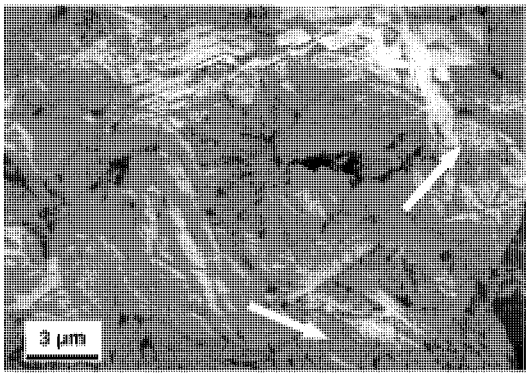

Fig. 4: *Post mortem SEM-image of an $LiCoO_2$ electrode stabilised at 4.3 V vs. Li/Li⁺ in EC/PC (1/1), 1M $LiPF_6$. The arrows are pointing to the SEI layer between the oxide crevices.*

Figure 5 shows the result of a film forming process on $LiCoO_2$ if 2% vinylene carbonate is added to the electrolyte EC/PC (1/1), 1M $LiPF_6$. A porous film could be observed on the oxide surface. It is very likely that in this case the film consists of reaction products of the polymerisation of VC, as can be observed in the case of the reduction of VC at the surface of graphite negative electrode material.

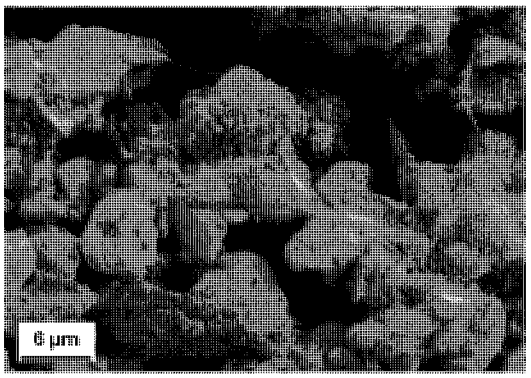

Fig. 5: *Post mortem SEM-image of an $LiCoO_2$ electrode stabilized at 4.3 V vs. Li/Li⁺ in the electrolyte EC/PC (1/1) with 2% VC, 1M $LiPF_6$.*

References

[1] E. Peled, J. Electrochem. Soc. **126,** 2047 (1979).

[2] D. Aurbach, K. Gamolsky, B. Markovsky, G. Salitra, Y. Gofer, U. Heider, R. Oesten, M. Schmidt, J. Electrochem. Soc. **147,** 1322 (2000).

[3] F. Kong, R. Kostecki, G. Nadeau, X. Song, K. Zaghib, K. Kinoshita, F. McLarnon, J. Power Sources **58**, 97 (1998).

[4] M. E. Spahr, T. Palladino, H. Wilhelm, A. Würsig, D. Goers, H. Buqa, M. Holzapfel, P. Novák, J. Electrochem. Soc., **151**, A1383 (2004).

OXYGEN REDUCTION REACTION IN POLYMER ELECTROLYTE FUEL CELLS

H. Kuhn, A. Wokaun, G.G. Scherer
+41(0)56 310 2350
holger.kuhn@psi.ch

The oxygen reduction reaction (ORR) is accounted for to be the limiting process in polymer electrolyte fuel cells (PEFCs) at high cell potentials, due to the slow kinetics. For a deeper understanding of this process and to further improve the performance of fuel cells, suitable experiments and in addition a model is needed to explain the ORR kinetics. With the pseudo reference electrode arrangement the single electrode reactions are accessible independently, hence allowing electrochemical impedance spectroscopy (EIS) to characterize electrode kinetics. The model itself provides a reaction mechanism by which it is possible to assign single reaction steps.

Experimental

The detailed experimental setup is explained elsewhere [1].

Model, Simulation, and Validation

Contrary to the hydrogen oxidation reaction (HOR), the ORR is still under discussion in the literature, but always following a proposed pathway by Damjanovic [2] or Wroblowa [3]. All pathways have in common that they consider two adsorbed species on the catalyst surface. We consider the following pathway for low current densities [4,5] and the corresponding reaction rates $\nu_{1\text{-}4}$

$$O_2 \leftrightarrow 2O_{ad} \quad (1)$$

$$O_{ad} + e^- \leftrightarrow O_{ad}^- \quad (2)$$

$$O_{ad}^- + H^+ \leftrightarrow OH_{ad} \quad (3)$$

$$OH_{ad} + H^+ + e^- \leftrightarrow H_2O \quad (4)$$

$$\nu_1 = k_1(1-\theta_O-\theta_H)^2 - k_2\theta_O^2 \quad (5)$$

$$\nu_2 = k_3\theta_O \quad (6)$$

$$\nu_3 = k_4\theta_O \quad (7)$$

$$\nu_4 = k_5\theta_{OH} - k_6(1-\theta_O-\theta_{OH}) \quad (8)$$

k_3, k_5 and k_6 are potential dependent and include constants like k_1 and k_4. The derivation of the impedance is an extension of Armstrong's kinetic theory of the two-step case [6].

Experimental data and modeling results are displayed in Figure 1. With this model as a background, we are able to denote some features of the impedance spectra to single reaction steps, which allows for a specific investigation of these steps at different electrodes. We observe a capacitive semi-circle at high frequencies, which is due to charge transfer kinetics. Even the reaction rates ν_2 and ν_4 are distinguishable. The inductive semi-circle at low frequencies can be attributed to adsorbed species, especially to reaction rates ν_1 and ν_3.

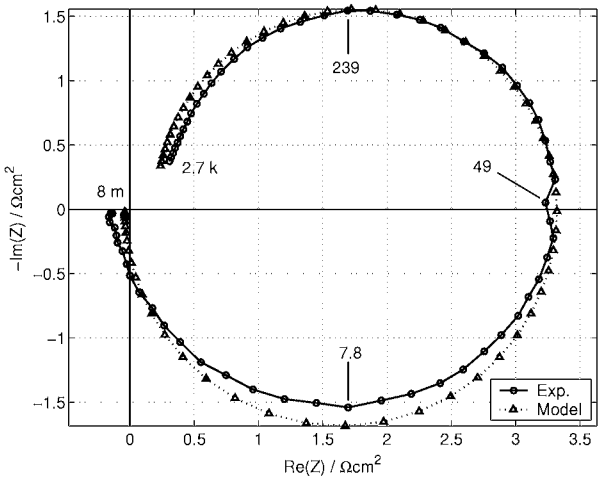

Fig. 1: *Experimental data and model results of the ORR. Single steps can be denoted to the semi-circles.*

We were able to fit a set of impedance spectra at different current densities, at different over-potentials respectively, with the same set of kinetic rate constants just by adjusting the over-potential. We found a linear relationship between the current densitiy and the potential, as it is demanded by the Butler-Volmer equation for low over-potentials.

Conclusions

The combination of established half-cell measurements in PEFC on the one hand and two models on the other hand, one for the HOR [1] and one for the ORR, allows for a detailed investigation of single electrode reactions. The reaction mechanisms may deliver a deeper insight and a better understanding of the processes at the individual electrodes within a PEFC. Investigations of electrodes of different compositions, e.g., platinum or ionomer loading, allow for an optimization of the single electrodes individually.

References

[1] H. Kuhn, B. Andreaus, A. Wokaun, G.G. Scherer, Electrochim. Acta **51**, 1622 (2006).

[2] A. Damjanovic, V. Brusic, Electrochim. Acta **12**, 615 (1967).

[3] H.S. Wroblowa, Y.C. Pan, G. Razumne., J. Electroanal. Chem. **69**, 195 (1976).

[4] H. Kuhn, A. Wokaun, G.G. Scherer, Electrochim. Acta, accepted (2006).

[5] T. Jakob, Fritz-Haber-Institut, Berlin, priv. communication (2005).

[6] R.D. Armstrong, M. Henderson, J. Electroanal. Chem. **39**, 81 (1972).

CHARACTERIZATION OF PLATINUM AND CARBON CO-SPUTTERED CATALYST LAYERS

A. Reiner, X. Wei, M. Döbeli[1], M. Horisberger, A. Wokaun, G.G. Scherer
+41(0)56 310 5165
andreas.reiner@psi.ch

The catalyst layers of today's polymer electrolyte fuel cells (PEFCs) predominantly contain platinum nanoparticles, supported on high surface area carbon. Normally, these catalysts are prepared by chemical wet impregnation methods, which have several drawbacks that could possibly be avoided by an alternative dry preparation method. Hence, the motivation for the preparation and characterization of platinum and carbon co-sputtered layers are achieving a large electrochemically active platinum surface at a simultaneously low Platinum loading. Additionally, the sputter process can have advantages related to an easy variation of Pt loading and substrate and furthermore the high compatibility to micro-fabrication processes.

Experimental

The samples were prepared by simultaneous sputtering of platinum and carbon, resulting in platinum nanoparticles dispersed in a carbon matrix [1]. Layers of different thicknesses were deposited onto glassy carbon plates. The samples have been analysed by Rutherford Backscattering Spectrometry [2] at the PSI/ETH Laboratory for Ion Beam Physics. The measurements have been performed using a 2 MeV ^{4}He beam and a silicon detector and data analysis using the RUMP software [3]. RBS can provide qualitative and quantitative information about the co-sputtered film.

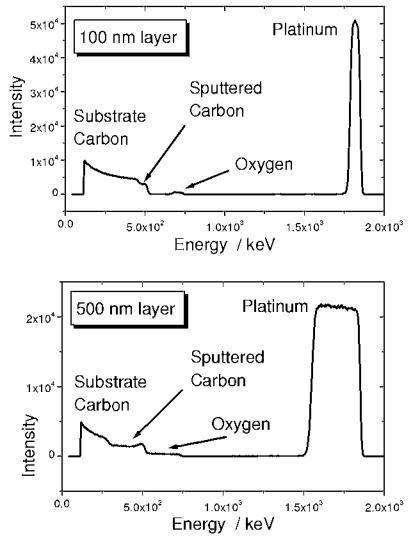

Fig. 1: *RBS measurements of co-sputtered films with thicknesses of 100 and 500 nm on glassy carbon.*

[1] ETH Zürich

Therefore, in addition to the platinum distribution within the layer, the platinum loading can also be precisely determined. The RBS spectra (intensity vs. energy of scattered ions) for two different film thicknesses are displayed in Fig. 1. The spectra show a platinum signal (between 1600 and 1800 keV) and a carbon signal (up to ca. 500 keV). It is difficult to trace the oxygen signal (between 600 and 700 keV). Impurities from copper and argon, eventually from the sputtering process, are negligible. A comparison with RUMP simulations shows that all 3 elements are more or less uniformly distributed throughout the layers (rectangular shape of the signals). The RBS data contains information about the number of atoms per geometric surface area. Consequently, the platinum loading can be calculated and plotted against the layer thickness. Thicker layers represent higher Pt loadings, which are indicated by broader signals (compare the spectra for 100 nm and 500 nm from Fig. 1) [4].

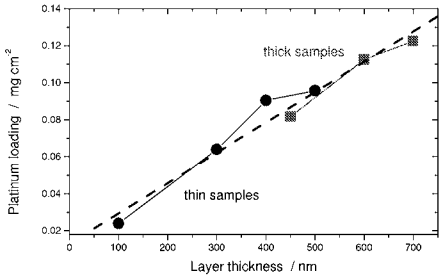

Fig. 2: *Dependence of platinum loading on sputtered layer thickness as determined by RBS.*

As displayed in Figure 2, a linear relationship between the layer thickness and the platinum loading is observed. Hence, the platinum loading of the sputter-deposited film can be controlled precisely by the sputter time. As the direct RBS investigation of substrates such as porous gas diffusion electrodes and polymer membranes is prone to a quite large error, the values obtained for glassy carbon substrates can serve as calibration data.

Conclusions

Co-sputtering Pt and C on glassy carbon provides layers, which consist of Pt nanoparticles in a C matrix. The elementary distribution within the layers is very homogenous. Additionally, it has been shown that the Pt loading can be easily varied by tuning the layer thickness and therefore the sputter time. Finally, it can be concluded that RBS is a powerful tool for the investigation of Pt/C co-sputtered films.

References

[1] F. Hajbolouri, ETH Zürich, Dissertation Nr. 15525 (2004).

[2] W.K. Chu, J.W. Mayer, M.A. Nicolet in: Backscattering Spectrometry, Academic Press (1978).

[3] L.R. Doolittle, Nucl. Instr. and Meth. **B15**, 227 (1986).

[4] A. Reiner, F. Hajbolouri, M. Döbeli, A. Wokaun, G.G. Scherer, Proc. 3rd European PEFC Forum, Lucerne (2005).

UNDER POTENTIAL DEPOSITION OF HYDROGEN ON PLATINUM INVESTIGATED BY IMPEDANCE SPECTROSCOPY

A. Reiner, H. Kuhn, A. Wokaun, G.G. Scherer
+41(0)56 310 5165
andreas.reiner@psi.ch

The reduction of the noble metal content in the catalyst layers of polymer electrolyte fuel cells (PEFCs) is of utmost importance for their cost competitiveness. Hence, the utilization of platinum has to be increased without performance penalty. The platinum surface fraction available for underpotential deposition of hydrogen (H_{upd}) in contact to the solid electrolyte gives an indication of the utilization. AC impedance measurements in the H_{upd} region yield kinetic data for these processes.

Experimental

Impedance measurements require a stable electrochemical surface in the H_{upd} potential region during the measuring time. However, smooth polycrystalline electrodes show declining H_{upd} signals, probably due to impurity adsorption. Hence, roughened polycrystalline electrodes showing stable adsorption peaks were used [1].

The platinum disc electrode exhibits a geometric diameter of 250 µm and a surface roughness of 4. All experiments were carried out at 21° C with a Pt wire as counter electrode and a reversible hydrogen reference electrode (RHE). The solution was 0.5 M H_2SO_4, saturated with purified Ar.

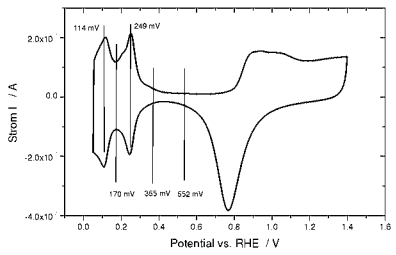

Fig. 1: *Cyclic voltammogram of a 250 µm Pt disc electrode in 0.5 M H_2SO_4 at a scan rate of 100 mV/s. Indicated are the different dc potentials used for the impedance measurements.*

Results and Discussion

A characteristic cyclic voltammogram (CV) of a roughened electrode in 0.5 M H_2SO_4 is shown in Fig. 1. The indicated dc potentials were chosen in the way to cover the double layer and the H_{upd} region. The impedance measurements were performed by imposing a sinusoidal voltage (amplitude 10 mV) onto the respective dc voltage within the frequency range of 0.1 to 10^6 Hz. For a dc potential of 552 mV (open squares) the Bode Plot (Fig. 2) exhibits at low and middle frequencies a ~ 45° declining branch, while the curve levels off in the high frequency region. It clearly reflects a capacitive behaviour, due to the fact that the potential chosen is located within the double layer region.

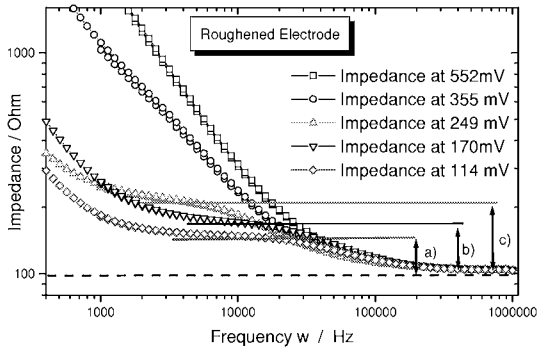

Fig. 2: *Impedance spectra at different dc potentials using a roughened electrode in 0.5 M H_2SO_4.*

Additionally, to the above described characteristics, the measurements at dc potentials located in the H_{upd} region (249 mV, 170 mV, and 114mV) indicate a plateau in the mid-frequency range. The impedance at high frequencies (dashed line) represents the electrolyte resistance, which is in the range of 100 Ω. The difference to the resistance in the mid frequency range represents the charge transfer resistance. These values are about 0.27, 0.18 and 0.12 Ω*cm^2 (see a), b) and c)) for the different dc potentials. Investigations using single crystals showed resistance values in the range between 0.3 and 0.6 Ω*cm^2 [2]. The impedance curve at a dc potential of 355 mV shows a transition state between the two types of impedance responses described above, this can be attributed to the fact that this dc potential is located between the H_{upd} and the double layer region.

Conclusions

Electrochemically roughened electrodes show stable behaviour in the H_{upd} region. Hence, it was possible to record impedance spectra with dc potentials in the double layer and the H_{upd} region. Depending on the position of the dc potential, the curves show predominant capacitive behaviour (double layer region) and, additionally in the H_{upd} region, features of a charge transfer process.

Applying a quite simple equivalent circuit consisting of a solution resistance, double layer capacity, and parallel to that a combination of charge transfer resistance and adsorption capacity, it was possible for the first time to extract resistance data concerning the H_{upd} process on polycrystalline platinum.

References

[1] A. Reiner, B. Steiger, G.G. Scherer, A. Wokaun, J. Power Sources, online (Dec. 2005).

[2] S. Morin, H. Dumont, B.E. Conway, J. Electroanal. Chem. **355,** 39 (1996).

THE ELECTROCHEMISTRY LABORATORY

On the occasion of the 57th Annual Meeting of the International Electrochemical Society 2005 in Busan, South Korea, a joint Seminar between PSI and RCECS (Research Center of Energy Storage and Conversion) was held at the Seoul National University (SNU).

Some impressions from our spirited annual Christmas party 2005

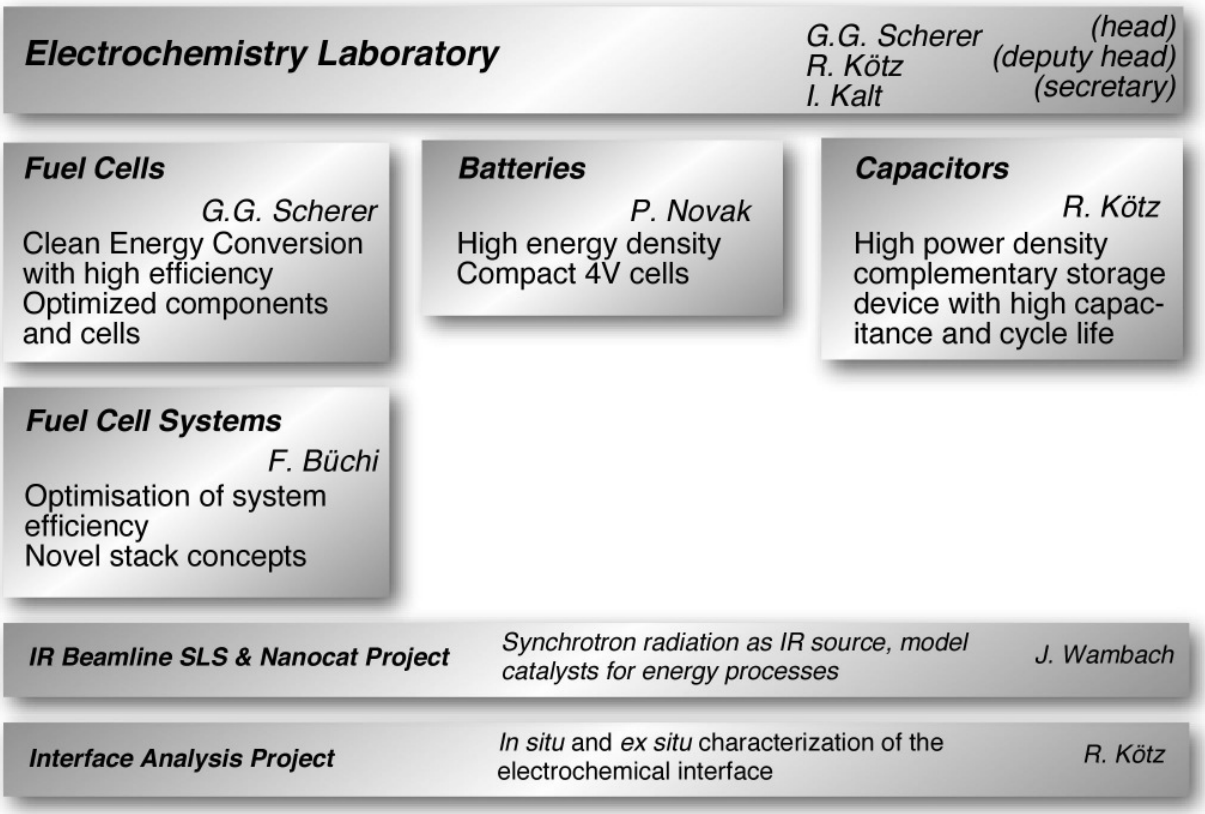
Electrochemistry Laboratory
G.G. Scherer (head)
R. Kötz (deputy head)
I. Kalt (secretary)
Fuel Cells
G.G. Scherer
Clean Energy Conversion with high efficiency
Optimized components and cells
Batteries
P. Novak
High energy density
Compact 4V cells
Capacitors
R. Kötz
High power density complementary storage device with high capacitance and cycle life
Fuel Cell Systems
F. Büchi
Optimisation of system efficiency
Novel stack concepts
IR Beamline SLS & Nanocat Project
Synchrotron radiation as IR source, model catalysts for energy processes
J. Wambach
Interface Analysis Project
In situ and ex situ characterization of the electrochemical interface
R. Kötz

ECL-PERSONNEL

Staff

Alkan Gürsel Selmiye, Dr. ♦ Arcaro Manuel ♦

Büchi Felix, Dr. ♦ Buqa Hilmi, Dr. ♦

Czekaj Izabela, Dr. ♦ (since February) ♦

Deiss Erich, Dr. (until June) ♦

Foelske Annette, Dr. ♦

Geiger Friederike ♦ Gloor Thomas • Gubler Lorenz, Dr. ♦

Hahn Matthias, Dr. ♦ Holzapfel Michael, Dr. ♦

Kaiser Hermann ♦ Kalt Isabella, ♦ Kötz Rudiger, Dr. ♦

Marmy Christian ♦

Novak Petr, Dr. ♦

Paganelli Gino (until January) ♦

Sauter Jean-Claude ♦ Scheifele Werner ♦ Scherer Günther G., Dr. ♦
Schneider Ingo, Dr. ♦ Steiger Beat, Dr. (until May) ♦

Tsukada Akinori ♦

Ufheil Joachim, Dr. ♦

Vetter Jens, Dr. ♦

Wambach Jörg, Dr. ♦ Wei Xun, Dr. (since July) ♦

PhD Students

Beck-Lempola Nina (until September) ♦ Ben Youcef Hicham (since May) ♦

Boillat Pierre (since December) ♦

Campana Flavio (until June) ♦

Ernst Frank ♦

Farquet Patrick (since January) ♦ Freunberger Stefan ♦

Hardwick Laurence ♦

Kramer Denis ♦ Kuhn Holger ♦ Kuhnke Markus (until July) ♦

La Mantia Fabio (since June) ♦

Reiner Andreas ♦ Reum Mathias ♦ Rosciano Fabio ♦ Ruch Patrick (since November) ♦

Santis Marco ♦ Slaski Michal ♦

Wimmer Jean (until March) ♦ Würsig Andreas (until March) ♦

AWARDS

P. Farquet, C. Padeste, H.H. Solak, S. Alkan Gürsel, G.G. Scherer	Best Poster *Polymer nanostructures grafted onto polymer substrates* TNT 2005, 6th International Conference in "Trends in NanoTechnology", Oviedo, Spain, August 29 – September 2 , 2005.
P. Novak	For the year 2005 *Technology Award of the Battery Division of the Electrochemical Society, Inc.*
C. Padeste, P. Farquet, H.H. Solak, S. Alkan Gürsel, G.G. Scherer	Best Poster *Functional Polymer Micro- and Nanostructures Grafted onto Polymer Substrates* NanoEurope 2005, International Fair and Conference for Innovation and Market Entries with Nano and Microtechnology, St. Gallen, September 12-14, 2005.
D. Kramer, I.A. Schneider	Christian Friedrich Schönbein "Contribution to Science" Medal for the outstanding contributions to the *Understanding of the fundamentals of the spatially resolved characterization of polymer electrolyte fuel cells* 3rd European Polymer Electrolyte Fuel Cell Forum, Lucerne, July 8, 2005.

THESE PHD STUDENTS FROM ECL GRADUATED IN 2005

Dr. Leif Steuernagel

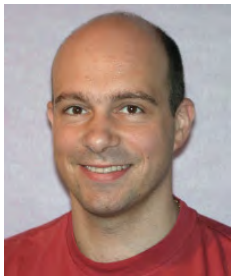

Synthese von Vinylverbindungen zur Darstellung oxidationsstabiler Membranen für die Brennstoffzellenanwendung
Ph.D. Thesis, No. 15749, ISBN No. 3-89720-779-6,
ETH Zürich, January 2005.

Advisor at university:	Prof. A. Wokaun
Advisor at TU Clausthal:	Prof. D.E. Kaufmann
Advisors at PSI:	Prof. A. Wokaun
	Dr. G.G. Scherer

Dr. Andreas Würsig

In situ Massenspektrometrie und Röntgendiffraktometrie zur Charakterisierung von Elektroden für Lithiumionen-Batterien
PhD Thesis No. 16059, ETH Zürich, May 2005.

Advisor at university:	Prof. R. Nesper
Advisors at PSI:	Prof. A. Wokaun
	PD Dr. P. Novak

Dr. Flavio Campana

Investigation of dimensional changes and film morphology at graphite electrodes in aprotic solutions by in situ atomic force microscopy
University of Bern, June 2005.

Advisor at university:	Prof. H. Siegenthaler
Advisor at PSI:	Dr. R. Kötz

EXCHANGE STUDENTS, DIPLOMA THESES, SUMMER STUDENTS

M. Bernasconi	*Charakterisierung von Membranen für die Brennstoffzelle, Durchführen von Brennstoffzellenversuchen, Realisierung von Testaufbauten* ETH Zürich, November 2004 – February 2005.
J. Schneider	*Thermal characterization of radiation-grafted films and membranes* ETH Zürich, December 2004 – March 2005.
F. Fürholz	*Experimente zur sub-mm Stromdichteverteilung in PEFC* Universität Basel, February – April 2005
M. Papra	*Untersuchung des dynamischen Verhaltens der Parallelschaltung einer PE-Brennstoffzelle und einer Superkapazität* Hochschule Wismar, Germany, February – April, 2005.
O. Schneider	*IR-Spektroskopische in situ Untersuchungen an verschiedenen Elektrolyten für Li-Ionen-Akkumulatoren* ETH Zürich, February – March 2005.
M. Keller	*Charakterisierung von Stromabnehmern für Brennstoffzellen* ETH Zürich, March – July 2005
A. Tiefenauer	*CFD Modellierung eines luftgekühlten PEFC-Stapels* Zürcher Hochschule Winterthur, May – June 2005.
P. Kirch	*Halbzellenmessungen in Polymerelektrolyt Brennstoffzellen* TU Karlsruhe, Germany, May – August 2005.
M. Lechermann	*Untersuchung der Fehlerquellen der lokalen Strommessung in PEFC* Universität Wien, Austria, June – August 2005.
M. Rubio-Munoz	*Charakterisierung von Membranen in der Direktmethanol Brennstoffzelle* Universidad de Murcia, Spain, July – September 2005.
U. Frischknecht	*Untersuchung und Modellierung der lokalen Stromdichteverteilung in PEFC* Universität Basel, September – December 2005.
T. Schulze	*Prozessuntersuchungen in Brennstoffzellen in Abhängigkeit einer Druckdifferenz* ETH Zürich, September – October 2005.

SEMINAR, INVITED SPEAKERS

Prof. P. Schmuki Universität Erlangen	*Approaches in electrochemical nanotechnology* January 24, 2005.
Dr. G.R. Patzke ETH Zürich	*Solvothermal synthesis of transition metal oxides: from solvothermal fields to in situ studies* February 21, 2005.
Prof. K.A. Friedrich Deutsches Zentrum für Luft- und Raumfahrt, Stuttgart	*Grundlegende Untersuchungen zur Reaktivität und Alterung in Polymer-Brennstoffzellen* February 28, 2005.
Dr. P. Holtappels EMPA, Dübendorf	*Electrochemical properties of solid oxid fuel cell materials* March 7, 2005.
Dr. T. Yamaki Japan Atomic Energy Research Institute, Takasaki	*Our radiation processing techniques for development of polymer electrolyte fuel cell membranes and others* March 21, 2005.
Prof. D. Fermin Universität Bern	*Organisation and charge transport properties of ultra thin assembly of nanoparticles at metal surfaces* April 4, 2005.
Dr. M. Hirayama Zürcher Hochschule Winterthur	*Polymers at surfaces and interfaces at ZHW* May 2, 2005.
Dr. M. Osman ETH Zürich	*Polymer-layered silicate nanocomposites* May 23, 2005.
Prof. H. Siegenthaler Universität Bern	*Electrolytic STM in fundamental and applied electrochemistry* May 30, 2005.
Prof. E. Roduner Universität Stuttgart	*Elektronen-Spin-Resonanz-Untersuchungen zur Stabilität von Brennstoffzellenmembranen* June 13, 2005.
Prof. A. Stemmer ETH Zürich	*Towards biological micro-power generators* June 27, 2005.
Prof. S. Mukerjee Northeastern University, Boston	*Fundamental aspects of durability at the polymer electrolyte-electrode interface* July 11, 200.
Dr. H. Gasteiger General Motors Corp., Honeoye Falls, NY	*Degradationsmechanismen von PEM Brennstoffzellenkomponenten* July 15, 2005.
Dr. E. Figgemeier Universität Basel	*Functionalized surfaces for energy conversion - self-assembled monolayers of metal complexes investigated by electrochemical and scanning probe techniques* September 12, 2005.

Dr. R. von Helmolt
Adam Opel AG,
Rüsselsheim

Hydrogen storage technology for fuel cell vehicles
September 19, 2005.

Prof. T. Pajkossy
Chemical Research
Center, Budapest

Impedance studies on single crystalline noble metal electrodes
November 21, 2005.

Prof. K. Jüttner
Dechema AG,
Frankfurt

Elektrochemische Eigenschaften leitfähiger Polymere und deren Anwendungsmöglichkeiten in der Reaktions- und Oberflächentechnik
November 28, 2005.

Dr. L. Kibler
Universität Ulm

Wozu sind Einkristallelektroden gut?
Beziehungen zwischen Struktur und Aktivität
December 5, 2005.

CONFERENCES – WORKSHOPS

Electrochemistry and Automotive Industry

21st One-Day-Symposium
May 11, 2005
Organizers: G.G. Scherer and R. Kötz

With contributions from:

Dr. P. Schmutz, EMPA Dübendorf
Dr. F. Büchi, PSI, Villigen
Prof. G. Nauer, Universität Wien, Austria
Dr. M. Broussely, SAFT, Poitiers, France
Prof. W. Tillmetz, ZSW, Ulm, Germany
Dr. M. Ullrich, Volkswagen AG, Wolfsburg, Germany

REVIEW ACTIVITIES OF THE LABORATORY

Journals

Advanced Materials ◆

Carbon ◆ Chemical Communications ◆ Chemistry of Materials ◆

Electrochimica Acta ◆ Electrochemistry Communications ◆ Electrochemical Solid State Letters ◆

Fire Safety Science ◆ Fuel Cells ◆

Green Chemistry ◆

Journal of American Society of Mechanical Engineers ◆ Journal of Applied Electrochemistry ◆ Journal of the Electrochemical Society ◆ Journal of Materials Chemistry ◆ Journal of Nuclear Materials ◆ Journal of Physical Chemistry ◆ Journal of Physics and Chemistry of Solids ◆ Journal of Polymer Science ◆ Journal of Solid State Chemistry ◆ Journal of Power Sources ◆

Solid State Ionics ◆

Thermochimica Acta ◆

Organisations

Alexander von Humboldt-Stiftung, Germany ◆

Christian Doppler Gesellschaft, Wien, Austria ◆

2nd **E**uropean Hydrogen Conference, Zaragoza, Spain ◆

Memorial University of Newfoundland, Canada ◆ **M**istra, The Swedish Foundation for Strategic Environmental Research ◆

PSI FOKO, Switzerland ◆

US-Israel Binational Science Foundation, Israel ◆

Co-Referee's Report for Dissertations

F. **C**ampana, PSI/University Bern ◆

A. **W**ürsig, PSI/ETH ◆

INDUSTRIAL PARTNERS

The Laboratory had the pleasure to collaborate with the following industrial partners during the year 2005:

BASF AG, Ludwigshafen, Germany ◆

Ciba SC, Basel, Switzerland ◆ Construction Développment Michelin SA (CDM), Givisiez, Switzerland ◆ CEKA Elektrowerkzeuge AG, Wattwil, Switzerland ◆

DaimlerChrysler, Deutschland ♦ Degussa, Creavis Technology & Innovation, Marl, Germany ◆

Ferro GmbH, Frankfurt/Main, Germany ◆

Honeywell Chemical Specialties, Seelze, Germany ♦ Hoppecke Batterien, Brilon, Germany ◆

Johnson Matthey, UK ◆

Maxwell Technologies SA, Rossens, Switzerland ◆ MES-DEA, Stabio, Switzerland ◆

Nissan Motors Co., Ltd. Yokosuka, Japan ◆

PEMEAS GmbH, Frankfurt, Germany ◆

Straumann Institut AG, Waldenburg, Switzerland ◆

TIMCAL AG, Bodio, Switzerland ◆

Umicore, Hanau-Wolfgang, Germany ◆

Volvo, Sweden ◆

Weidmann Plastics, Rapperswil, Switzerland ◆

PROJECT COLLABORATIONS WITH EXTERNAL PARTNERS

SBF

F.N. Büchi Project Leader	*HYTRAN (Hydrogen and Fuel Cell Technologies for Road Transport)* EU-Project
P. Novák Project Leader	*ALiSTORE (Advanced lithium energy storage systems based on the use of nano-powders and nano-composite electrodes/electrolytes)* EU-Project (Network of Excellence)
P. Novák Project Leader	*CAMELiA (Calendar life mastering of Li-ion accumulator)* EU-Project
P. Novák Project Leader	*LiBERAL (Lithium battery evaluation and research – accelerated life test direction)* EU-Project

BFE

F.N. Büchi Project Leader	*Numerische Modellierung von PE Brennstoffzellen mit der FE-Methode* mit ZHW, Winterthur
R. Kötz Project Leader	*Integrated micro-supercapacitor* with NTB, Buchs, Institute for Micro- and Nanotechnology
G.G. Scherer Project Leader	*Polymer Elektrolyt Brennstoffzellen mit H_2 und Methanol als Brennstoff*

Gebert Ruef Stiftung

F.N. Büchi Project Leader PSI	*SIMPEM* (*Simulation von Polymer Elektrolyt Brennstoffzellen und Stapeln)* mit ZHW, Winterthur

Industry

P. Dietrich Project Leader	*Research collaboration* Construction Développment Michelin SA (CDM), Givisiez
L. Gubler Project Leader	*Eignung von Polyisobutylen basierten Filmen als Grundpolymer für die Strahlenpfropfung* BASF AG, Ludwigshafen, Germany
L. Gubler Project Leader	*Charakterisierung von Celtec®-V Membranen für die Direkt Methanol Brennstoffzelle* Pemeas Fuel Cell Technologies, Frankfurt (Main), Germany
P. Novák Project Leader	*Elektrochemische Charakterisierung von Oxiden für Lithiumionen-Batterien* Ferro GmbH, Frankfurt (Main), Germany
P. Novák Project Leader	*Entwicklung eines Batterieseparators auf Basis der keramischen Membranfolie der CREAVIS* Degussa AG, CREAVIS Technologies & Innovation, Marl, Germany

P. Novák Project Leader	*Behandlung der Graphite für die negative Elektrode der Lithiumionen-Batterie* TIMCAL SA, Bodio
P. Novák Project Leader	*Rechargeable magnesium batteries (Project No. 1)* Nissan Motor Co. Ltd., Yokohama, Japan
P. Novák Project Leader	*Rechargeable magnesium batteries (Project No. 2)* Nissan Motor Co. Ltd., Yokohama, Japan
P. Novák Project Leader	*Characterization of graphite electrodes* Nissan Motor Co. Ltd., Yokohama, Japan
P. Novák Project Leader	*Elektrochemische Charakterisierung von Oxiden für Lithiumionen-Batterien* Industriepartner A
P. Novák Project Leader	*Industrieprojekt* Industriepartner B
G.G. Scherer Project Leader	*Diagnostics of polymer electrolyte fuel cells* Nissan Motor Co. Ltd. Yokohama, Japan
G.G. Scherer Project Leader	*Diagnostics of polymer electrolyte fuel cells* Automotive Industries
J. Vetter Project Leader	*Electrochemical characterization of polymeric organic active materials* CIBA SC, Basel

KTI

F. N. Büchi Project Leader PSI	*Brennstoffzellenstapel mit erweiterter Funktionalität* mit CEKA AG, Wattwil und FH Bern
R. Kötz Project Leader	*Optimized electrochemical capacitors*

Nationalfonds

R. Kötz Project Leader	*Scanning probe microscopy of the solid electrolyte interface*
P. Novák Project Leader	*Synthesis and characterization of advanced electroactive materials for electrodes of rechargeable lithium-ion batteries*

TEACHING ACTIVITIES

University Level Teaching

PD Dr. P. Novák, Prof. Dr. A. Wokaun	*Technische Elektrochemie* ETH Zürich, WS 2005/2006
PD Dr. P. Novák	*Technische Elektrochemie* Praktikum, ETH Zürich, SS 2005
Prof. Dr. A. Wokaun, Dr. J. Gass, Dr. G.G. Scherer	*Technik erneuerbarer Energien, Teil 2* ETH Zürich, WS 2004/2005

PUBLICATIONS

Peer Reviewed Papers

S. Alkan Gürsel, C. Padeste, H.H. Solak, G.G. Scherer
Microstructured polymer films by X-ray lithographic exposure and grafting
Nucl. Instr. and Meth. in Phys. Res. B **236**, 449-455 (2005).

O. Barbieri, M. Hahn, A. Herzog[1], R. Kötz
Capacitance limits of high surface area activated carbons for double-layer capacitors
Carbon **43/6**, 1303-1310 (2005).
[1] EMPA Dübendorf

F. N. Büchi, A.B. Geiger, R.P. Neto[1]
Dependence of current distribution on water management in PEFC of technical size
J. Power Sources **145**, 62-67 (2005).
[1] IST, Lisbon, Portugal

H. Buqa, A. Würsig, D. Goers, L. Hardwick, M. Holzapfel, P. Novák, F. Krumeich[1], M.E. Spahr[2]
Behavior of highly crystalline graphites in lithium-ion cells with propylene carbonate containing electrolytes
J. Power Sources **146**, 134-141 (2005).
[1] ETH Zürich
[2] TIMCAL SA, Bodio

H. Buqa, D. Goers, M. Holzapfel, M.E. Spahr[1], P. Novák
High rate capability of graphite negative electrodes for lithium-ion batteries
J. Electrochem. Soc. **152**, A474-A481 (2005).
[1] TIMCAL SA, Bodio

F.P. Campana, R. Kötz, J. Vetter, P. Novák, H. Siegenthaler[1]
In situ atomic force microscopy study of dimensional changes during Li^+ ion intercalation/de-intercalation in highly oriented pyrolytic graphite
Electrochem. Commun. **7**, 107-112 (2005).
[1] University of Bern

E. Deiss
Spurious chemical diffusion coefficients of Li^+ in electrode materials evaluated with GITT
Electrochim. Acta **50**, 2927-2932 (2005).

V.-M. Graubner[1], D. Clemens[2], T. Gutberlet, R. Kötz, T. Lippert, O. Nuyken[1], B. Schnyder, A. Wokaun
Neutron reflectometry and spectroscopic ellipsometry studies of cross-linked poly(dimethylsiloxane) after irradiation at 172 nm
Langmuir **21,** 8940-8946 (2005).
[1] TU Munich, Germany
[2] Hahn-Meitner-Institut, Berlin, Germany

L. Gubler, S. Alkan Gürsel, G.G. Scherer
Radiation grafted membranes for polymer electrolyte fuel cells
Fuel Cells **5**, 317-335 (2005).

L. Gubler, N. Prost, S. Alkan Gürsel, G.G. Scherer
Proton exchange membranes prepared by radiation grafting of styrene / divinylbenzene onto poly(ethylene-alt-tetrafluoroethylene) for low temperature fuel cells
Solid State Ionics **176,** 2849-2860 (2005).

M. Hahn, A. Würsig, R. Gallay[1], P. Novák, R. Kötz
Gas evolution in activated carbon / propylene carbonate based double-layer capacitors
Electrochem. Commun. **5**, 925-930 (2005).
[1] Maxwell Technologies SA, Rossens

M. Holzapfel, C. Jost[1], A. Prodi-Schwab[1], F. Krumeich[2], A. Würsig, H. Buqa, P. Novák
Stabilization of lithiated graphite in an electrolyte based on ionic liquids: An electrochemical and scanning electron microscopy study
Carbon **43**, 1488-1498 (2005).
[1] Degussa AG, Marl, Germany
[2] ETH Zürich

M. Holzapfel, H. Buqa, W. Scheifele, P. Novák, F.-M. Petrat[1]

A new type of nano-sized silicon/carbon composite electrode for reversible lithium insertion
Chem. Commun. **12**, 1566-1568 (2005).
[1] Degussa AG, Marl, Germany

M. Holzapfel, H. Buqa, F. Krumeich[1], P. Novák, F.-M. Petrat[2], C. Veit[2]

Chemical vapor deposited silicon/graphite compound material as negative electrode for lithium-ion batteries
Electrochem. Solid State Let. **8**, A516-A520 (2005).
[1] ETH Zürich
[2] Degussa AG, Marl, Germany

D. Kramer, E. Lehmann, G. Frei, P. Vontobel, A. Wokaun, G.G. Scherer

An on-line study of fuel cell behavior by thermal neutrons
Nucl. Instr. and Meth. A **542**, 52-60 (2005).

D. Kramer, J. Zhang[1], R. Shimoi[1], E. Lehmann, A. Wokaun, K. Shinohara[1], G.G. Scherer

In situ diagnostic of two-phase flow phenomena in polymer electrolyte fuel cells by neutron imaging
Part A. Experimental, data treatment, and quantification
Electrochim. Acta **50**, 2603-2614 (2005).
[1] Nissan Motor Co. Ltd., Yokosuka, Japan

M. Kuhnke, T. Lippert, G.G. Scherer, A. Wokaun

Micro-Fabrication of flow field channels in glassy carbon by a combined laser and reactive ion etching process
Surf. Coat. Technol. **200**, 730-733 (2005).

P. Novák, D. Goers, L. Hardwick, M. Holzapfel, W. Scheifele, J. Ufheil, A. Würsig

Advanced in situ characterization methods applied to carbonaceous materials
J. Power Sources **146**, 15-20 (2005).

F. Raimondi, G.G. Scherer, R. Kötz, A. Wokaun

Nanoparticles in energy technology – examples from electrochemistry and catalysis
Angew. Chem. Int. Ed. **44**, 2190-2209 (2005) & Angew. Chemie, **117**, 2228-2248 (2005).

T.J. Schmidt[1], K. Simbeck[2] G.G. Scherer

Influence of cross-linking on performance of radiation-grafted and sulfonated FEP 25 membranes in H_2-O_2 PEFC
J. Electrochem. Soc. **152** (1), A93-A97 (2005).
[1] Pemeas, Frankfurt (Main), Germany
[2] Adam Opel AG, Mainz-Kastel, Germany

I.A. Schneider, H. Kuhn, A. Wokaun, G.G. Scherer

Fast locally resolved electrochemical impedance spectroscopy in polymer electrolyte fuel cell
J. Electrochem. Soc. **152** (10) A2092-A2103 (2005).

I.A. Schneider, H. Kuhn, A. Wokaun, G.G. Scherer

Study of water balance in a polymer electrolyte fuel cell by locally resolved electrochemical impedance spectroscopy
J. Electrochem. Soc. **152** (12) A2383-A2389 (2005).

I.A. Schneider, D. Kramer, A. Wokaun, G.G. Scherer

Spatially resolved characterization of PEFCs using simultaneously neutron radiography and locally resolved impedance spectroscopy
Electrochem. Commun. **7**, 1393-1397 (2005).

J. Ufheil, M.C. Bärtsch, A. Würsig, P. Novák

Maleic anhydride as an additive to γ-butyrolactone solutions for Li-ion batteries
Electrochim. Acta **50**, 1733-1738 (2005).

J. Ufheil, A. Würsig, O. Schneider, P. Novák

Acetone as oxidative decomposition product in propylene carbonate containing battery electrolyte
Electrochem. Commun. **7**, 1380-1384 (2005).

J. Vetter, H. Buqa, M. Holzapfel, P. Novák

Impact of co-solvent chain branching on lithium-ion battery performance
J. Power Sources **146**, 355-359 (2005).

J. Vetter, P. Novák, M.R. Wagner, J.O. Besenhard[1], M. Winter[1], M. Wohlfahrt-Mehrens[2], C. Vogler[2], A. Hammouche[3]

Ageing mechanisms in lithium-ion batteries
J. Power Sources **147**, 269-281 (2005).
[1] TU Graz, Austria
[2] ZSW, Ulm, Germany
[3] RWTH, Aachen, Germany

A. Würsig, H. Buqa, M. Holzapfel, F. Krumeich[1], P. Novák

Film formation at positive electrodes in lithium-ion batteries
Electrochem. Solid State Let. **8**, A34-A37 (2005).
[1] ETH Zürich

Other Papers

F.N. Büchi, M. Reum, S.A. Freunberger, A. Delfino[1]

On the efficiency of automotive H_2/O_2 PE fuel cell systems
Proc. 3rd European PEFC Forum, Luzern, July 4-8 (2005).
[1] CDM, Givisiez

H. Buqa, M. Holzapfel, A. Würsig, F. Krumeich[1], M.E. Spahr[2], P. Novák

Post mortem SEM-analyses of film formation on electrode materials in lithium-ion batteries
Extended Abstracts, Lithium Battery Discussion - Electrode Materials, Arcachon, France, May 22-27 (2005).
[1] ETH Zürich
[2] TIMCAL SA, Bodio

E. Deiss

Reply to "Comments on 'spurious potential dependence of diffusion coefficients in Li+ insertion electrodes measured with PITT' [E. Deiss, Electrochim. Acta 47 (2002) 4027-4037] by A. Eftekhari"
Electrochim. Acta **50**, 2545 (2005).

Th. Dumont, T. Lippert, M. Döbeli, H. Grimmer, P. Novák, A. Würsig, A. Wokaun

Influence of experimental parameters on the Li-content of $LiMn_2O_4$ electrodes produced by pulsed laser deposition
Proc. European Materials Research Society Spring Meeting, Strasbourg, France, May 31 - June 3 (2005).

F.O. Ernst, S.E. Pratsinis[1], J. Ufheil, P. Novák

Electrochemically active nanosized spinels made by flame spray pyrolysis
Chemie Ingenieur Technik **77**, 1217 (2005).
[1] ETH Zürich

S.A. Freunberger, F.N. Büchi, N. Djilali[1]

Electrical and thermal coupling in PEFC stacks – a CFD-analysis
Proc. 3rd European PEFC Forum, Luzern, B065, July 4-8 (2005).
[1] University of Victoria, Canada

L. Gubler, S. Alkan Gürsel, M. Slaski, F. Geiger, G.G. Scherer, A. Wokaun

Radiation grafted fuel cell membranes: Current state of the art at PSI
Proc. 3rd European PEFC Forum, Lucerne, B113, July 4–8 (2005).

L. Gubler, M. Slaski, G.G. Scherer, A. Wokaun

Radiation grafted fuel cell membranes: Prospects of advanced monomer combinations
Proc. Fuel Cell Seminar, Palm Springs, USA, November 14–18, 195-198 (2005).

M. Hahn, O. Barbieri, R. Kötz

The evolution of electrical double layer in nanoporous carbon electrodes
Grundlagen und Anwendungen der Elektrochemischen Oberflächentechnik, Gesellschaft Deutscher Chemiker, Frankfurt (Main), GDCH-Monographie **32**, 229-239, 2004, ISBN 3-936028-30-3 (2005).

L. Hardwick, P. Novák

Detection of surface disorder on graphite electrodes using Raman microscopy
Grundlagen und Anwendungen der Elektrochemischen Oberflächentechnik, Gesellschaft Deutscher Chemiker, Frankfurt (Main), GDCh-Monographie **32**, 220-228 (2005).

L. Hardwick, H. Buqa, P. Novák

Graphite surface disorder detection using Raman microscopy
Proc. SSI-15 International Conference on Solid State Ionics, Baden-Baden, Germany, July 17-22 (2005).

M. Holzapfel, H. Buqa, W. Scheifele, P. Novák, F.-M. Petrat[1]

Nano-scale silicon as negative electrode material for lithium-ion batteries
Proc. 22nd International Seminar and Exhibit on Batteries and Small Fuel Cells, Fort Lauderdale, Florida, USA, March 14-17 (2005).
[1] Degussa AG, Marl, Germany

C. Jost[1], M. Pascaly[1], A. Prodi-Schwab[1], M. Holzapfel, P. Novák

Ionic liquids for safe high performance lithium-ion batteries
Proc. 1st International Congress on Ionic Liquids, Salzburg, Austria, June 19-22 (2005).
[1] Degussa AG, Marl, Germany

R. Kötz, P. Dietrich, M. Hahn, F. Büchi

Supercaps – Eigenschaften und Fahrzeuganwendungen
5. Fachtagung Brennstoffzelle, Hamburg, Germany, April 19-20, VDI-Berichte 1874, 175-188 (2005).

R. Kötz, M. Hahn, O. Barbieri, F. Campana, A. Foelske, A. Würsig, P. Novák, R. Gallay[1]

Pseudo capacitive processes and lifetime aspects of electrochemical double-layer capacitors
Proc. 15th International Seminar on Double Layer Capacitors and Hybrid Energy Storage Devices, Deerfield Beach, USA, December 5–7 (2005).
[1] Maxwell Technologies SA, Rossens

R. Kötz, M. Hahn, O. Barbieri, F. P. Campana, R. Gallay[1]

Lifetime aspects of electrochemical double layer capacitors
56th Annual ISE Meeting, Busan, Korea, September 26-28, Abstract No. 3C-004-IL (2005).
[1] Maxwell Technologies SA, Rossens

M. Kuhnke, G. Dumitru[1], T. Lippert, E. Ortelli[2], G.G. Scherer, A. Wokaun

Micro machining of carbon materials and laser micro patterning of metal films used as masks for reactive ion etching
Proc. 6th International Symposium on Laser Precision Microfabrication (LPM), Williamsburg, USA, April 4-8 (2005).
[1] FHNW, Windisch
[2] Dyconex AG, Bassersdorf

P. Novák, A. Würsig

Gas development on electrode/electrolyte interfaces in lithium-ion batteries
56th Annual ISE Meeting, Busan, Korea, September 26-28, Abstract No. 3A-039-IL (2005).

P. Novák, A. Würsig, H. Buqa, M. Holzapfel, M. Hahn, R. Kötz

Oxidative and reductive gas development on electrode/electrolyte interfaces in carbonate based electrolytes
Extended Abstracts, Lithium Battery Discussion - Electrode Materials, Arcachon, France, May 22-27 (2005).

A. Reiner, F. Hajbolouri, M. Döbeli[1], A. Wokaun, G.G. Scherer

Co-sputtering: A novel platinum-carbon catalyst preparation method
Proc. 3rd European PEFC Forum, Lucerne, July 4-8 (2005).
[1] ETH Zürich

M. Reum, S.A. Freunberger, F. Fürholz, F.N. Büchi

First investigations of the local current density distribution over the flow field channel and rib
Proc. 3rd European PEFC Forum, Lucerne, July 4-8 (2005).

M. Santis, S.A. Freunberger, M. Papra, F.N. Büchi

Experimental investigation of the propagation of local current density variations to adjacent cells in PEFC stacks
Proc. 3rd International Conference on Fuel Cell Science, Engineering and Technology, Ypsilanti, MI, USA, May 23-25 (2005).

M. Santis, F.N. Büchi

Homogenization of the current density distribution in polymer electrolyte fuel cells
Proc. 3rd European PEFC Forum, Lucerne, July 4-8 (2005).

G.G. Scherer, F.N. Büchi

Appliances and portable power: Power Pac
Energy Research in ETH Domain, Science and Technology for Sustainable Energy, ISBN 3-9521409-4-5, 54 (2005).

I.A. Schneider, D. Kramer, H. Kuhn, L. Gubler, A. Wokaun, G.G. Scherer

Advanced in situ diagnostic methods for polymer electrolyte fuel cells at PSI
Fuel Cell Seminar Abstracts, Fuel Cell Seminar, Palm Springs, USA, November 14-18 (2005).

I.A. Schneider, A. Wokaun, G.G. Scherer

Analysis of performance losses in polymer electrolyte fuel cells by locally resolved electrochemical impedance spectroscopy
Proc. 3rd European PEFC Forum, Lucerne, July 4–8 (2005).

M.E.Spahr[1], H. Wilhelm[1], D. Goers, H. Buqa, A. Würsig, L. Hardwick, P. Novák, F. Krumeich[2], J. Dentzer[3], C. Vix-Guterl[3]

Influence of the surface properties of graphite materials used in secondary lithium batteries
Proc. CARBON 2005, Gyeongju, Korea, July 30 (2005).
[1] TIMCAL SA, Bodio
[2] ETH Zürich
[3] ICSI, Mulhouse, France

M.E. Spahr[1], H. Wilhelm[1], D. Goers, H. Buqa, A. Würsig, L. Hardwick, P. Novák, F. Krumeich[2], J. Dentzer[3], C. Vix-Guterl[3]

Active surface area of graphite and its reactivity towards lithium battery electrolytes
Extended Abstracts 2nd International Conference on Polymer Batteries and Fuel Cells, Las Vegas, Nevada, USA, June 12-17 (2005).
[1] TIMCAL SA, Bodio
[2] ETH Zürich
[3] ICSI, Mulhouse, France

J. Ufheil, F. Ernst, H. Buqa, S.E. Pratsinis[1], P. Novák

Tailor made nano particles for batteries by flame spray pyrolysis
Meeting Abstracts, 207th Electrochem. Soc. Meeting, Quebec, Canada, May 15-20, **05-1,** 1688 (2005).
[1] ETH Zürich

J. Vetter, M. Holzapfel, A. Würsig, J. Ufheil, P. Novák

In situ study on CO_2 evolution at lithium-ion battery cathodes
Proc. 3rd International Conference on Materials for Advanced Technologies (ICMAT) & 9th International Conference on Advanced Materials (IUMRS-ICAM), Singapore, July 3-8 (2005).

TALKS

Invited Talks

F.N. Büchi

Brennstoffzellen: Technologie, Anwendungen, Perspektiven
Energieagentur der Wirtschaft, Uzwil, Januray 11, 2005.

F.N. Büchi

Analysis and exploitation of along the channel gradients
Computational Fuel Cell Dynamics-III, Banff, Canada, March 19-24, 2005.

F.N. Büchi

The ultimate possibilities of a hybrid electric power rain
BFE Forschungstagung, Villigen PSI, June 15, 2005.

H. Buqa

Untersuchungen zur Grenzfläche Anode/Elektrolyt in Lithiumionen-Batterien
Sonderforschungsbereich 595, TU-Darmstadt, Germany, December 8, 2005.

L. Gubler

Trends in membrane electrode development for PEFC
European Materials Research Society (E-MRS) Spring Meeting, Strasbourg, France,
May 31 - June 3, 2005.

L. Gubler

Radiation grafted membranes for low temperature fuel cells
National Research Council Canada, Institute for Fuel Cell Innovation, Vancouver, Canada, September 15, 2005.

L. Gubler

Die Brennstoffzelle – was trägt sie bei zur Lösung der Energieproblematik ?
Technische Gesellschaft Zürich, September 26, 2005.

M. Hahn	*Activated carbons for high power supercapacitors: Capacitance and voltage limitations* Carbon for Energy Storage and Environment Protection (CESEP), Orléans, France, October 2-6, 2005.
M. Holzapfel	*Nano-scale silicon as negative electrode material for lithium-ion batteries* 22nd International Seminar and Exhibit on Batteries and Small Fuel Cells, Fort Lauderdale, Florida, USA, March 14-17, 2005.
R. Kötz	*Supercaps – Eigenschaften und Fahrzeuganwendungen* 5. Fachtagung Brennstoffzelle VDI, Hamburg, Germany, April, 2005.
R. Kötz	*New powertrain technologies reshape the passenger car - Realisation of the HY-LIGHT demonstration vehicle* 3rd European PEFC Forum, Lucerne, July 4-8, 2005.
R. Kötz	*Lifetime aspects of electrochemical double layer capacitors* Keynote Lecture 56th Annual ISE Meeting, Busan, Korea, September 26-30, 2005.
R. Kötz	*Electrochemical double-layer capacitors: Limitations and applications* PSI-RCECS Joint Seminar, Seoul National University, Korea, October 4, 2005.
P. Novák	*Electrodes for lithium-ion batteries* International Workshop on Future Concepts in Energy Related Catalysis, Monte Verità, Ascona, March 16, 2005.
P. Novák	*Oxidative and reductive gas development on electrode/electrolyte interfaces in carbonate based electrolytes* Lithium Battery Discussion - Electrode Materials, Arcachon, France, May 25, 2005.
P. Novák	*What happens on the various electrode/electrolyte interfaces in a lithium-ion battery?* Batteries 2005, Paris, France, June 14, 2005.
P. Novák	*Gas development on electrode/electrolyte interfaces in lithium-ion batteries* 56th Annual ISE Meeting, Busan, Korea, September 26-30, 2005.
P. Novák	*Interface processes in lithium-ion batteries* PSI - RCECS Joint Seminar, Seoul National University, Seoul, Korea, October 4, 2005.
P. Novák	*Lithiumionen-Batterien* Hoppecke Batterien GmbH & Co. KG, Brilon, Germany, November 23, 2005.
G.G. Scherer	*Electrocatalysis in polymer electrolyte fuel cells: The role of water at the interface gas diffusion electrode / solid polymer electrolyte* 3rd Gerischer Symposium, Berlin, Germany, July 6–8, 2005.
G.G. Scherer	*Electrocatalysis for polymer electrolyte fuel cells - practical implications* International Workshop on Future Concepts in Energy Related Catalysis, Monte Verità, Ascona, March 13–17, 2005.
G.G. Scherer	*Polymer electrolyte fuel cells - The role of water at the interface gas diffusion electrode / solid polymer electrolyte* ELECTROCHEM 2005, University of Northumbria, Newcastle upon Tyne, UK, September 4–7, 2005.
G.G. Scherer	*Recent progress in the development of in situ diagnostic methods for polymer electrolyte fuel cells* 56th Annual ISE Meeting, Busan, Korea, September 25-30, 2005.

G.G. Scherer	*Polymer electrolyte fuel cells research and development activities at Paul Scherrer Institut* PSI – RCECS Joint Seminar, Seoul National University, Seoul, Korea, October 4, 2005.
J. Ufheil	*Tailor made nano particles for batteries by flame spray pyrolysis* 207th Electrochem. Soc. Meeting, Quebec, Canada, May 18, 2005.

Contributions to Media

F.N. Büchi et al.	TV-Sendung NZZ Format, Swissmade, Vorstellung PowerPac SF-DRS, January 23, 2005.
P. Dietrich et al.	TV-Sendung NZZ Format, Swissmade, Vorstellung HY-LIGHT-Fahrzeug SF-DRS, January 16, 2005.

Other Talks

F.N. Büchi	*The ultimate possibilities of a hybrid electric power train* 21st One-Day-Symposium Electrochemistry Laboratory, Villigen PSI, May 11, 2005.
A. Foelske, B. Steiger, N.K. Beck, R. Kötz, G.G. Scherer, A. Wokaun	*Electrochemically pretreated $Bi_2Pt_{2-y}Ir_yO_7$ pyrochlores – an X-ray photoelectron spectroscopy study* ECASIA 05, Vienna, Austria, September 25-30, 2005.
S.A. Freunberger, F.N. Büchi, N. Djilali[1]	*Cell-to-cell coupling in PEFC stacks* 2nd Fuel Cell Research Symposium Modelling and Experimental Validation, Stuttgart, Germany, March 3-4, 2005. [1] University of Victoria, Canada
S.A. Freunberger, F.N. Büchi, N. Djilali[1]	*Electrical and thermal coupling in PEFC stacks – a CFD-analysis* 3rd European PEFC Forum, Lucerne, July 4-8, 2005. [1] University of Victoria, Canada
L. Gubler, S. Alkan Gürsel, M. Slaski, F. Geiger, G.G. Scherer, A. Wokaun	*Radiation grafted fuel cell membranes: Current state of the art at PSI* 3rd European PEFC Forum, Lucerne, July 4-8, 2005.
L. Gubler, T. Finsterwald, M. Keller, G.G. Scherer	*Investigations on the proton conductivity of various proton exchange membranes* International Conference on Solid State Ionics, Baden-Baden, Germany, July 17-22, 2005.
L. Gubler, M. Slaski, G.G. Scherer, A. Wokaun	*Radiation grafted fuel cell membranes: Prospects of advanced monomer combinations* Fuel Cell Seminar, Palm Springs, USA, November 14-18, 2005.
L. Hardwick, H. Buqa, P. Novák	*Graphite surface disorder detection using Raman microscopy* International Conference on Solid State Ionics, Baden-Baden, Germany, July 6, 2005.
R. Kötz, M. Hahn, O. Barbieri, F. Campana, A. Foelske, A. Würsig, P. Novák, R. Gallay[1]	*Pseudo-capacitive processes and lifetime aspects of electrochemical double-layer capacitors* 15th International Seminar on Double Layer Capacitors and Hybrid Energy Storage Devices, Deerfield Beach, USA, December 5 –7, 2005. [1] Maxwell Technologies SA, Rossens
D. Kramer, E. Lehmann, G. Kühne, A. Wokaun, G.G. Scherer	*The prospect of imaging with cold neutrons for fuel cell research* ICON Workshop, Villigen, October 13, 2005.

D. Kramer, J. Zhang[1], Y. Ono[1], E. Lehmann, A. Wokaun, K. Shinohara[1], G.G. Scherer

In situ investigation of two-phase flow phenomena in polymer electrolyte fuel cells by neutron imaging
3rd European PEFC Forum, Lucerne, B055, July 4-8, 2005.
[1] Nissan Motor Co. Ltd., Yokosuka, Japan

D. Kramer, I.A. Schneider, E. Lehmann, A. Wokaun, G.G. Scherer

The investigation of two-phase flow in polymer electrolyte fuel cells by neutron imaging and locally resolved electrochemical impedance spectroscopy
Energy for a Sustainable Future 5, Villigen PSI, June 9-10, 2005.

D. Kramer, J. Zhang[1], E. Lehmann, A. Wokaun, K. Shinohara[1], G.G. Scherer

Investigation of two-phase flow phenomena in polymer electrolyte fuel cells by neutron imaging
2nd Fuel Cell Research Symposium, Stuttgart, Germany, March 3-4, 2005.
[1] Nissan Motor Co. Ltd., Yokosuka, Japan

D. Kramer, J. Zhang[1], E. Lehmann, A. Wokaun, K. Shinohara[1], G.G. Scherer

Investigation of two-phase flow in polymer electrolyte fuel cells with neutron imaging
7th SINQ User Meeting, Villigen, January 27, 2005.
[1] Nissan Motor Co. Ltd, Yokosuka, Japan

H. Kuhn, B. Andreaus, G.G. Scherer, A. Wokaun

Measuring and modelling the single electrode reactions in PEFC
2nd FC Research Symposium Modelling and Validation, DLR Stuttgart, Germany, March 3-4, 2005.

H. Kuhn, B. Andreaus, G.G. Scherer, A. Wokaun

Investigation of the single electrode reactions in polymer electrolyte fuel cells
3rd PEFC Forum, Lucerne, B076, July 4-8, 2005.

M. Kuhnke, T. Lippert, G.G. Scherer, A. Wokaun

Fabrication and characterization of micro-structured glassy carbon electrodes for model fuel cells
3rd European PEFC Forum, Lucerne, B043, July 4-8, 2005.

A. Reiner, F. Hajbolouri, M. Döbeli[1], A. Wokaun, G.G. Scherer

Platinum nanoparticles dispersed in a carbon matrix for fuel cell catalysis
E-MRS 2005 Spring Meeting, Strasbourg, France, Mai 31 – June 03, 2005.
[1] ETH Zürich

A. Reiner, N. Beck, H. Kuhn, A. Wokaun, G.G. Scherer

Activities in electrocatalyst development at Paul Scherrer Institut
Projekttreffen des O2 RedNet, Universität Bonn, Germany, November 24-25, 2005.

M. Reum, S.A. Freunberger, F.N. Büchi

Micro scale current density distribution PEFC
2nd Fuel Cell Research Symposium: Modelling and Experimental Validation, Stuttgart, Germany, March 3-4, 2005.

G.G. Scherer, L. Gubler, S. Alkan-Gürsel, M. Slaski, F. Geiger , A. Wokaun

Recent developments and trends in radiation grafted fuel cell membranes at Paul Scherrer Institut
56th Annual ISE Meeting, Busan, Korea, September 25-30, 2005.

I.A. Schneider, H. Kuhn, A. Wokaun, G.G. Scherer

Locally resolved electrochemical impedance spectroscopy in polymer electrolyte fuel cell
2nd Fuel Cell Research Symposium: Modelling and Validation, Stuttgart, Germany, March 3-4, 2005.

I.A. Schneider, D. Kramer, A. Wokaun, G.G. Scherer

Locally resolved electrochemical impedance spectroscopy and simultaneous neutron imaging of liquid water in a PEFC operated on air and pure oxygen
207th Meeting of the Electrochemical Society: Diagnostic Methods for Monitoring Fuel Cell Processes, Quebec, Canada, May 15–20 2005.

I.A. Schneider, D. Kramer, A. Wokaun, G.G. Scherer

Analysis of performance losses in polymer electrolyte fuel cells by locally resolved electrochemical impedance spectroscopy
3rd European PEFC Forum, B052, Lucerne, July 4–8 2005.

J. Vetter	*Lithium-ion batteries* Ciba SC, Basel, February 4, 2005.
J. Vetter, M. Holzapfel, W. Scheifele, J. Ufheil, P. Novák	*In situ study on CO_2 evolution in lithium-ion battery cathodes* 3rd International Conference on Materials for Advanced Technologies (ICMAT 2005) & 9th International Conference on Advanced Materials (ICAM 2005), Singapore, July 3-8, 2005.
J. Wambach	*Surface spectroscopic tools at the Paul Scherrer Institut for investigating catalytic processes* LEM-LVF Seminar, Paul Scherrer Institut, August 31, 2005.
K. Yoshizawa[1], K. Ikezoe[1], K. Shinohara[1], D. Kramer, E. Lehmann, G.G. Scherer	*Analysis of different gas diffusion layer materials in fuel cells* Mechanical Engineering Congress, Tokio, Japan, September 19-22, 2005. [1] Nissan Motor Co. Ltd., Yokosuka, Japan
J. Zhang[1], R. Shimoi[1], K. Shinohara[1], D. Kramer, E. Lehmann, G.G. Scherer	*Visualization and quantification of the water distribution inside an operating fuel cell by neutron radiography* 14th International Conference on the Properties of Water and Steam, Kyoto, Japan, August 29 - September 3, 2005. [1] Nissan Motor Co. Ltd., Yokosuka, Japan

POSTERS

S. Alkan Gürsel, J. Schneider, G.G. Scherer	*Proton exchange membranes based on poly(ethylene-alt-tetrafluoroethylene) for low temperature fuel cells* GRC 2005, Gordon Research Conference on Ion-Containing Polymers, Il Ciocco, Italy, May 1-6, 2005.
S. Alkan Gürsel, L. Gubler, M. Slaski, D. Kramer, A. Wokaun, G.G. Scherer	*Radiation-grafted membranes for polymer electrolyte fuel cells* E-MRS 2005 Spring Meeting, Strasbourg, France, May 31 - June 3, 2005.
S. Alkan Gürsel, J. Schneider, G.G. Scherer	*Thermal behaviour of proton exchange membranes based on poly(ethylene-alt-tetrafluoroethylene* PGS Fall Meeting, Neuchâtel, November 18, 2005.
H. Ben youcef, S. Alkan Gürsel, G.G. Scherer, A. Wokaun	*Radiation-induced grafting of styrene onto ETFE: Influence of synthesis conditions* PGS Fall Meeting, Neuchâtel, November 18, 2005.
F.N. Büchi, M. Santis, S.A. Freunberger	*Investigation of along the channel catalyst gradients* Gordon Research Conference on Fuel Cells, Smithfield, RI, USA, July 17-22, 2005.
I. Czekaj, M. Witko[1], K. Hermann[2], M. Muhler[3], M. van der Berg	*Theoretical and experimental research of surface morphology and properties of transition metal oxides* International Workshop Future Concepts in Energy Related Catalysis, Monte Verità, Ascona, March 13-17, 2005. [1] Polish Academy of Science, Cracow, Polen [2] MPG, Berlin, Germany [3] University of Bochum, Germany
I. Czekaj, G. Piazessi, O. Kröcher, A. Wokaun	*Modeling of the adsorption of isocyanic acid and the isocyanate radical on the TiO_2 anatase (101) and (001) surface by DFT cluster studies* C4 Workshop Competence Centre for Computational Chemistry, ETH Zürich, November 24, 2005.
P. Farquet, C. Padeste, H.H. Solak, S. Alkan Gürsel, G.G. Scherer	*Grafting of poly(glycidyl methacrylate) nanostructures onto flexible substrates using RAFT polymerization* PGS Fall Meeting, Neuchâtel, November 18, 2005.

L. Gubler, S.A. Gürsel, G.G. Scherer	*Radiation grafted fuel cell membranes* European Community H_2 / Fuel Cell Technology Platform Operation Review Days, Bruxelles, Belgium, December 8-9, 2005.
L. Hardwick, H. Buqa, A. Wokaun, P. Novák	*The study of lithium intercalation into graphite with Raman microscopy* International Workshop on Future Concepts in Energy Related Catalysis, Monte Verità, Ascona, March 13-17, 2005.
L. Hardwick, H. Buqa, P. Novák	*Variation of intercalation kinetics in graphite* 21st Annual SAOG Meeting, Fribourg, January 21, 2005.
L. Hardwick, F. La Mantia, F. Rosciano, A. Wokaun, P. Novák	*Analytical methods for lithium-ion battery characterization* EMPA PhD Student Poster Session, Dübendorf, October 20, 2005.
D. Kramer, I.A. Schneider, H. Kuhn, L. Gubler, A. Wokaun, G.G. Scherer	*Advanced in situ diagnostic methods for polymer electrolyte fuel cells at Paul Scherrer Institut* Fuel Cell Seminar, Palm Springs, USA, November 14-18, 2005.
D. Kramer, I.A. Schneider, H. Kuhn, E. Lehmann, A. Wokaun, G.G. Scherer	*The influence of flow direction on liquid distribution and performance in polymer electrolyte fuel cells* Gordon Research Conference on Fuel Cells, Smithfield, RI, USA, July 17-22, 2005.
H. Kuhn, B. Andreaus, M. Stampanoni, G.G. Scherer, A. Wokaun	*X-ray tomographic microscopy investigations of gas diffusion layers for polymer electrolyte fuel cells* Energy and Technology for a Sustainable Future 5, Villigen PSI, June 8-9, 2005.
H. Kuhn, B. Andreaus, G.G. Scherer, A. Wokaun	*Exploring the oxygen reduction reaction in a polymer electrolyte fuel cell* Efficient Oxygen Reduction for the Electrochemical Energy Conversion, ZSW, Ulm, Germany, February 8-9, 2005.
H. Kuhn, B. Andreaus, G.G. Scherer, A. Wokaun	*Exploring single electrode reactions in polymer electrolyte fuel cells* International Workshop on Future Concepts in Energy Related Catalysis, Monte Verità, Ascona, March 13-17, 2005.
M. Kuhnke, T. Lippert, G.G. Scherer, A. Wokaun	*Fabrication and characterization of micro-structured glassy carbon electrodes for micro fuel cells* 21st One-Day-Symposium Electrochemistry Laboratory, Villigen PSI, May 11, 2005.
T. Ogasawara[1], A. Débart[1], M. Holzapfel, P. Novák, P.G. Bruce[1]	*Electrode reactions in lithium-batteries: The O_2 cathode* 208th ECS Meeting, Los Angeles, USA, October 16-21, 2005. [1] University of St. Andrews, UK
A. Reiner, F. Hajbolouri, G.G. Scherer, A. Wokaun	*Platinum particles in a carbon matrix* 21st SAOG-GSSI conference, Advanced Nano Probe Techniques, University of Fribourg-Pérolles, January 21, 2005.
A. Reiner, F. Hajbolouri, S. Abolhassani-Dadras, T. Vad[1], G.G. Scherer, A. Wokaun	*A novel platinum-carbon catalyst via co-sputtering* 1st Workshop of the network: Efficient Oxygen Reduction for the Electrochemical Energy Conversion, Ulm, Germany, February 8-9, 2005. [1] FZ, Jülich, Germany
A. Reiner, B. Steiger, G.G. Scherer, A. Wokaun	*Morphology modifications and their influence on the electrochemical platinum surface activity* International Workshop on Future Concepts in Energy Related Catalysis, Monte Verità, Ascona, March 13-17, 2005.
A. Reiner, F. Hajbolouri, S. Abolhassani-Dadras, T. Vad[1], G.G. Scherer, A. Wokaun	*A novel catalyst geometry: Platinum nanoparticles in a carbon matrix* International Workshop on Future Concepts in Energy Related Catalysis, Monte Verità, Ascona, March 13-17, 2005. [1] FZ, Jülich, Germany

A. Reiner, F. Hajbolouri, M. Doebeli[1], A. Wokaun, G.G. Scherer	*Platinum nanoparticles in a carbon matrix a novel catalyst morphology* 208th ECS-Meeting, Los Angeles, USA, October 16-21, 2005. [1] ETH Zürich
J. Wambach, P. Lerch, J. Schneider, L. Schulz, Q. Cheng, H. Bächli, R. Abela, F. van der Veen	*The SLS infrared beamline "X01DC"* WIRMS-2005, Rathen, Germany, June 26 – 30, 2005.

PATENT APPLICATIONS

L. Gubler, S. Alkan Gürsel, G.G. Scherer	*A method for preparing a membrane to be assembled in a membrane electrode assembly and membrane electrode assembly* Patent Application No. 2005P01798EP, 2005.
L. Gubler, M. Slaski, G.G. Scherer	*A method for preparing a radiation grafted fuel cell membrane with enhanced chemical stability and a membrane electrode assembly* Patent Application No. 2005P01802EP, 2005.
R. Kötz, J.C. Sauter	*Centralized supercapacitor voltage balancing* Patent Application No. PCT/EP05/054564, 2005
F.-M. Petrat[1], M. Holzapfel, H. Buqa, P. Novák, H. Wiggers[1], B. Recken[1]	*Verfahren zur Herstellung von beschichteten Kohlenstoffpartikeln und deren Verwendung in Anodenmaterialien für Lithiumionen-Batterien* Patent Application No. DE 10 2005 011 940.9 2005. [1] Degussa AG, Marl, Germany
A. Prodi-Schwab[1], M. Holzapfel, C. Jost[1], P. Novák, V. Hennige[1], C. Hying[1]	*Filmbildner freies Elektrolyt-Separator-System sowie dessen Verwendung in elektrochemischen Energiespeichern* Patent Application No. DE 10 2005 029 124.4, 2005. [1] Degussa AG, Marl, Germany
I.A. Schneider, G.G. Scherer	*Fast locally resolved electrochemical impedance spectroscopy in polymer electrolyte fuel cells* Patent Application No. EP 05 015 055.6, 2004.

CONFERENCES, WORKSHOPS & EXHIBITIONS

F.N. Büchi	*Power Pac Fuel Cell System* Industriemesse, Hannover, Germany, April 11-16, 2005.
R. Kötz	*56th Annual ISE Meeting,* Busan, Korea, September 25-30, 2005. Symposium Organizer
P. Novák	*CARBON 2005* Gyeongju, Korea, July 3-7, 2005. Symposium Organizer
G.G. Scherer	*2nd European Hydrogen Energy* Conference Zaragoza, Spain, November 22-25, 2005. Member, Scientific and Programme Committee
G.G. Scherer	*International Workshop Future Concepts in Energy Related Catalysis* Monte Verità, Ascona, March 13–17, 2005. Co-Organizer
G.G. Scherer	*European Materials Research Society (E-MRS) Spring Meeting, Symposium L: Hydrogen and Fuel Cells* Strasbourg, France, May 31 - June 3, 2005. Co-Organizer

MEMBERSHIPS IN EXTERNAL COMMITTEES

F.N. Büchi	*International Society of Electrochemistry* Regional Representative Switzerland
R. Kötz	*International Society of Electrochemistry* Past Chair of Div. 3, Electrochemical Energy Storage and Conversion
P. Novák	*International Society of Electrochemistry* Member of Executive Committee (Treasurer) and Council
P. Novák	*International Society of Electrochemistry* Member of Scientific Meeting Committee
G.G. Scherer	*International Society of Electrochemistry* Co-Chair Divison 3; Electrochemical Energy Storage and Conversion
G.G. Scherer	*Beirat Forschungsallianz Brennstoffzellen Baden-Württemberg, Germany* Deputy Speaker
G.G. Scherer	*Maturitätprüfungskommission der Kantonsschulen Baden, Wettingen und Wohlen* Mitglied
G.G. Scherer	*MISTRA, The Swedish Foundation for Strategic Environmental Research* Member International Advisory Board
G.G. Scherer	*Agence National de Recherche, Plan d'Action National sur l'Hydrogene et les Piles à Combustibles, PAN-H, France* Expert Etranger

Paul Scherrer Institut, 5232 Villigen PSI, Switzerland
Tel. +41 (0)56 310 21 11, Fax +41 (0)56 310 21 99
www.psi.ch